

UC Riverside

UC Riverside Electronic Theses and Dissertations

Title

Treatment and Resource Recovery of Brackish Desalination Brine: Antiscalant Chemistry, a Southern California Case Study, and UV Persulfate Treatment Train to Remove Hardness Ions

Permalink

<https://escholarship.org/uc/item/4b54f1fz>

Author

Tang, Xinyu

Publication Date

2024

Peer reviewed|Thesis/dissertation

UNIVERSITY OF CALIFORNIA
RIVERSIDE

Treatment and Resource Recovery of Brackish Desalination Brine: Antiscalant
Chemistry, a Southern California Case Study, and UV Persulfate Treatment Train to
Remove Hardness Ions

A Dissertation submitted in partial satisfaction
of the requirements for the degree of

Doctor of Philosophy

in

Chemical and Environmental Engineering

by

Xinyu Tang

December 2024

Dissertation Committee:

Dr. Haizhou Liu, Chairperson

Dr. Robert Jinkerson

Dr. Samantha Ying

Copyright by
Xinyu Tang
2024

The Dissertation of Xinyu Tang is approved:

Committee Chairperson

University of California, Riverside

Acknowledgements

Words cannot fully convey my sincere gratitude to my advisor, Dr. Haizhou Liu, for his invaluable guidance, unwavering support, and continuous patience throughout my Ph.D. journey. His insightful advice and encouragement were essential in navigating the challenges of this path. Dr. Liu's dedication as a principal investigator and his passion for research have greatly inspired me. His critical thinking, networking skills, and excellence in technical writing have profoundly influenced my development. Dr. Liu not only helped me grow as a researcher but also instilled the confidence to seize every opportunity to share my work. I could not have asked for a better mentor to guide me through this experience.

I would also like to thank my dissertation committee members, Dr. Robert Jinkerson and Dr. Samantha Ying, for their time, support, and valuable feedback during the dissertation defense and graduation process.

My heartfelt thanks go to my lab mates and friends. Dr. Soyeon Kum provided essential guidance, from training me on experimental setups and instruments to engaging in valuable discussions about research and career development. I am grateful to Dr. Liang Wu, Dr. Cheng Tan, and Sitao Liu for their friendship and insightful advice on research, career, and life beyond graduation. Their support made my Ph.D. journey more enjoyable. I also extend my thanks to Andrew Sanchez, Ananta Azad, and Phung Quan for the time spent together in the lab over the years.

Lastly, I am deeply grateful to my parents for their unwavering support, both emotional and financial. I also want to express my gratitude to my dear girlfriend, Mingkun Ma, for

being by my side. Their presence helped me endure the darkest moments of my Ph.D. life.

This doctoral dissertation includes work published in the following journals: Chapter 2 (published in ACS ES&T Engineering), Chapter 3 (published in Environmental Science: Water Research & Technology), Chapter 4 (published in Separation and Purification Technology), and Chapter 5 (published in ACS ES&T Water). Co-authors include Dr. Soyoon Kum and Dr. Haizhou Liu.

My Ph.D. research was supported by funding to Dr. Liu from the United States Bureau of Reclamation (DWPR-R19AC00092), California Department of Water Resources Agricultural Drainage Program, United States Department of Agriculture (2022-67022-37869), and an INTERN supplement to a U.S. National Science Foundation Career Award (CBET-1653931). I also extend my thanks to Carlos Quintero and Richard Haller at the Santa Ana Watershed Project Authority (SAWPA) for their assistance with sampling coordination, and to Phung Quan, Ananta Azad, and Miranda Aiken at UC Riverside for their help with brine collection and processing.

ABSTRACT OF THE DISSERTATION

Treatment and Resource Recovery of Brackish Desalination Brine: Antiscalant Chemistry, a Southern California Case Study, and UV Persulfate Treatment Train to Remove Hardness Ions

by

Xinyu Tang

Doctor of Philosophy, Graduate Program in Chemical and Environmental Engineering
University of California, Riverside, December 2024
Dr. Haizhou Liu, Chairperson

This dissertation addresses key challenges in brine management from inland desalination and the reuse of agricultural drainage water, both critical for sustainable water resource management in arid regions. While the first three studies focus on managing and treating brine from inland desalination, the fourth explores gypsum scaling mitigation in reverse osmosis (RO) desalination of agricultural drainage water, broadening the application of these findings.

The first study investigates a 116-km brine pipeline in Southern California, where brine chemistry and solid precipitation lead to scaling, impacting pipeline efficiency. Results highlight the need for enhanced brine pretreatment and operational optimization to mitigate scaling. The second study introduces an ultraviolet-driven persulfate oxidation (UV/PS) method to degrade antiscalants, which facilitates efficient calcium removal through subsequent chemical demineralization, demonstrating an innovative approach to brine treatment. The third study extends this approach by combining UV/PS, chemical

demineralization, microfiltration, and secondary RO, resulting in over 75% freshwater recovery in the secondary membrane desalination and significant mineral recovery, showcasing the potential for sustainable inland brine management.

The fourth study shifts focus on the desalination of high-salinity agricultural drainage water, where gypsum scaling due to calcium and sulfate poses a severe challenge. This study evaluates the effectiveness of three antiscalants (DTPMP, NTMP, and PAA) under varied pH conditions to prevent gypsum scaling during RO. Findings reveal distinct mechanisms for each antiscalant, with DTPMP providing the most effective inhibition. These insights offer targeted strategies to improve RO efficiency and facilitate the reuse of agricultural drainage water.

Collectively, this dissertation presents an integrated approach to inland brine management, resource recovery, and agricultural water reuse. The findings contribute practical, scalable solutions for enhancing water treatment infrastructure in water-scarce regions and offer foundational insights for future advancements in sustainable desalination processes.

Table of Contents

Acknowledgements.....	iv
Abstract.....	vi
Chapter 1.....	1
Inland Brackish Water Desalination Brine Management Overview.....	2
Brine Composition and Environmental Impact	3
Traditional Brine Disposal Methods and Limitations.....	4
Inland Brine Line System in Southern California.....	5
UV/Persulfate Oxidation and Chemical Demineralization for Brine Treatment.....	6
Agricultural Drainage Water Desalination and Antiscalant Application	6
Research Gaps and Motivations.....	8
Objectives of PhD Dissertation.....	9
Reference	12
Chapter 2.....	18
Abstract.....	19
Introduction.....	20
Methods and Materials.....	23
Major Discharge Points and Brine Sampling Location	23
Chemical Modeling on Theoretical Solid Formation in the Brine Line	25
Simulation of Solid Formation from the Brine	25
Analytical Methods.....	26
Results and Discussion	26

Brine Chemistry in the Brine Line.....	26
Solid Formation Potential in the Brine Line.....	29
Effects of Antiscalants on Solid Formation Potentials in the Brine Line.....	31
Engineering Implication.....	33
Conclusions.....	35
Supporting Information.....	36
Reference	43
Chapter 3.....	47
Abstract.....	48
Introduction.....	49
Materials and Methods.....	52
Chemicals and Solutions.....	52
Experimental Setup.....	53
Analytical Methods for Water Samples.....	55
Results and Discussion	56
Antiscalant DTPMP Degradation by UV/persulfate.....	56
Chemical Demineralization by NaOH Softening	57
Chemical Demineralization by Lime Softening	58
Microfiltration Performance Following Chemical Demineralization.....	59
Engineering Implications on Freshwater Recovery.....	60
Conclusions.....	61
Supporting information.....	62

References.....	71
Chapter 4.....	79
Abstract.....	80
Introduction.....	81
Materials and Methods.....	85
Sampling of Brackish RO Brine.....	85
Experimental Details on Brine Treatment.....	85
Analytical Methods.....	87
Results and Discussion.....	88
Phosphonate Antiscalant Degradation by UV/persulfate.....	88
Removal of Hardness Ions from the Brine by Chemical Demineralization.....	90
Mineral Recovery after Chemical Demineralization.....	91
Fresh Water Recovery from the Brine Following UV/PS and CDM.....	92
Implications.....	93
Supporting Information.....	94
References.....	101
Chapter 5.....	107
Abstract.....	108
Introduction.....	110
Methods and Materials.....	113
Chemicals and Materials.....	113
Experimental Setup and Design.....	113

Analytical Methods.....	115
Results and Discussions.....	115
Effect of Different Antiscalant on Gypsum Scaling.....	115
Membrane Scaling Surface Characterization.....	117
Effect of pH on Gypsum Scaling.....	118
Mechanisms of Antiscalant Inhibition on Gypsum Scaling	118
Effect of NOM on Gypsum Scaling.....	123
Engineering Implications	124
Conclusions.....	125
Supporting information.....	126
Reference	133
Chapter 6.....	138
Brine Line Scaling Case Study in Inland Desalination Systems	139
Enhancing Brine Treatment through Antiscalant Removal via UV/PS.....	139
Integrated Multi-Stage Brine Treatment for Water and Mineral Recovery.....	140
Gypsum Scaling Control in Agricultural Drainage Water Desalination	141
Future Work and Broader Implications	142
Appendix A.....	145
Appendix B.....	153
Appendix C.....	163
Appendix D.....	181

List of Tables

Table 2-1. Chemical composition of brine from 8 sampling sites.....	38
Table 2-2. Saturation indices and FSS concentration of brine from 8 sampling sites.* ...	39
Table 3-1. Chemical composition of brackish water desalination brine solutions.	63
Table 4-1. Major chemical constituents of the inland brackish RO brine.	95
Table 5-1. Chemical compositions of two types of synthetic drainage water.	127

List of Figures

Figure 1-1. Overview of dissertation research scope.....	11
Figure 2-1. (A) Five major brine dischargers and studied brine line branch in Inland Southern California brine line map. (B) Three major dischargers and 8 sampling sites in the brine line branch chosen for this study.	37
Figure 2-2. Theoretical solids amount of brine samples at 8 sampling sites in brine line branch.....	40
Figure 2-3. Dissolved calcium concentration profile from induction time experiments with brines from three inland desalination treatment plants.....	41
Figure 2-4. Effects of secondary antiscalant on calcium precipitation in oversaturated desalination brine from desalination plant DWTP #1 under different stirring rates in lab simulation experiments.	42
Figure 3-1. A schematic of the UV/PS-CDM-MF brine pre-treatment developed in this study.....	64
Figure 3-2. Contribution of persulfate dose to DTPMP degradation (A) effect of UV/persulfate on DTPMP degradation and (B) observed pseudo first-order rates of DTPMP degradation.	65
Figure 3-3. Total calcium concentration of CDM process by NaOH softening with 5 M NaOH. (A) the CDM process with UV/PS pre-treatment at pH 7.8, pH 9, and pH 10.2; (B) The CDM process for controls and CDM process with UV/PS pre-treatment at pH 10.2.....	66
Figure 3-4. Total calcium concentration of the CDM process by lime softening (16.5 mM of $\text{Ca}(\text{OH})_2$ and 11.7 mM of NaHCO_3).	67
Figure 3-5. Total calcium concentration change during the CDM process after 0, 5, 10, and 20 minutes UV/PS pre-treatment, (A) NaOH softening at pH 10.2; (B) lime softening (16.5 mM of $\text{Ca}(\text{OH})_2$ and 11.7 mM of NaHCO_3).	68
Figure 3-6. Normalized permeate flux decline as a function of cumulative normalized volume throughput in the solutions of (A) NaOH softening (5 M NaOH, pH 10.2) and (B) lime softening demineralization without and with UV/PS pre-treatment.....	69
Figure 3-7. Calcite saturation index calculations for calcite in the treated brine after UV/PS-CDM (NaOH softening) and UV/PS-CDM (lime softening).....	70

Figure 4-1. Schematic of sequential persulfate-based photochemical pre-treatment, chemical demineralization, microfiltration, and reverse osmosis (UV/PS-CDM-MF-RO) system.	96
Figure 4-2. Antiscalant degradation by UV/persulfate treatment (A) effect of UV irradiation time and (B) observed pseudo-first-order rates of antiscalant degradation. ...	97
Figure 4-3. Total calcium and magnesium concentration of CDM process after adjustment to pH 10.2 with 5 M NaOH: (A) calcium and (B) magnesium.	98
Figure 4-4. The amount of recovered minerals from the brine after the CDM process. ..	99
Figure 4-5. Normalized permeate flux decline as a function of water recovery for RO feed solutions: (A) pH 7.8, (B) pH 5, and (C) pH 10.2.	100
Figure 5-1. Effect of antiscalant type and concentration on RO permeate flux. (A) Effect of different antiscalants on RO permeate flux.	128
Figure 5-2. Effects of different antiscalants on the scaling layer of RO membrane surface after 24 hours of RO desalination using synthetic drainage water I as the feedwater. (A) [DTPMP]=1 μ M; (B) [NTMP]=1 μ M; (C) [PAA]=1 μ M; (D) without any antiscalant.	129
Figure 5-3. (A) Effect of pH on normalized flux (flux / flux (pH 11, 5 μ M DTPMP)) at 12 hours with different antiscalants. (B) Effect of pH on concentration of total charges of antiscalants species (Φ).	130
Figure 5-4. Effect of acidic pH on particle size of gypsum precipitates and percentage of calcium as solid at 12 hours of RO desalination.	131
Figure 5-5. Effect of NOM on RO permeate flux and membrane surface characteristics.	132

Chapter 1

Introduction

Inland Brackish Water Desalination Brine Management Overview

Water scarcity is one of the most urgent challenges of the 21st century, impacting regions globally and threatening sustainable development in urban, industrial, and agricultural sectors.¹⁻³ The demand for water has continued to rise due to population growth, urbanization, and climate change, particularly in arid and semi-arid regions where freshwater resources are limited. In these areas, desalination has emerged as a practical approach to augment freshwater supplies by treating brackish groundwater.⁴⁻⁶ Inland brackish water desalination, primarily through reverse osmosis (RO), enables the conversion of saline groundwater into potable water and is increasingly adopted to support municipal and industrial water demands.

However, desalination has its own environmental and operational challenges, particularly the production of highly saline brine, which is a concentrated byproduct containing dissolved salts, minerals, and other contaminants.^{7,8} While coastal desalination plants often discharge brine directly into the ocean, inland facilities do not have this option, creating significant obstacles for brine disposal and management. Inland brine management solutions must account for the environmental impacts of saline discharge on soil and groundwater and the high operational costs associated with traditional disposal methods.⁹⁻¹² In recent years, research has intensified to find sustainable, cost-effective methods for inland brackish water desalination brine disposal or reuse, thereby improving the feasibility of inland brackish water desalination as a reliable freshwater source.

Brine Composition and Environmental Impact

Inland brackish water desalination brine is often enriched with scale-forming ions such as calcium, magnesium, and silica, which result in a unique chemical profile that can exacerbate environmental challenges when disposed of untreated brine.^{13,14} Inland brackish water desalination brine typically has total dissolved solids (TDS) concentrations ranging from 5,000 to 10,000 mg/L, depending on the composition of the source water and specific desalination process parameters.^{15,16} These high concentrations of TDS make untreated brine potentially harmful to soil and groundwater quality if improperly disposed of.

In addition to scale-forming ions, brine contains residual chemicals from the desalination process itself, notably antiscalants. Phosphonate-based antiscalants are commonly added to the feedwater in RO systems to prevent scale formation on membranes, helping maintain operational efficiency and prolong membrane life.¹⁷⁻¹⁹ However, these antiscalants become concentrated in the brine, which interferes with further treatment processes and limits options for brine disposal or reuse.²⁰ If released into the environment, brine with high concentrations of antiscalants can inhibit the natural precipitation of minerals, potentially leading to adverse ecological effects. The combination of high salinity, scale-forming ions, and residual antiscalants poses a formidable challenge for sustainable inland brackish water desalination brine management.

Traditional Brine Disposal Methods and Limitations

Traditional disposal methods for inland brackish water desalination brine include deep well injection, evaporation ponds, and land application.^{21–23} Each of these methods has significant limitations, making them less ideal for large-scale inland brackish water desalination facilities. Deep well injection involves injecting brine into deep, isolated geological formations, but it carries risks of subsurface scaling, groundwater contamination, and, in some cases, induced seismic activity. Additionally, the cost of drilling and maintaining deep injection wells is high, making this option economically infeasible in many regions.

Evaporation ponds are another conventional disposal method, where brine is stored in large open basins and allowed to evaporate naturally. While this method is simple and effective in arid regions with high evaporation rates, it requires large land areas and is unsuitable in densely populated regions or areas with high land value.^{12,24} The environmental risks associated with evaporation ponds include infiltration of salts and contaminants into the soil and the potential for damage to local ecosystems due to the high concentration of dissolved contaminants.

Land application, where brine is used for irrigation, is an alternative that has been explored in agricultural settings. However, this method is limited by the tolerance of specific crops to saline conditions and the long-term risk of soil degradation due to salt accumulation. Repeated application of brine to agricultural land can lead to salinization, reducing soil productivity and ultimately making the land unsuitable for crops. Given these limitations, there is a growing need for advanced treatment technologies that reduce

brine volume, enhance resource recovery, and provide safe disposal options for inland brackish water desalination facilities.

Inland Brine Line System in Southern California

In inland arid regions, brine from desalination plants can be discharged into a pipeline infrastructure known as a brine line. This system transports brine over long distances via gravity flow to a centralized treatment facility along the coast or main waterways, where the brine is treated, and the volume is reduced before disposal.

In response to the need for brine disposal, a 116-km brine line infrastructure was constructed to collect and transport $4.8 \times 10^4 \text{ m}^3$ of brine per day from multiple inland desalination facilities in Riverside and San Bernardino Counties, California, to a coastal treatment plant in Orange County, California. This brine line benefits the inland region by removing more than 450 tons of salt per day.²⁵ However, the brine line historically experienced severe scaling issues. The concentration of inorganic solids in the brine increased from the entry point to the end point of the brine line, suggesting that solid formation occurred in the pipeline infrastructure.²⁶ One of the main challenges in managing brine lines is scaling, where minerals precipitate and accumulate on the inner pipe walls due to oversaturation. This scaling causes solid buildup and pipe clogging, significantly increasing maintenance costs and reducing the infrastructure's lifespan. The degree of mineral precipitation depends on factors such as brine oversaturation, flow turbulence, and the presence of antiscalants. Therefore, it is urgent to understand what affects solids formation and how to better manage brine pipeline infrastructure.

UV/Persulfate Oxidation and Chemical Demineralization for Brine Treatment

Advanced oxidation processes (AOPs) and chemical demineralization methods have shown promise in addressing the unique challenges of inland brackish water desalination brine. Among these, UV/persulfate photochemical treatment (UV/PS) has emerged as an effective approach for degrading phosphonate-based antiscalants, one of the main components that hinder further treatment of the brine.^{27–30} In the UV/PS process, persulfate ions are activated by UV light to produce sulfate radicals, which are highly reactive and capable of breaking down organic compounds such as persistent antiscalants and deactivating their precipitation inhibitive capacity.³¹

Degradation of antiscalants through UV/PS oxidation facilitates subsequent treatment steps, such as chemical demineralization (CDM), by allowing the precipitation of scale-forming ions like calcium and magnesium, which are otherwise inhibited by the antiscalants. Chemical demineralization, a process in which alkaline reagents are added to precipitate dissolved ions, further softens the brine and reduces the risk of fouling in downstream processes such as microfiltration (MF) and secondary RO.^{32–34} Integrating UV/PS with CDM and MF forms a comprehensive treatment train capable of enhancing freshwater recovery and enabling the recovery of valuable minerals from brine, making inland brackish water desalination more sustainable and economically viable.

Agricultural Drainage Water Desalination and Antiscalant Application

In addition to inland desalination, agricultural drainage water has also emerged as a potential alternative freshwater source, particularly in arid regions with intensive agriculture. Reusing drainage water can help alleviate water scarcity by providing an

additional water source for irrigation or other non-potable applications. However, drainage water from agricultural fields often has high salinity levels and elevated concentrations of calcium and sulfate, which complicate direct reuse without treatment. Agricultural drainage water typically contains total dissolved solids (TDS) ranging from 3,000 to 30,000 mg/L, with major constituents including hardness ions, sodium, sulfate, and chloride.³⁵ Calcium concentrations within hardness ions range from 200 to 600 mg/L, while sulfate levels vary between 2,000 and 20,000 mg/L.³⁵ Without proper treatment and reuse, discharging this drainage water can degrade soil productivity and pose significant environmental risks.

Reverse osmosis (RO) is a promising membrane desalination process that is able to reduce salinity of agricultural drainage water and produce potable water.³⁶⁻³⁹ However, gypsum scaling, a common issue in the desalination of drainage water, can reduce RO membrane efficiency by forming deposits on the membrane surface, impeding water flow, and increasing operational costs.⁴⁰ To prevent scaling, antiscalants such as diethylenetriaminepentakis-methylphosphonic acid (DTPMP), nitrilotri-methylphosphonic acid (NTMP), and polyacrylic acid (PAA) are commonly used.¹⁹ Each of these antiscalants has different inhibition mechanisms and effectiveness based on the specific chemical conditions of the feedwater. Optimizing antiscalant dosage and application conditions and understanding antiscalant interaction with scale-forming ions are crucial to improving membrane desalination performance and achieving sustainable drainage water reuse.

Research Gaps and Motivations

Despite advancements in inland brackish water desalination and drainage water desalination, several critical research gaps remain:

1. Downstream brine disposal via brine line systems:

The factors that affect solid formation within the brine pipeline infrastructure remain poorly understood, necessitating further investigation to mitigate scaling and operational challenges.

2. Downstream sustainable brine treatment:

Limited research exists on the integrated application of UV/PS-CDM-MF-RO processes. Further investigations are needed to optimize each step and evaluate the combined effectiveness of these processes in reducing salinity, degrading antiscalants, and enhancing mineral recovery.

3. Upstream antiscalant application in primary RO desalination:

While antiscalants are widely used to prevent membrane scaling, the mechanisms by which they inhibit the precipitation of various minerals in complex brine solutions are not fully understood. Specifically, the interactions between antiscalants and ions such as calcium and sulfate require further study to optimize antiscalant selection and dosage. This dissertation aims to address these research gaps by collecting and analyzing brine samples from local brine pipeline system, exploring a multi-step brine treatment train, and investigating the application of antiscalants in agricultural drainage water desalination. By advancing inland brackish water desalination brine treatment and

drainage water reuse, this research seeks to contribute to sustainable saline water management solutions for water-scarce regions.

Objectives of PhD Dissertation

The overarching objective of this PhD dissertation is to develop sustainable and efficient inland brackish water desalination brine management strategies and explore the impact of antiscalants during agricultural drainage water desalination. The research focuses on both downstream brine management and upstream antiscalant applications. Specifically, it addresses:

1. Downstream brine management methods:

This includes analyzing current brine disposal through brine line systems and investigating a novel integrated treatment process (Figure 1-1). It evaluates factors affecting solid formation during brine transportation. Then it integrates and evaluates advanced oxidation processes, chemical demineralization, and microfiltration techniques to improve brine treatability, enhance water recovery, and facilitate resource reclamation.

2. Upstream antiscalant application in primary RO desalination:

This involves optimizing antiscalant use and illustrating their inhibition mechanisms for gypsum scaling. The goal is to improve membrane performance and reduce scaling (Figure 1-1).

The specific objectives are as follows:

1. Characterize brine transport and scaling dynamics in pipeline infrastructure systems:

Analyze brine composition and scaling potential along brine pipeline networks connected with multiple inland brackish water desalination facilities. Identify factors

that promote solid precipitation and scaling, and propose strategies to mitigate scaling risks and improve pipeline performance.²¹

2. Evaluate UV/persulfate photochemical treatment for antiscalant degradation:

Investigate the efficacy of UV/PS oxidation in degrading phosphonate-based and commercial antiscalants in brine and its impact on subsequent treatment steps.^{41,42}

3. Evaluate a newly proposed treatment process for maximizing fresh water and mineral recovery:

Integrate UV/PS oxidation, CDM, MF and RO to examine this comprehensive brine treatment process. This process aims to increase water recovery and reclaim valuable minerals, such as calcium and magnesium, from inland brackish water desalination brine while creating a sustainable brine treatment framework.^{41,42}

4. Understand antiscalant application for agricultural drainage water desalination:

Evaluate the performance of different antiscalants (DTPMP, NTMP, and PAA) in mitigating gypsum scaling during RO desalination of agricultural drainage water.

Investigate the effects of pH and natural organic matter (NOM) on antiscalant effectiveness to determine optimal conditions for reducing membrane scaling and enhancing RO performance. In addition, elucidate the antiscalant inhibition mechanisms on gypsum precipitation under varying chemical conditions.⁴³

Through these objectives, this dissertation seeks to address challenges in downstream inland brackish water desalination brine disposal, sustainable brine treatment, and upstream antiscalant application. The findings aim to advance innovative and

environmentally friendly water treatment technologies, contributing to sustainable water management solutions.

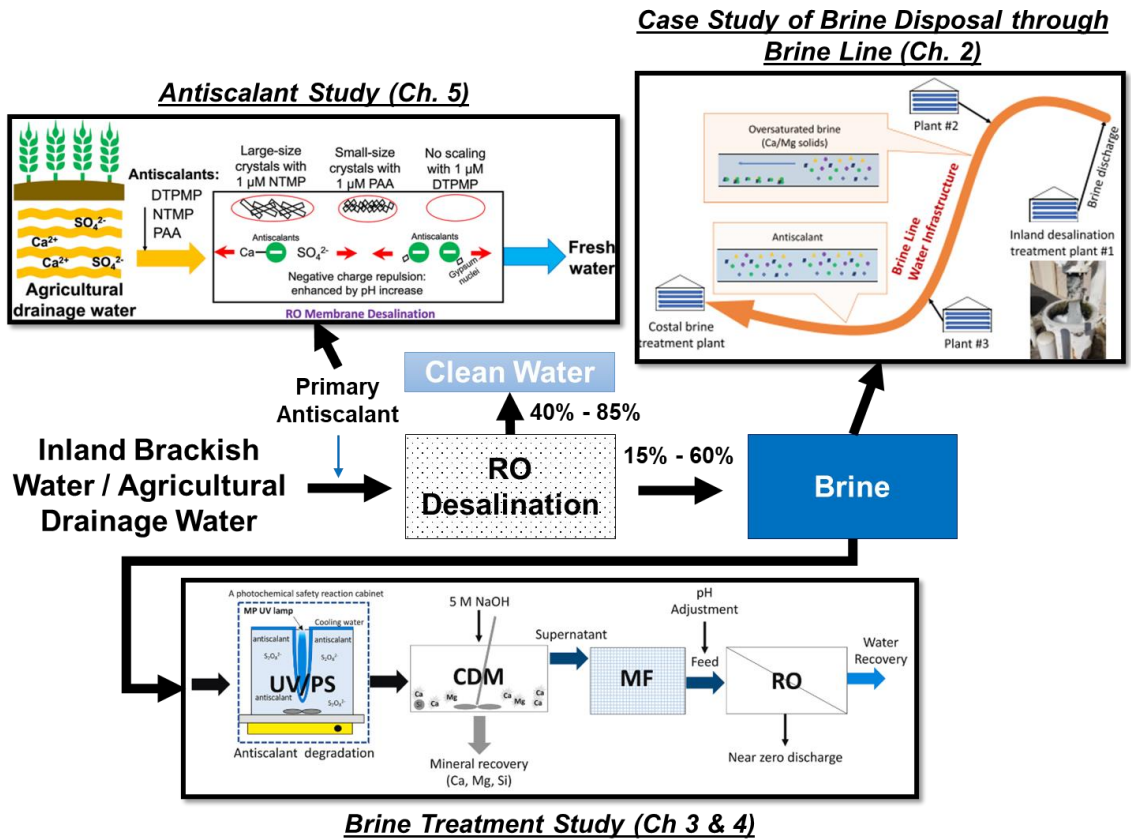


Figure 1-1. Overview of dissertation research scope

Reference

- (1) Mekonnen, M. M.; Hoekstra, A. Y. Sustainability: Four Billion People Facing Severe Water Scarcity. *Sci Adv* **2016**, *2* (2).
<https://doi.org/10.1126/sciadv.1500323>.
- (2) Schwabe, K.; Nemati, M.; Landry, C.; Zimmerman, G. Water Markets in the Western United States: Trends and Opportunities. *Water* (Switzerland). MDPI AG January 1, 2020. <https://doi.org/10.3390/w12010233>.
- (3) Yoon, J. H.; Wang, S. Y. S.; Gillies, R. R.; Kravitz, B.; Hipps, L.; Rasch, P. J. Increasing Water Cycle Extremes in California and in Relation to ENSO Cycle under Global Warming. *Nat Commun* **2015**, *6*.
<https://doi.org/10.1038/ncomms9657>.
- (4) Khanzada, N. K.; Khan, S. J.; Davies, P. A. Performance Evaluation of Reverse Osmosis (RO) Pre-Treatment Technologies for in-Land Brackish Water Treatment. *Desalination* **2017**, *406*, 44–50. <https://doi.org/10.1016/j.desal.2016.06.030>.
- (5) Greenlee, L. F.; Lawler, D. F.; Freeman, B. D.; Marrot, B.; Moulin, P. Reverse Osmosis Desalination: Water Sources, Technology, and Today's Challenges. *Water Research*. Elsevier Ltd **2009**, pp 2317–2348.
<https://doi.org/10.1016/j.watres.2009.03.010>.
- (6) Landsman, M. R.; Sujanani, R.; Brodfuehrer, S. H.; Cooper, C. M.; Darr, A. G.; Davis, R. J.; Kim, K.; Kum, S.; Nalley, L. K.; Nomaan, S. M.; Oden, C. P.; Paspureddi, A.; Reimund, K. K.; Rowles, L. S.; Yeo, S.; Lawler, D. F.; Freeman, B. D.; Katz, L. E. Water Treatment: Are Membranes the Panacea? In *ANNUAL REVIEW OF CHEMICAL AND BIOMOLECULAR ENGINEERING, VOL 11*; Doherty, M. F., Segalman, R. A., Eds.; **2020**; Vol. 11, pp 559–585.
<https://doi.org/10.1146/annurev-chembioeng-111919-091940>.
- (7) Morillo, J.; Usero, J.; Rosado, D.; El Bakouri, H.; Riaza, A.; Bernaola, F. J. Comparative Study of Brine Management Technologies for Desalination Plants. *Desalination* **2014**, *336* (1), 32–49. <https://doi.org/10.1016/j.desal.2013.12.038>.

- (8) Bond, P.; Veerapaneni, S. Zeroing in on ZLD Technologies for Inland Desalination. *J Am Water Works Assoc* 2008, 100 (9).
<https://doi.org/10.1002/j.1551-8833.2008.tb09722.x>.
- (9) Xu, P.; Cath, T. Y.; Robertson, A. P.; Reinhard, M.; Leckie, J. O.; Drewes, J. E. Critical Review of Desalination Concentrate Management, Treatment and Beneficial Use. *Environ Eng Sci* 2013, 30 (8), 502–514.
<https://doi.org/10.1089/ees.2012.0348>.
- (10) Mezher, T.; Fath, H.; Abbas, Z.; Khaled, A. Techno-Economic Assessment and Environmental Impacts of Desalination Technologies. *Desalination* 2011, 266 (1–3), 263–273. <https://doi.org/10.1016/j.desal.2010.08.035>.
- (11) Pramanik, B. K.; Shu, L.; Jegatheesan, V. A Review of the Management and Treatment of Brine Solutions. *Environmental Science: Water Research and Technology*. Royal Society of Chemistry July 1, 2017, pp 625–658.
<https://doi.org/10.1039/c6ew00339g>.
- (12) Ahmed, M.; Shayya, W. H.; Hoey, D.; Al-Handaly, J. Brine Disposal from Inland Desalination Plants Research Needs Assessment. *Water Int* 2002, 27 (2), 194–201.
<https://doi.org/10.1080/02508060208686992>.
- (13) Rahardianto, A.; Gao, J.; Gabelich, C. J.; Williams, M. D.; Cohen, Y. High Recovery Membrane Desalting of Low-Salinity Brackish Water: Integration of Accelerated Precipitation Softening with Membrane RO. *J Memb Sci* 2007, 289 (1–2), 123–137. <https://doi.org/10.1016/j.memsci.2006.11.043>.
- (14) Boerlage, S. F. E.; Kennedy, M. D.; Bremere, I.; Witkamp, G. J.; Van Der Hoek, J. P.; Schippers, J. C. The Scaling Potential of Barium Sulphate in Reverse Osmosis Systems. *J Memb Sci* 2002, 197 (1–2), 251–268. [https://doi.org/10.1016/S0376-7388\(01\)00654-8](https://doi.org/10.1016/S0376-7388(01)00654-8).
- (15) Semiat, R.; Sutzkover, I.; Hasson, D. Scaling of RO Membranes from Silica Supersaturated Solutions. *Desalination* 2003, 157 (1–3), 169–191.
[https://doi.org/10.1016/S0011-9164\(03\)00398-9](https://doi.org/10.1016/S0011-9164(03)00398-9).

- (16) Greenlee, L. F.; Testa, F.; Lawler, D. F.; Freeman, B. D.; Moulin, P. Effect of Antiscalant Degradation on Salt Precipitation and Solid/Liquid Separation of RO Concentrate. *J Memb Sci* 2011, 366 (1–2), 48–61.
<https://doi.org/10.1016/j.memsci.2010.09.040>.
- (17) Hasson, D.; Drak, A.; Semiat, R. Induction Times Induced in an RO System by Antiscalants Delaying CaSO₄ Precipitation; Vol. 157.
www.elsevier.com/locate/desal.
- (18) Jain, T.; Sanchez, E.; Owens-Bennett, E.; Trussell, R.; Walker, S.; Liu, H. Z. Impacts of Antiscalants on the Formation of Calcium Solids: Implication on Scaling Potential of Desalination Concentrate. *Environ Sci (Camb)* 2019, 5 (7), 1285–1294. <https://doi.org/10.1039/c9ew00351g>.
- (19) Yu, W.; Song, D.; Chen, W.; Yang, H. Antiscalants in RO Membrane Scaling Control. *Water Research*. Elsevier Ltd September 15, 2020.
<https://doi.org/10.1016/j.watres.2020.115985>.
- (20) Greenlee, L. F.; Testa, F.; Lawler, D. F.; Freeman, B. D.; Moulin, P. The Effect of Antiscalant Addition on Calcium Carbonate Precipitation for a Simplified Synthetic Brackish Water Reverse Osmosis Concentrate. *Water Res* 2010, 44 (9), 2957–2969. <https://doi.org/10.1016/j.watres.2010.02.024>.
- (21) Tang, X. Y.; Kum, S.; Liu, H. Z. Inland Desalination Brine Disposal: A Baseline Study from Southern California on Brine Transport Infrastructure and Treatment Potential. *ACS ES&T ENGINEERING* 2022, 2 (3), 456–464.
<https://doi.org/10.1021/acsestengg.1c00276>.
- (22) Jensen, V. B.; Darby, J. L. Brine Disposal Options for Small Systems in California’s Central Valley. *J Am Water Works Assoc* 2016, 108 (5), E276–E289.
<https://doi.org/10.5942/jawwa.2016.108.0045>.
- (23) Semblante, G. U.; Lee, J. Z.; Lee, L. Y.; Ong, S. L.; Ng, H. Y. Brine Pre-Treatment Technologies for Zero Liquid Discharge Systems. *Desalination* 2018, 441 (January), 96–111. <https://doi.org/10.1016/j.desal.2018.04.006>.

- (24) Kim, M. S.; Cha, D.; Lee, S. M.; Jeong, H.; Lee, C. Prediction of Brine Evaporation Rate in a Pond: Development of Different Models under Controlled Meteorological Conditions and Comparative Evaluation. *Desalination* 2023, 551. <https://doi.org/10.1016/j.desal.2023.116415>.
- (25) Inland Empire Brine Line - Santa Ana Watershed Project Authority. <https://sawpa.org/inland-empire-brine-line/>, accessed on 06/30/2021.
- (26) Owens-Bennett, E. L.; Trussell, B.; Monroy, I. TECHNICAL MEMORANDUM - Proposed Solids Formation Recovery Formula for the Inland Empire Brine Line; 2016.
- (27) Greenlee, L. F.; Freeman, B. D.; Lawler, D. F. Ozonation of Phosphonate Antiscalants Used for Reverse Osmosis Desalination: Parameter Effects on the Extent of Oxidation. *Chemical Engineering Journal* 2014, 244, 505–513. <https://doi.org/10.1016/j.cej.2014.02.002>.
- (28) Rott, E.; Minke, R.; Bali, U.; Steinmetz, H. Removal of Phosphonates from Industrial Wastewater with UV/FeII, Fenton and UV/Fenton Treatment. *Water Res* 2017, 122, 345–354. <https://doi.org/10.1016/j.watres.2017.06.009>.
- (29) Wang, Z.; Chen, G.; Patton, S.; Ren, C.; Liu, J.; Liu, H. Degradation of Nitrilotris-Methylenephosphonic Acid (NTMP) Antiscalant via Persulfate Photolysis: Implications on Desalination Concentrate Treatment. *Water Res* 2019, 159, 30–37. <https://doi.org/10.1016/j.watres.2019.04.051>.
- (30) Xu, Z. Bin; Wang, W. L.; Huang, N.; Wu, Q. Y.; Lee, M. Y.; Hu, H. Y. 2-Phosphonobutane-1,2,4-Tricarboxylic Acid (PBTCA) Degradation by Ozonation: Kinetics, Phosphorus Transformation, Anti-Precipitation Property Changes and Phosphorus Removal. *Water Res* 2019, 148, 334–343. <https://doi.org/10.1016/j.watres.2018.10.038>.
- (31) Li, W.; Patton, S.; Gleason, J. M.; Mezyk, S. P.; Ishida, K. P.; Liu, H. UV Photolysis of Chloramine and Persulfate for 1,4-Dioxane Removal in Reverse-Osmosis Permeate for Potable Water Reuse. *Environ Sci Technol* 2018, 52 (11), 6417–6425. <https://doi.org/10.1021/acs.est.7b06042>.

- (32) Rioyo, J.; Aravinthan, V.; Bundschuh, J.; Lynch, M. Research on ‘High-PH Precipitation Treatment’ for RO Concentrate Minimization and Salt Recovery in a Municipal Groundwater Desalination Facility. *Desalination* 2018, 439, 168–178. <https://doi.org/10.1016/J.DESAL.2018.04.020>.
- (33) Rahardianto, A.; McCool, B. C.; Cohen, Y. Accelerated Desupersaturation of Reverse Osmosis Concentrate by Chemically-Enhanced Seeded Precipitation. *Desalination* 2010, 264 (3), 256–267. <https://doi.org/10.1016/J.DESAL.2010.06.018>.
- (34) Gabelich, C. J.; Williams, M. D.; Rahardianto, A.; Franklin, J. C.; Cohen, Y. High-Recovery Reverse Osmosis Desalination Using Intermediate Chemical Demineralization. *J Memb Sci* 2007, 301 (1–2), 131–141. <https://doi.org/10.1016/j.memsci.2007.06.007>.
- (35) Cohen, Y. Membrane Desalination of Agricultural Drainage Water: Water Recovery Enhancement and Brine Minimization. UC Berkeley: University of California Water Resources Center 2008.
- (36) Shih, W. Y.; Rahardianto, A.; Lee, R. W.; Cohen, Y. Morphometric Characterization of Calcium Sulfate Dihydrate (Gypsum) Scale on Reverse Osmosis Membranes. *J Memb Sci* 2005, 252 (1–2), 253–263. <https://doi.org/10.1016/j.memsci.2004.12.023>.
- (37) Gabelich, C. J.; Yun, T. I.; Coffey, B. M.; Suffet, I. H. Pilot-Scale Testing of Reverse Osmosis Using Conventional Treatment and Microfiltration. *Desalination* 2003, 154 (3), 207–223. [https://doi.org/10.1016/S0011-9164\(03\)80036-X](https://doi.org/10.1016/S0011-9164(03)80036-X).
- (38) Afonso, M. D.; Jaber, J. O.; Mohsen, M. S. Brackish Groundwater Treatment by Reverse Osmosis in Jordan. *Desalination* 2004, 164 (2), 157–171. [https://doi.org/10.1016/S0011-9164\(04\)00175-4](https://doi.org/10.1016/S0011-9164(04)00175-4).
- (39) Agashichev, S. P.; El-Dahshan, M. E. Reverse Osmosis Incorporated into Existing Cogenerating Systems as a Sustainable Technological Alternative for United Arab Emirates. *Desalination* 2003, 157 (1–3), 33–49. [https://doi.org/10.1016/S0011-9164\(03\)00381-3](https://doi.org/10.1016/S0011-9164(03)00381-3).

- (40) Le Gouellec, Y. A.; Elimelech, M. Calcium Sulfate (Gypsum) Scaling in Nanofiltration of Agricultural Drainage Water. *J Memb Sci* 2002, 205 (1–2), 279–291. [https://doi.org/10.1016/S0376-7388\(02\)00128-X](https://doi.org/10.1016/S0376-7388(02)00128-X).
- (41) Kum, S.; Tang, X.; Liu, H. Treatment of Brackish Water Inland Desalination Brine via Antiscalant Removal Using Persulfate Photolysis. *Environ Sci (Camb)* 2023, 9 (4), 1137–1146. <https://doi.org/10.1039/d2ew00924b>.
- (42) Kum, S.; Tang, X.; Liu, H. Recovery of Fresh Water and Minerals from Inland Brackish Desalination Brine via Persulfate-Based Photochemical Treatment and Demineralization. *Sep Purif Technol* 2024, 342, 126994. <https://doi.org/10.1016/j.seppur.2024.126994>.
- (43) Tang, X.; Liu, H. Mechanisms of Alleviating Gypsum Scaling by Antiscalants during Membrane Desalination: Implications on Agricultural Drainage Water Reuse. *ACS ES and T Water* 2024, 4 (8), 3486–3494. https://doi.org/10.1021/ACSESTWATER.4C00298/ASSET/IMAGES/LARGE/EW4C00298_0005.JPEG.

Chapter 2

Inland Desalination Brine Disposal: a Baseline Study from Southern California on Brine Transport Infrastructure and Treatment Potential

Previously published in *ACS ES&T Engineering*

Tang, X.; Kum, S.; Liu, H. Inland Desalination Brine Disposal: A Baseline Study from Southern California on Brine Transport Infrastructure and Treatment Potential. *ACS ES&T Engineering*. 2022, 2, 456-464 DOI: 10.1021/acsestengg.1c00276.

Abstract

In the inland region of Southern California, a 116-km brine line distribution system transports brackish desalination brine to the coast for treatment and ocean discharge, however, solid precipitation and pipeline scaling occurred in the brine line. This case study investigated brine chemistry and solid precipitation behaviors in the brine line system. Brine chemical composition at multiple sites along the brine line was measured and the theoretical type and amount of solid formation was predicted using chemical modeling. Lab-scale simulation experiments were performed to evaluate the impacts of antiscalant application on solid formation in the brine line. Sampling data showed that pre-existing solids discharged from inland brackish desalination plants accumulated in the brine line which may lead to scaling problems. Chemical modeling predicted that calcite, dolomite, silica and hydroxyapatite were oversaturated but not precipitated. Lab simulation data suggested that the delayed solid formation was mostly due to the presence of antiscalants, especially secondary antiscalants in low flow turbulence conditions. Results suggest that to minimize scaling issues in the brine line infrastructure, two strategies of active on-site brine pretreatment to remove antiscalants and hardness ions, and operational optimization on the brine line for better flow control and real-time monitoring should be considered.

Keywords: Brackish water desalination brine, Solid formation, Antiscalant, Flow turbulence, Induction time

Introduction

Water scarcity has become a worldwide issue, especially in arid inland area.¹⁻³ In response, inland brackish water becomes an increasingly viable water resource and reverse osmosis (RO) brackish water desalination is widely employed to produce clean drinking water.⁴⁻⁸ The major challenge to the wide application of inland desalination is the disposal of the desalination concentrate, a byproduct wastewater known as brine that can account for up to 25% volume of brackish feedwater.⁹ Compared to other types of brine, inland brackish desalination brine has a modest salinity – typical total dissolved solid (TDS) concentration is 5000-9000 mg/L, but with a high level of various scale-forming precursors (*e.g.*, calcium, magnesium, silicate) and oversaturated with respect to different minerals.¹⁰⁻¹³ In addition, antiscalants that transitorily inhibit solid formation are also ubiquitously present in the brine.¹⁴ Therefore, a proper handling of inland brine disposal is needed to prevent brine line scaling and adverse environmental impact, such as damaging aqueous ecosystem and deteriorating vegetation growth and soil productivity.¹⁵

Current brine disposal options include direct ocean discharge, sewer discharge, evaporation pond and deep well injection.^{13,16,17} In inland arid area, a viable option is to discharge brine from different inland desalination plants into a pipeline infrastructure that is known as brine line. This water infrastructure transports brine via a long-distance, gravity-driven manner to a centralized facility along the coast or main waterways, where a reduced volume of brine will be disposed after treatment. If the centralized facility is located far from natural water body, a thermal treatment of brine is needed to achieve

zero liquid discharge. Compared to other brine disposal methods, a brine line that collects inland brine for centralized treatment is a practical approach to manage a large number of inland desalination facilities and protect the groundwater. As brackish groundwater desalination becomes more important to inland regions, more brine line infrastructure will be constructed in the future.

A major challenge to brine line management is scaling – a phenomenon when minerals precipitate on the inner pipe wall from oversaturated brine. Scaling results in solid build-up and pipe clogging, thus significantly increasing the maintenance cost of brine line and reducing the longevity of water infrastructure. The extent of solid precipitation from the brine depends on several factors including the oversaturation ratio, flow turbulence and the presence of antiscalants – a group of organic chemicals that are typically added in the feedwater during desalination process to alleviate membrane scaling issue.^{18–22}

Antiscalants are subsequently rejected by RO membranes and concentrated in the brine. Antiscalant is the organic chemical that contains active gradients with function groups including phosphonate, carboxylic acid or other chelating agents and its concentration ranges between 2 and 10 μM .^{14,23} The presence of antiscalant can delay nucleation and crystal growth for a finite duration of time (known as induction time).^{14,24–28}

Flow turbulence can also affect solid formation kinetics in the brine line. The mixing energy has a dominant impact on crystal growth process.²⁹ However, the impact of flow turbulence on solid formation in brackish water desalination brine remains unknown. Prior studies focusing on scaling and solid formation phenomenon in a real brine line system are very limited, and there is little knowledge on how to control the rate of

nucleation and crystal growth in real brackish water desalination brine. A case study on a real brine line system will generate much needed knowledge on inland brine disposal management.

In the semi-arid Inland Southern California, a 70,000-km² region known as Inland Empire that compasses Riverside and San Bernardino Counties, a brine line infrastructure in operation provides a unique setting of its kind in the world. Inland Empire has a population of approximately 4.5 million with a fast growing economy and booming housing market.³⁰ The water demand for agricultural, industrial and municipal use, driven by increasing population and economy, keeps growing. To alleviate severe water scarcity in this region, inland brackish water desalination has been employed and expanded to meet the growing water demand, which in its companion generates a large amount of brine. In response to the need for brine disposal, a 116-km brine line infrastructure was constructed to collect and transport 4.8×10^4 m³ of brine per day from multiple inland desalination facilities in Riverside and San Bernardino Counties, Calif., to a coastal treatment plant in Orange County, Calif. This brine line benefits the inland region by removing more than 450 tons of salt per day.³¹ However, the brine line historically experienced severe scaling issues that induced high maintenance cost. The concentration of inorganic solids in the brine increased from the entry point to the end point of the brine line, suggesting that solid formation occurred in the pipeline infrastructure.³² Therefore, it is urgent to understand what affects solids formation and how to better manage brine pipeline infrastructure.

By collecting and analyzing samples from the unique brine line in Inland Southern California, this study aimed to quantitatively characterize chemistry of inland desalination brine, predict theoretical solid formation potential in the brine line using chemical modeling, fundamentally understand the impacts of antiscalant, flow turbulence on the solid formation phenomenon in brine line, and acquire knowledge for better brine transport infrastructure management.

Methods and Materials

Major Discharge Points and Brine Sampling Location

The whole brine line system in Inland Southern California receives brine from 5 major inland brackish desalination water treatment plants: Arlington desalter, Temescal desalter, Perris and Menifee desalters, Chino I desalter and Chino II desalter that account for more than 95% of brine discharge volume (Figure 1A).³² For a better control of the experimental design and system control, this study focused on the most unique and important branch of the brine line system (Figure 1B). This brine line branch historically experienced severe scaling issues and accounts for approximately 40% of the total inland brine volume, the largest of all branches. It mainly receives brine from three discharging points: Arlington desalter (labelled as DWTP #1 of Site S1), Temescal desalter (labelled as DWTP #2 of Site S6) and a side stream brine discharged from Perris and Menifee desalters (labelled as DWTP #3 leading to Site S3) (Figure 1B). These three discharge points in combination account for nearly 100% of calcium loading and flow rate in this branch of brine line.³² Primary antiscalants (Table S1) carried over from the RO desalination process are present in brine samples from DWTP #1, DWTP #2 and DWTP

#3 (Figure 1B). In addition, a secondary antiscalant (Table S1) is added to the RO brine discharged from DWTP #1 right before entering the brine line, whereas no secondary antiscalant was added in other two facilities. Therefore, the brine line branch chosen in this study provides a unique setting to study brine chemistry and solid formation.

A total of 8 sampling sites along the brine line were selected to collect brine samples on January 20, 2021. In addition to the three desalination facilities' sites prior to entering the brine line (Sites S1, S3 and S6), five sites in the brine line were chosen (Figure 1B). The brine line is divided into three sections based on the sites: Section A (between Site S1 and Site S2), Section B (between Site S4 and Site S5), and Section C (between Site S7 and Site S8; Figure 1B). Additionally, one brine sample was collected at DWTP #1 prior to the addition of secondary antiscalant. The hydraulic retention time of Section A, B and C is 6, 1.5 and 1 hours, respectively. The flow rate of brine from DWTP #1, DWTP #2 and DWTP #3 is 1744, 14718, 6355 m³/day, respectively. Therefore, the brine from DWTP #3 has the highest flow rate and has a dominant impact on brine chemistry from Site S4 to Site S8.

Fresh brine samples were collected from the 8 sampling locations and then stored into 9.5-L sample bottles sealed without headspace within a 2-hour time span. Following that, the samples were analyzed within 2 hours for suspended solids, pH, alkalinity, anions concentration measurement. An additional 150 mL of brine samples were collected from each location, immediately filtered using 0.1- μ m syringe filters, acidified by concentrated nitric acid onsite and then stored in three 50-mL centrifuge tubes without headspace.

These acidified brine samples were subsequently measured for dissolved cation concentrations.

Chemical Modeling on Theoretical Solid Formation in the Brine Line

Chemical equilibrium model simulation was conducted using Visual Minteq (version 3.1) software to calculate the theoretical amount and type of solid formation at different sampling locations of the brine line.³³ Only inorganic solids precipitation was considered in the chemical model. This is because dissolved organic carbon (DOC) concentration is very low compared to calcium and magnesium concentration in the brine (Table 1). Calcium and magnesium complexation with organic matter is negligible at this low level. Measured chemical compositions and temperature of brine samples at each site were input parameters of the chemical model in a closed system. The saturation indices with respect to various possible solids were predicted by the software. Predicted oversaturated solids were subsequently selected, and theoretical type and amount of solid formation in the brine at equilibrium were calculated. More details on the chemical modeling are provided in supporting information (Text S1).

Simulation of Solid Formation from the Brine

To evaluate the kinetics of solid formation in the brine, lab-scale simulation experiment was conducted in 2-L stirred rectangular batch-reactors at 23 ± 1 °C that simulates the brine line temperature. Specifically, 1-L brine samples collected from different sites were transferred to the reactor as soon as possible after sampling. Experiments were conducted under three stirring rates of 0, 350 and 700 revolutions per minutes (rpm) for up to 72

hours. At designated time intervals, 3-mL sample was withdrawn, filtered using 0.1- μ m filters, acidified and measured for dissolved calcium and magnesium concentrations.

Analytical Methods

Dissolved calcium, magnesium, sodium and silica concentrations were quantified using EPA standard methods 3005 with an inductively coupled plasma mass spectrometry (ICP-MS).³⁴ Alkalinity in brine samples without pretreatment was measured using a titration method.³⁴ Phosphate was determined by vanadomolybdophosphoric acid colorimetric method.³⁴ Ammonium was determined by phenate method. Nitrite and nitrate were determined by using standard colorimetric methods.³⁴ Total suspended solids (TSS), Volatile suspended solids (VSS) and fixed suspended solids (FSS) were determined by the standard method 2540D-E.³⁴ Dissolved organic carbon (DOC) was determined by a TOC analyzer. pH and total dissolved solids (TDS) were determined by pH meter and conductivity meter. Triplicate measurements of each sample were conducted in all brine quality measurements.

Results and Discussion

Brine Chemistry in the Brine Line

Field sampling data showed that brine chemical parameters are different at each desalination plant, which is due to different feed brackish groundwater and different recovery rate (79% at DWTP #1, 86% at DWTP #2, 75% at DWTP #3). The solution pH of the brine along the 8 sampling locations are relatively stable, ranging between 7.7 and 7.9 (Table 1). TDS concentration of brine along the brine line is in the range of 3300 mg/L to 5300 mg/L, validating high salinity of brackish desalination brine, and brine

from DWTP #3 has the highest TDS concentration among brines from three plants (Table 1). The alkalinity of desalination brine varied at different desalination plants discharged into the brine line (Table 1). For example, alkalinity of brines from DWTP #1 (Site S1) and DWTP #2 (Site S6) are similar at approximately 1600 mg/L, but alkalinity of brine originated from DWTP #3 (Site S3) is much lower at 500 mg/L. Alkalinity along the brine line first decreases from 1600 mg/L (Site S2) to 660 mg/L (Site S4) and then increases to 1000 mg/L (Site S7) as a result of mixing and dilution effects of the three desalination brines discharged into the brine line. Bicarbonate mainly contributes to alkalinity. The presence of bicarbonate in the inland brackish water originates from dissolution of carbonate species from aquifer minerals in equilibrium with brackish groundwater.

Calcium is a major constituent in the inland desalination brine, ranging between 840 and 1178 mg/L (Table 1). There is also a considerable amount of magnesium in the brine, ranging between 150 and 300 mg/L (Table 1). Sources of these two hardness ions are from dissolution and equilibrium with aquifer calcium and magnesium minerals in groundwater. Brines from DWTP #1 and DWTP #2 were similar with respect to magnesium concentration, but the brine from DWTP #3 is 50% less compared with the other two brines. Sodium concentration in these three brines ranged from 500 to 1000 mg/L. In addition, dissolved silica concentration in the brine discharged from the three plants were approximately 50 mg Si/L and stayed relatively stable along the brine line (Table 1).

Regarding nutrients, inland brackish brine is very rich in nitrate, with its concentration ranging between 30 and 110 mg N/L (Table 1). The elevated level of nitrate unique in inland desalination brine is mainly attributed to the historical agricultural activity in this region and a long-term application of nitrogen fertilizer and groundwater contamination. In addition, phosphate, nitrite and ammonium ion concentrations were nearly negligible at most sites along the brine line branch, except that the brine at Site S3 that had the highest concentrations of phosphate, nitrite and ammonium ion (Table 1), which could be attributed to the collection of a small volume of industrial wastewater that contains a certain level of nitrogen and phosphorus at DWTP #3. Dissolved organic carbon (DOC) concentration along the brine line is generally low, consistent with other observations that brackish water is low in organic content compared to surface water.

TSS and FSS concentration in the brine represents total and inorganic solids that can contribute to brine line scaling. Brines discharged from DWTP #1 and DWTP #2 had negligible amount of pre-existing solids, but brine at Site S3 has the highest solid concentration (Table 1), suggesting that solid pre-existing in the brine was discharged from DWTP #3. TSS concentration is 12 mg/L higher than FSS concentration in brine from DWTP #3, indicating that pre-existing organic solids account for a small fraction of TSS and inorganic solids play a dominant role in brine line scaling (Table 1). These solids further transported downstream from Site S3 and increased solid concentration in Sections B and C of the brine line (Table 1). In Section A of the brine line section, FSS concentration did not change from Site S1 to Site S2, indicating that no solid formation occurs in this section. In Section B, FSS concentration declined from 32 mg/L to 12

mg/L. In Section C, FSS concentration also declined from 18 mg/L to 6.5 mg/L (Table 1). The decrease of FSS concentration in Section B and C of the brine line indicates an accumulation of pre-existing inorganic solids instead of new solids formation took place in the brine line, which was also supported by stable dissolved calcium, magnesium, silica concentration along the brine line (Table 1). Calculation shows that approximately 340 and 255 kg/day of inorganic solids accumulated in Section B and C of the brine line, respectively (Figure S1). The accumulation of pre-existing solids in the brine line is likely due to the settling effects of the suspended solids in the brine under low-turbulent flow conditions.

Solid Formation Potential in the Brine Line

Chemical modeling predicts the theoretical maximal amount and type of formed solid from the oversaturated brine based on chemical equilibrium. Modeling result shows that four solids are oversaturated and can precipitate in the brine line: calcite $\text{CaCO}_{3(s)}$, dolomite $\text{CaMg}(\text{CO}_3)_2(s)$, silica solid $\text{SiO}_{2(s)}$ and hydroxyapatite $\text{Ca}_{10}(\text{PO}_4)_6(\text{OH})_2(s)$. For brines from DWTP #1, DWTP #2 and DWTP #3, calcite accounts for the majority of the predicted solid composition, accounting for 52%, 90%, 62% of total theoretical solids, respectively (Figure 2). Dolomite is predicted to only exist in brine from DWTP #1, accounting for 38% of total theoretical solids (Figure 2). Silica solid is predicted to exist in brines from all three plants, accounting for 10%-30% of total theoretical solids. Hydroxyapatite concentration is predicted to only exist in the brine originating from DWTP #3, accounting for approximately 5 % of the solids. The predicted solid

composition and concentration at other sites along the brine line are mainly a result of mixing and dilution effects of the three main dischargers.

Hydroxyapatite has the highest saturation index, but the lowest theoretical solids amount at all sites, due to the lowest K_{sp} value (Log K_{sp} of calcite, dolomite, silica solid and hydroxyapatite is -8.5, -17.1, -4 and -44.3, respectively) of the solid and the low level of phosphate in the brine (Table 2 and Figure 2). Dolomite has a higher saturation index than calcite and silica solid along the brine line, but its theoretical concentration equals zero at all sites except for Site S1 and Site S2. In contrast, calcite and silica solid have the lower saturation index but relatively higher theoretical concentration along the brine line. This is due to the fact that when different oversaturated solids start to precipitate, solution composition also changes and then solids initially supersaturated are no longer supersaturated at the end point of precipitation, which lead to different theoretical solid concentrations.

Total theoretical solid concentrations of brine from DWTP #1 and DWTP #2 are similar at approximately 1100 mg/L, due to the direct impact of brine discharged from brackish desalination plants (Figure 2). The theoretical solids concentration of brine from DWTP #3 is only 340 mg/L, due to its low alkalinity and low saturation index of calcite and silica solid (Table 2). After the mixing of brine from DWTP #3 into Section B of the brine line, total theoretical solids concentration drops to 460 mg/L at Site S4, mainly due to dilution effects by the large volume of brine mixing from DWTP #3 (Figure 2). After mixing with oversaturated brine from DWTP #2 (Site S7), total theoretical solids concentration increases to 690 mg/L. The trend of theoretical solids concentration along

the brine line is consistent with the trend of saturation index of calcite, which in turn rationalizes the prediction that calcite is the dominant theoretical solid.

The experimentally measured FSS concentration, however, was much lower than the theoretical solids concentration at all sites (Table 2), suggesting that the extent of solid formation is heavily impacted by the kinetics of solid precipitation. The slower-than-expected rate of solid formation in the brine is mainly due to the existence of antiscalants.

Effects of Antiscalants on Solid Formation Potentials in the Brine Line

The presence of residual primary antiscalant (Table S1) in the brine is effective on delaying solids formation from the desalination brine (Figure 3). The primary antiscalant concentration carried over into the brine from DWTP #1, DWTP #2 and DWTP #3 is approximately 20, 32 and 5 mg/L, respectively. But the type of primary antiscalants at these sites are different. Lab precipitation simulation experiments show that the induction time of calcium precipitation in the three desalination brines ranged between 1 and more than 4 hours under 700 rpm stirring rate (Figure 3). The induction time of magnesium precipitation in the three desalination brines was also more than 4 hours under 700 rpm stirring rate (Figure S2). These results indicate the primary antiscalant is capable of delaying solids formation even considering that the three brine samples have different chemical compositions.

Because a secondary antiscalant with active gradient of carboxylic acid and other chelating agents was injected into the RO brine discharged from DWTP #1, brines samples were taken with and without the secondary antiscalants (Table S1) from DWTP #1 to further evaluate its effect on solid precipitation. Results show that the presence of a

secondary antiscalant further delayed the precipitation of calcium solids, decreased solids formation rate and created a two-stage calcium precipitation curve (Figure 4). For example, under 700 rpm stirring rate and in the absence of secondary antiscalant, the induction time for calcium precipitation in the brine was 3 hours and then a linear precipitate rate was observed (Figure 4A). In contrast, in the presence of 10 mg/L secondary antiscalant, a two-stage calcium precipitation curve was observed. The first-stage induction time increased to 4 hours. After that, calcium precipitation lasted for 2 hours before it was further delayed for an additional 50 hours (Figure 4A). Overall, under the same stirring rate, the brine with secondary antiscalant had a longer induction time and slower calcium precipitation rate than the brine without secondary antiscalant (Figure 4). The trend is consistent with previous observations that the presence of antiscalant delays calcium precipitation in the brine.³⁵

Lab-scale simulation experiments also show that the addition of secondary antiscalant (Table S1) at a concentration of 10 mg/L was as effective as the presence of primary antiscalant on the inhibition of magnesium solid precipitation within 72 hours (Figure S3). The induction time of magnesium precipitation was much longer than that of calcium precipitation. (Figure 4 vs. Figure S3). The results suggest that the antiscalants used for the brine line are more effective on inhibition of magnesium precipitation than calcium precipitation.

Flow turbulence also affects the effectiveness of antiscalants on nucleation and solid formation process. Due to the complexity of actual brine line system from aspect of pipeline configuration and diameters, three different stirring rates were chosen in lab-

scale induction time experiment to qualitatively illustrate the impact of flow turbulence on solids formation phenomenon in brine line. With the stirring rate increasing from 0 to 700 rpm, flow turbulence increased, and a shorter induction time and faster calcium precipitation kinetics were observed (Figure 4). When the brine was in static condition at 0 rpm, the induction time was beyond 72 hours (Figure 4C). In brines without secondary antiscalant, the induction time decreased from 6 to 3 hours when the stirring speed increased from 350 to 700 rpm (Figure 4A vs. 4B). In brines with secondary antiscalant, the induction time also decreased from 8 to 4 hours when the stirring speed increased from 350 to 700 rpm (Figure 4A vs. 4B). This phenomenon could be due to the mechanism that increase of flow turbulence can accelerate detachment between antiscalant and calcium and magnesium and it can also accelerate collision between cations and anions, particles and particles and then induce flocs formation, facilitating solids precipitation.

Engineering Implication

Extensive sampling data along the brine line show that inland brackish water desalination brine is heavily oversaturated with multiple hardness solids (*e.g.*, calcite and dolomite) and silica solid. Consequently, there is a high risk for solids formation in the brine pipeline. In addition, primary antiscalant universally exists in brackish water desalination brine and secondary antiscalant is also dosed into brine sometimes to prevent solids formation, which makes brine chemistry even more complex. Moreover, brine flow turbulence conditions also affect the effectiveness of antiscalant in delaying solid formation in the brine line. Furthermore, pre-existing solids discharged from desalination

plants can accumulate in the brine line via particle setting effects. Based on the unique inland brine chemistry, it is important to minimize solid formation risk and scaling issues in the brine line for better water infrastructure management. Data from this study points to two overall strategies for inland brine line management: (1) active on-site brine pretreatment to reduce solid loading; and (2) better brine line management to minimize *in situ* solid formation and accumulation.

Regarding active brine pre-treatment before discharging into the brine line, two treatment options can be implemented. First, solid removal unit operations can be installed to remove pre-existing solids from the brine at the desalination facilities, including coagulation and sedimentation followed by microfiltration. Second, to minimize potential solid formation risks in the brine line, it is important to transform oversaturated brine to undersaturated brine before discharging from inland desalination facilities. To reach this goal, the removal of antiscalants from the brine is critical. One potential pretreatment train is to degrade antiscalants by ultraviolet light based advanced oxidation process.³⁶ The removal of antiscalants will accelerate the precipitation of oversaturated hardness ions, *e.g.*, calcite and dolomite, which can be subsequently removed via a solid separation unit process.¹³ This treatment train will result in additional resource recovery of minerals and the production of a clear brine with minimal scaling risks.

In cases where active on-site pretreatment options are not possible, several design and operational options on the brine line can be considered to minimize *in situ* solid formation and accumulation. First, it is important to control brine flow rate to an optimal level to avoid extremely low or high flow turbulence, because a high flow turbulence

renders the effectiveness of carried-over primary antiscalant, and a low flow turbulence facilitates the accumulation of pre-existing solids in the brine. Second, it is useful to have a monitoring system along the brine line to transmit real-time important brine chemical characteristics including temperature, pH, alkalinity, hardness levels, to predict the brine oversaturation levels and solid potential risks. Third, based on the real-time data, mild adjustment can be made along the brine line to stabilize the brine chemistry and avoid in situ solid formation, e.g., dosing additional antiscalants and pH adjustment.

Conclusions

In this study, we conducted a case study on an inland brine line in southern California. By analyzing brine samples at different sites along the brine line and major desalination treatment facilities, we evaluated brine chemistry, theoretical solids formation and impact of antiscalant and flow turbulence on solids formation. This study shows inland brackish water desalination brine is supersaturated with respect to calcite, dolomite, silica solid and hydroxyapatite, with calcium solids the major minerals oversaturated in the brine. Both primary antiscalant and secondary antiscalant can be effective in delaying solids formation. Pre-existing solids discharged from desalination plants could accumulate in the brine line and lead to scaling issues in the long term. Results suggest that to minimize scaling issues in the brine line infrastructure, two strategies of active on-site brine pretreatment to remove antiscalants and hardness ions, and operational optimization on the brine line for better flow control and real-time monitoring should be considered.

Supporting Information

Please refer to Appendix A for supporting information, which includes:

Text S1, Visual Minteq calculation steps; Figure S1, solids accumulation rate in different sections of brine line; Figure S2, dissolved magnesium concentration profile from induction time experiments with brines from three inland desalination treatment plants.

Table S1, Antiscalant information at Arlington desalter and Temescal desalter. Figure S3, magnesium induction time experiment for brine at DWTP #1 with or without secondary antiscalant under different stirring rate.

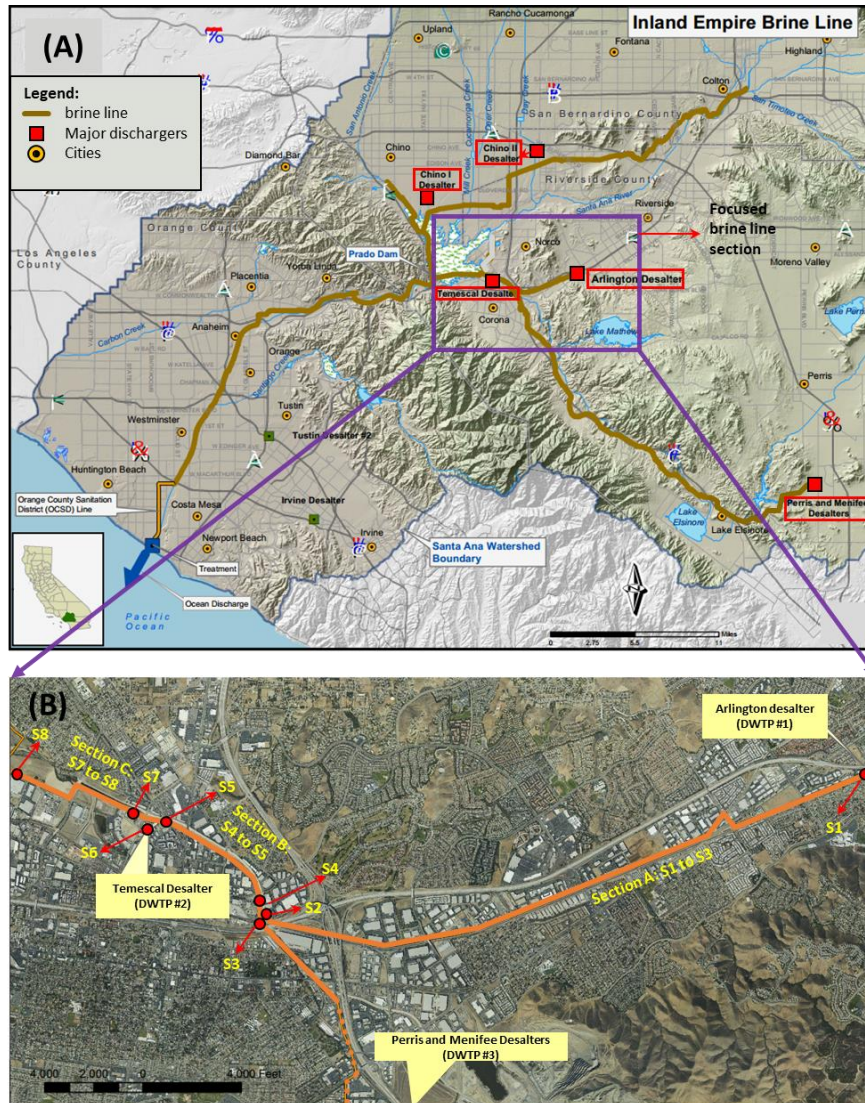


Figure 2-1. (A) Five major brine dischargers and studied brine line branch in Inland Southern California brine line map. (B) Three major dischargers and 8 sampling sites in the brine line branch chosen for this study. Site S1 (discharge point of DWTP #1 to acquire brine with secondary antiscalant), Site S2 (end point of Section A of the brine line), Site S3 (end point of side brine line from DWTP #3), Site S4 (start point of Section B of brine line), Site S5 (end point of Section B of brine line), Site S6 (discharge point of DWTP #2), Site S7 (start point of Section C of brine line), Site S8 (end point of Section C of the brine line).

Table 2-1. Chemical composition of brine from 8 sampling sites.

Parameters	DWTP #1		DWTP #2		DWTP #3		Section A		Section B		Section C	
	Site S1	Site S6	Site S6	Site S6	Site S3	Site S2	Site S4	Site S5	Site S7	Site S8		
pH	7.8	7.7	7.7	7.7	7.7	7.9	7.8	7.7	7.9	7.9		
Alkalinity (mg/L as CaCO₃)	1629±8	1588±25	508±16	1638±14	663±0	658±36	1017±16	1013±0				
Ca²⁺ (mg/L)	840±10	1178±29	847±45	827±35	870±37	905±13	968±19	943±83				
Mg²⁺ (mg/L)	301±6	293±3	154±7	302±13	149±47	187±4	218±4	210±16				
Na⁺ (mg/L)	464±18	674±20	977±34	510±24	912±4	742±23	818±6	699±48				
NO₃⁻ (mg N/L)	65.2	104.8	31.4	68.1	39.8	87.8	62.4	107.6				
NO₂⁻ (mg N/L)	ND*	ND*	1.3	ND*	1.2	0.2	0.6	0.3				
NH₄⁺ (mg N/L)	ND*	ND*	1.0	ND*	0.7	0.1	0.4	0.1				
PO₄³⁻ (mg P/L)	0.1	0.3	5.9	0.1	7.6	3.6	4.5	2.5				
SO₄²⁻ (mg/L)	1101±24	1490±53	1031±89	1104±6	995±18	558±12	1149±47	932±24				
Cl⁻ (mg/L)	897±7	1531±11	2574±36	909±25	2340±21	2371±4	2013±47	2046±4				
H₄SiO₄ (mg Si/L)	51±2	52±0	56±1	52±1	62±0	62±1	49±1	41±6				
FSS (mg/L)	0.8	1.9	40.4	0.4	31.6	10.9	17.7	6.5				
TSS (mg/L)	1.5	4	52.4	0.9	42.9	18.3	24.1	11.9				
TDS (mg/L)	3268	4608	5258	3364	5153	4709	4844	4733				
DOC (mg C/L)	5.9	5.0	3.1	6.5	3.1	3.5	3.9	3.8				

* ND = non-detectable

Table 2-2. Saturation indices and FSS concentration of brine from 8 sampling sites.*

Theoretical solid	Saturation index							
	Site S1	Site S2	Site S3	Site S4	Site S5	Site S6	Site S7	Site S8
Calcite β -CaCO _{3(s)}	2.0	2.1	1.5	1.7	1.6	2.0	2.0	2.0
Dolomite CaMg(CO ₃) _{2(s)}	3.9	4.1	2.5	2.9	2.9	3.6	3.6	3.6
Silica SiO _{2(s)}	1.3	1.3	1.3	1.3	1.3	1.3	1.3	1.2
Hydroxyapatite Ca ₁₀ (PO ₄) ₆ (OH) _{2(s)}	7.9	8.2	13.0	13.7	12.5	9.3	13.5	12.7
FSS	Concentration (mg/L)							
Predicted FSS	1066	1076	343	461	468	1104	687	671
Measured FSS	0.8	0.4	40.4	31.6	10.9	1.9	17.7	6.5

Site S1 refers to brine at Site S1 (DWTP #1); Site S3 refers to brine at Site S3 (originated from DWTP #3); Site S6 refers to brine at Site S6 (DWTP #2). Section A: Site S1 to Site S2, including brine at Site S1 and brine at Site S2; Section B: Site S4 to Site S5, including brine at Site S4 and brine at Site S5; Section C: Site S7 to Site S8, including brine at Site S7 and brine at Site S8.

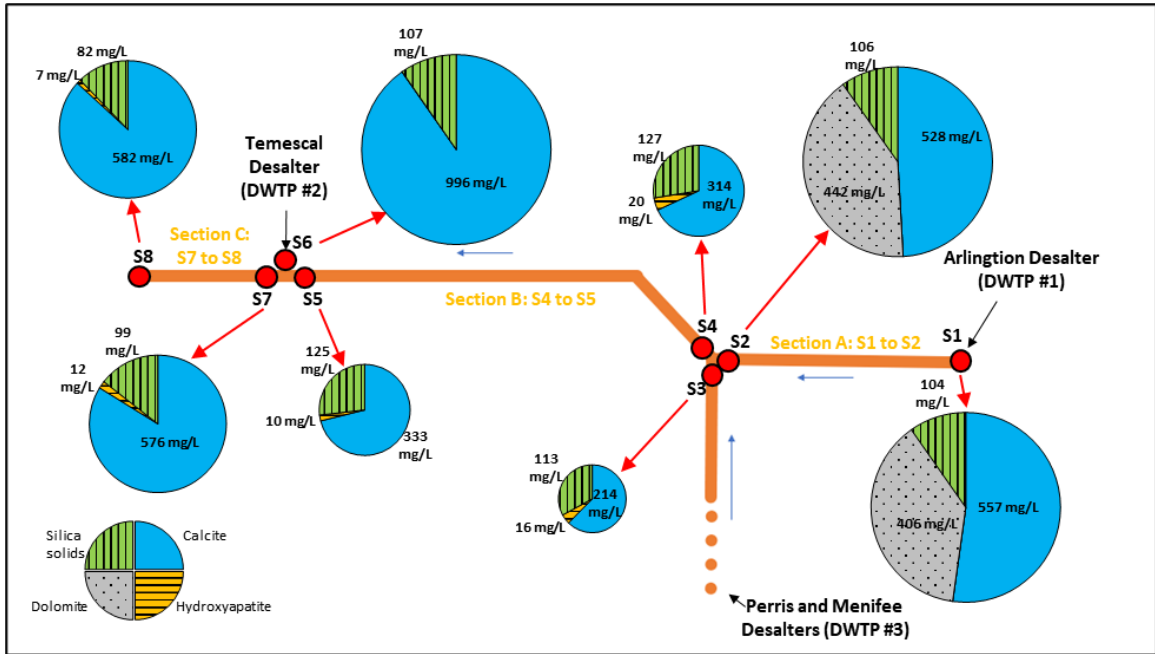


Figure 2-2. Theoretical solids amount of brine samples at 8 sampling sites in brine line branch. (Concentration results in this figure was calculated by Visual Minteq and detailed calculation steps was shown in Text S1)

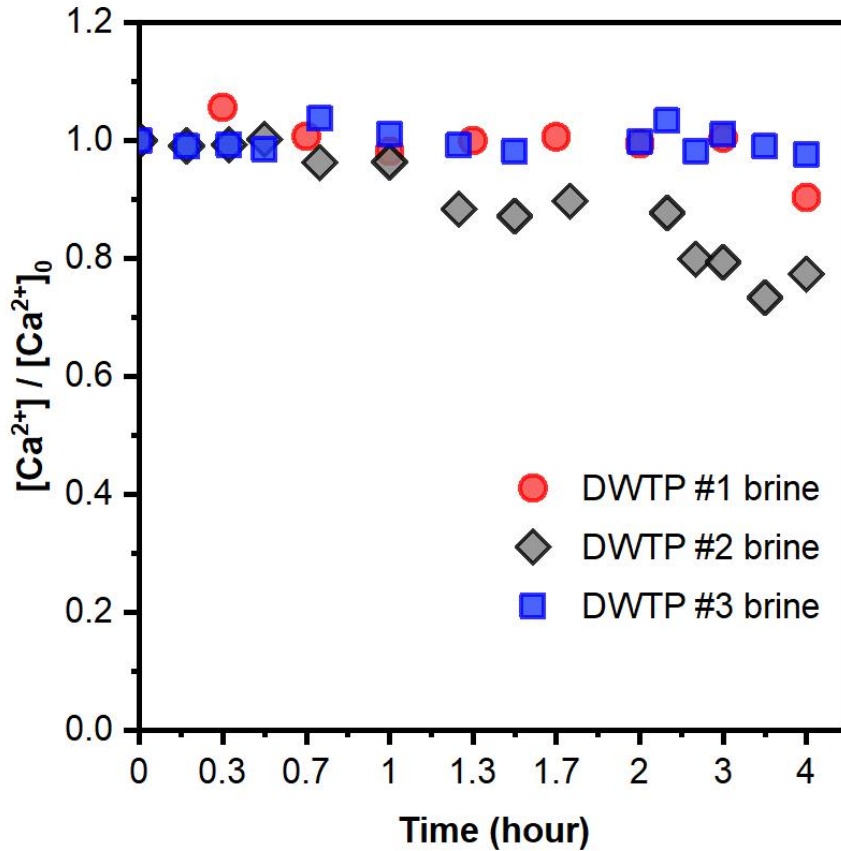


Figure 2-3. Dissolved calcium concentration profile from induction time experiments with brines from three inland desalination treatment plants (DWTPs #1, #2 and #3 at Site S0, Site S6 and Site S3, respectively). Stirring rate = 700 rpm. Only residual primary antiscalants were present in these three brine samples. $[Ca^{2+}]_0$ refers to initial dissolved calcium concentration. $[Ca^{2+}]$ refers to dissolved calcium concentration at designated time point.

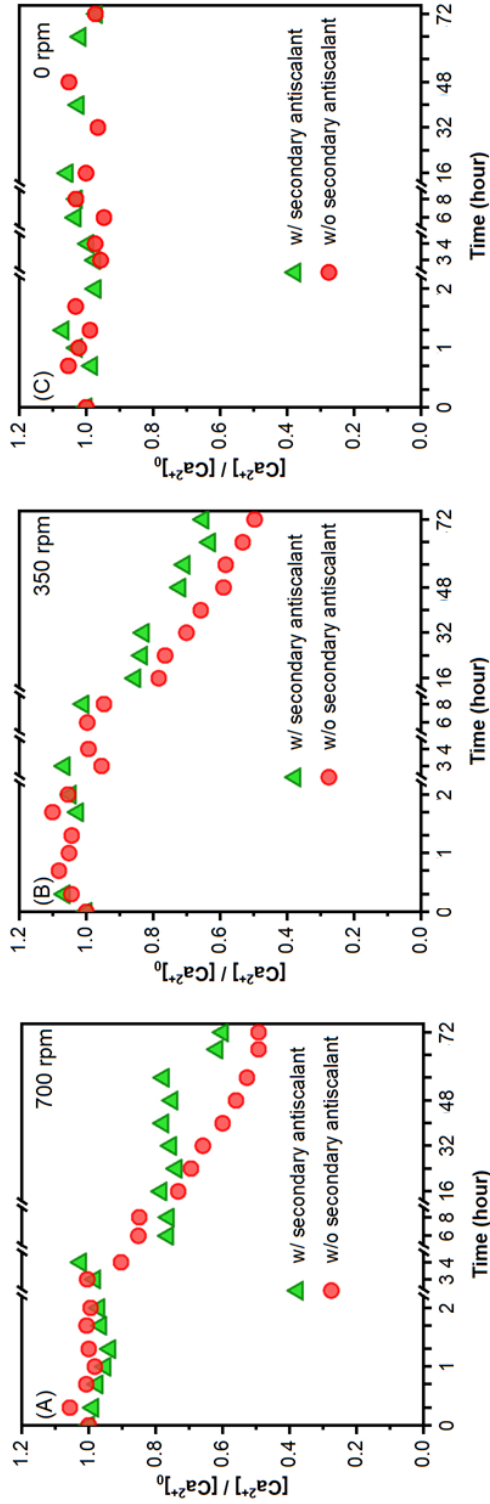


Figure 2-4. Effects of secondary antiscalant on calcium precipitation in oversaturated desalination brine from desalination plant DWTP #1 under different stirring rates in lab simulation experiments. (A) stirring rate = 700 rpm; (B) stirring rate = 350 rpm; (C) stirring rate = 0 rpm. Experiments were conducted under room temperature and all brine samples were acquired at onsite sampling sites. The brine samples all contain primary antiscalant.

Reference

- (1) United Nations Educational, S. and C. O. *The UN World Water Development Report 2015, Water for a Sustainable World*; 2015.
- (2) Sedlak, D. *Water 4.0: The Past, Present, and Future of the World's Most Vital Resource*; Yale University Press: New Haven, MA, 2014.
- (3) Asano, T.; Burdon, F.; Leverenz, H.; Tsuchihashi, R.; Tchobanoglous, G. *Water Reuse: Issues, Technologies and Applications*; McGraw-Hill: New York, NY, 2007.
- (4) Afonso, M. D.; Jaber, J. O.; Mohsen, M. S. Brackish groundwater treatment by reverse osmosis in Jordan. *Desalination* **2004**, *164* (2), 157–171. [https://doi.org/10.1016/S0011-9164\(04\)00175-4](https://doi.org/10.1016/S0011-9164(04)00175-4).
- (5) Pérez-González, A.; Urtiaga, A. M.; Ibáñez, R.; Ortiz, I. State of the art and review on the treatment technologies of water reverse osmosis concentrates. *Water Res.* **2012**, *46* (2), 267–283. <https://doi.org/10.1016/j.watres.2011.10.046>.
- (6) Fritzmann, C.; Löwenberg, J.; Wintgens, T.; Melin, T. State-of-the-art of reverse osmosis desalination. *Desalination* **2007**, *216* (1–3), 1–76. <https://doi.org/10.1016/J.DESAL.2006.12.009>.
- (7) Zhou, Y.; Tol, R. S. J. Evaluating the costs of desalination and water transport. *Water Resour. Res.* **2005**, *41* (3), 1–10. <https://doi.org/10.1029/2004WR003749>.
- (8) Greenlee, L. F.; Lawler, D. F.; Freeman, B. D.; Marrot, B.; Moulin, P. Reverse osmosis desalination: Water sources, technology, and today's challenges. *Water Res.* **2009**, *43* (9), 2317–2348. <https://doi.org/10.1016/J.WATRES.2009.03.010>.
- (9) Badruzzaman, M.; Oppenheimer, J.; Adham, S.; Kumar, M. Innovative beneficial reuse of reverse osmosis concentrate using bipolar membrane electrodialysis and electrochlorination processes. *J. Memb. Sci.* **2009**, *326* (2), 392–399. <https://doi.org/10.1016/j.memsci.2008.10.018>.
- (10) Rahardianto, A.; Gao, J.; Gabelich, C. J.; Williams, M. D.; Cohen, Y. High recovery membrane desalting of low-salinity brackish water: Integration of accelerated precipitation softening with membrane RO. *J. Memb. Sci.* **2007**, *289* (1–2), 123–137. <https://doi.org/10.1016/j.memsci.2006.11.043>.

- (11) Boerlage, S. F. E.; Kennedy, M. D.; Bremere, I.; Witkamp, G. J.; Van Der Hoek, J. P.; Schippers, J. C. The scaling potential of barium sulphate in reverse osmosis systems. *J. Memb. Sci.* **2002**, *197* (1–2), 251–268. [https://doi.org/10.1016/S0376-7388\(01\)00654-8](https://doi.org/10.1016/S0376-7388(01)00654-8).
- (12) Semiat, R.; Sutzkover, I.; Hasson, D. Scaling of RO membranes from silica supersaturated solutions. *Desalination* **2003**, *157* (1–3), 169–191. [https://doi.org/10.1016/S0011-9164\(03\)00398-9](https://doi.org/10.1016/S0011-9164(03)00398-9).
- (13) Greenlee, L. F.; Testa, F.; Lawler, D. F.; Freeman, B. D.; Moulin, P. Effect of antiscalant degradation on salt precipitation and solid/liquid separation of RO concentrate. *J. Memb. Sci.* **2011**, *366* (1–2), 48–61. <https://doi.org/10.1016/j.memsci.2010.09.040>.
- (14) Jain, T.; Sanchez, E.; Owens-Bennett, E.; Trussell, R.; Walker, S.; Liu, H. Impacts of antiscalants on the formation of calcium solids: Implication on scaling potential of desalination concentrate. *Environ. Sci. Water Res. Technol.* **2019**, *5* (7), 1285–1294. <https://doi.org/10.1039/c9ew00351g>.
- (15) Panagopoulos, A.; Haralambous, K. J. Environmental impacts of desalination and brine treatment - Challenges and mitigation measures. *Mar. Pollut. Bull.* **2020**, *161*, 111773. <https://doi.org/10.1016/J.MARPOLBUL.2020.111773>.
- (16) Malmrose, P. ; Lozier, J. ; Mickley, M. ; Reiss, R. ; Committee Report: Current Perspectives on Residuals Management for Desalting Membranes. *Am. Water Work. Assoc. J.* **2004**, *96*, 73–87.
- (17) Semblante, G. U.; Lee, J. Z.; Lee, L. Y.; Ong, S. L.; Ng, H. Y. Brine pre-treatment technologies for zero liquid discharge systems. *Desalination* **2018**, *441* (January), 96–111. <https://doi.org/10.1016/j.desal.2018.04.006>.
- (18) Shih, W. Y.; Rahardianto, A.; Lee, R. W.; Cohen, Y. Morphometric characterization of calcium sulfate dihydrate (gypsum) scale on reverse osmosis membranes. *J. Memb. Sci.* **2005**, *252* (1–2), 253–263. <https://doi.org/10.1016/j.memsci.2004.12.023>.
- (19) Xiao, J. (Alan); and, A. T. K.; Tomson, M. B. Prediction of BaSO₄ Precipitation in the Presence and Absence of a Polymeric Inhibitor: Phosphino-polycarboxylic Acid. *Langmuir* **2001**, *17* (15), 4668–4673. <https://doi.org/10.1021/LA001721E>.
- (20) Öner, M.; Doğan, Ö.; Öner, G. The influence of polyelectrolytes architecture on calcium sulfate dihydrate growth retardation. *J. Cryst. Growth* **1998**, *186* (3), 427–437. [https://doi.org/10.1016/S0022-0248\(97\)00518-6](https://doi.org/10.1016/S0022-0248(97)00518-6).

- (21) Ghafour, E. E. A. Enhancing RO system performance utilizing antiscalants. *Desalination* **2003**, *153* (1–3), 149–153. [https://doi.org/10.1016/S0011-9164\(02\)01117-7](https://doi.org/10.1016/S0011-9164(02)01117-7).
- (22) Amjad, Z. Applications of antiscalants to control calcium sulfate scaling in reverse osmosis systems. *Desalination* **1985**, *54* (C), 263–276. [https://doi.org/10.1016/0011-9164\(85\)80022-9](https://doi.org/10.1016/0011-9164(85)80022-9).
- (23) McCool, B. C.; Rahardianto, A.; Cohen, Y. Antiscalant removal in accelerated desupersaturation of RO concentrate via chemically-enhanced seeded precipitation (CESP). *Water Res.* **2012**, *46* (13), 4261–4271. <https://doi.org/10.1016/j.watres.2012.04.045>.
- (24) Nowack, B. Environmental chemistry of phosphonates. *Water Res.* **2003**, *37* (11), 2533–2546. [https://doi.org/10.1016/S0043-1354\(03\)00079-4](https://doi.org/10.1016/S0043-1354(03)00079-4).
- (25) Greenlee, L. F.; Testa, F.; Lawler, D. F.; Freeman, B. D.; Moulin, P. Effect of antiscalants on precipitation of an RO concentrate: Metals precipitated and particle characteristics for several water compositions. *Water Res.* **2010**, *44* (8), 2672–2684. <https://doi.org/10.1016/j.watres.2010.01.034>.
- (26) Hasson, D.; Drak, A.; Semiat, R. Induction times induced in an RO system by antiscalants delaying CaSO₄ precipitation. *Desalination* **2003**, *157* (1–3), 193–207. [https://doi.org/10.1016/S0011-9164\(03\)00399-0](https://doi.org/10.1016/S0011-9164(03)00399-0).
- (27) Choi, J. Y.; Lee, T.; Cheng, Y.; Cohen, Y. Observed Crystallization Induction Time in Seeded Gypsum Crystallization. *Ind. Eng. Chem. Res.* **2019**, *58* (51), 23359–23365. <https://doi.org/10.1021/acs.iecr.9b06050>.
- (28) Rahman, F. Calcium sulfate precipitation studies with scale inhibitors for reverse osmosis desalination. *Desalination* **2013**, *319*, 79–84. <https://doi.org/10.1016/j.desal.2013.03.027>.
- (29) Kurt Ohlinger, B. N.; Member, S.; Young, T. M.; Member, A.; Schroeder, E. D. Kinetics Effects on Preferential Struvite Accumulation in Wastewater. *J. Environ. Eng.* **1999**, *125*, 730–737.
- (30) BOND, V. P. Inland Empire helps drive California’s economic expansion <https://news.ucr.edu/articles/2019/12/19/inland-empire-helps-drive-californias-economic-expansion>, accessed on 06/30/2021.
- (31) Inland Empire Brine Line - Santa Ana Watershed Project Authority <https://sawpa.org/inland-empire-brine-line/>, accessed on 06/30/2021.

- (32) Owens-Bennett, E. L.; Trussell, B.; Monroy, I. *TECHNICAL MEMORANDUM - Proposed Solids Formation Recovery Formula for the Inland Empire Brine Line*; 2016.
- (33) Gustafsson, J. Visual Minteq 3.1. 2019.
- (34) APHA. *Standard Methods For the Examination of Water and Wastewater*; American Public Health Association: Washington (DC), 1989.
- (35) Greenlee, L. F.; Testa, F.; Lawler, D. F.; Freeman, B. D.; Moulin, P. The effect of antiscalant addition on calcium carbonate precipitation for a simplified synthetic brackish water reverse osmosis concentrate. *Water Res.* **2010**, *44* (9), 2957–2969. <https://doi.org/10.1016/j.watres.2010.02.024>.
- (36) Wang, Z.; Chen, G.; Patton, S.; Ren, C.; Liu, J.; Liu, H. Degradation of nitrilotris-methylenephosphonic acid (NTMP) antiscalant via persulfate photolysis: Implications on desalination concentrate treatment. *Water Res.* **2019**, *159*, 30–37. <https://doi.org/10.1016/j.watres.2019.04.051>.

Chapter 3

Treatment of Brackish Water Inland Desalination Brine via Antiscalant Removal Using Persulfate Photolysis

Previously published in *Environmental Science: Water Research & Technology*

Kum, S., Tang, X., & Liu, H. (2023). Treatment of Brackish Water Inland Desalination Brine via Antiscalant Removal Using Persulfate Photolysis. *Environmental Science: Water Research & Technology*, 9(4), 1137-1146. DOI:10.1039/d2ew00924b.

Abstract

Brine disposal is a challenging issue for brackish water desalination in inland regions. This study developed an ultraviolet-driven persulfate oxidation pre-treatment (UV/PS) followed by a chemical demineralization (CDM) and microfiltration to effectively treat brackish water desalination brine, specifically by degrading antiscalant during UV/PS and precipitating scale-forming calcium from the brine during CDM. To optimize calcium removal kinetics, the effects of persulfate dose and UV irradiation time during UV/PS were investigated and softening by NaOH and lime during CDM were evaluated. UV/PS pre-treatment successfully eliminated the scale inhibition effect of antiscalant, resulting in enhanced chemical demineralization performance. A few minutes of CDM operating time was sufficient to remove more than 85% of total calcium from the brine due to the fast sedimentation of calcium precipitates. Moreover, compared to a control (no pre-treatment), the subsequent microfiltration (MF) membrane fouling potential was reduced by 80%. Overall, the application of the UV/PS-CDM-MF combined process has the potential to remove more than 90% of calcium from the brackish desalination brine, and consequently recover a significant amount of fresh water (>90%) from the brine. Results from this study point to UV/PS-CDM process as a promising brine treatment technology to remove scale-forming precursors and improve water recovery.

Introduction

Freshwater scarcity has become a worldwide challenging issue.¹⁻³ To overcome freshwater scarcity in inland and semi-arid areas, including the Middle East, Southern California and Texas, reverse osmosis (RO) membrane desalination of brackish groundwater that contains total dissolved solids (TDS) ranging from 1 to 10 g/L is employed to generate freshwater.⁴⁻⁶ Water recovery of brackish water RO desalination is typically between 40% and 85%, depending on TDS and chemical composition of the feed water.⁷⁻¹⁰ Therefore, 15% to 60% of the feedwater becomes the RO concentrate waste, known as brine. However, the management of a RO concentrate stream remains challenging due to the high costs and adverse environmental impacts, especially in inland regions.¹¹⁻¹³ Current management options for inland desalination plants include ocean or surface water discharge through a brine line, deep well injection, evaporation pond, and landfill solidification.¹⁴⁻¹⁷ However, the cost of existing brine management can add up to more than 30% of the overall treatment cost,^{18,19} and direct disposal can have negative environmental impacts by increasing salinity and inducing secondary pollution.²⁰⁻²² In order to minimize the inland brine management cost and negative environmental effects, additional water recovery from brine is needed. The improvement of water recovery can be achieved by passing the primary brine through a secondary RO process.^{23,24} However, the major limitation to achieving high water recovery from the brine is mineral scaling by sparingly soluble salts (*e.g.*, calcite and gypsum) on the membrane surface.^{25,26} Therefore, an adequate brine treatment prior to the further

membrane process is necessary to reduce mineral scaling during the secondary RO process.

The major target constituents of brine pre-treatment are antiscalant and scale-forming precursors.^{17,27-29} Antiscalant is a vital chemical due to its scale inhibition effect, which improves the water recovery of the RO system; therefore, the type of antiscalant applied to the RO system has a significant impact on the operating and maintenance costs in the desalination plants.³⁰ Choosing the appropriate type of antiscalants depends on the feedwater composition.³¹ Among various types of antiscalants, phosphonate-based antiscalants are most commonly added to the feed water.³²⁻³⁴ Although antiscalants help prevent precipitation and increase water recovery at the main RO desalination stage, the presence of antiscalants in the brine hinder the removal of target scale-forming precursors at the brine treatment process;³⁵ therefore, the removal of antiscalant can benefit brine treatment. Several antiscalant separation techniques, including use of coagulant or surfactant, ion exchange, adsorption, nanofiltration, and chemically-enhanced seeded precipitation have been proposed.^{29,36-42} Additional chemical residuals may cause membrane fouling at the secondary RO process.^{43,44} Ion exchange and adsorption still need to be improved for the process sustainability, and antiscalant residual may still present after treatment.

Antiscalant degradation by advanced oxidation processes (AOPs) is a promising approach to remove phosphonate-based antiscalant compounds.^{28,45-47} The benefit of AOPs is the decomposition of antiscalants in brine to simple organic compounds.

Consequently, both scale inhibition effects during the demineralization process and the

possibility of membrane fouling by excessive antiscalant in the RO process can be reduced. Among various AOPs, an ultraviolet-driven persulfate oxidation process (UV/PS) has the potential to remove antiscalants effectively.⁴⁶ UV photolysis of persulfate ($S_2O_8^{2-}$) generates sulfate radical ($SO_4^{\cdot-}$), and it is a strong oxidant with similar oxidizing power ($E^0 = 2.5 - 3.1$ V) to HO^{\cdot} ($E^0 = 1.9 - 2.7$ V). $SO_4^{\cdot-}$ is also more selective toward organic contaminants.⁴⁸ However, little research has been performed on the application of UV/PS on brine treatment.

After antiscalant degradation, the removal of scale-forming precursors in brine can be achieved by demineralization processes. Among various demineralization techniques, chemical demineralization (CDM) is effective in the removal of scale-forming precursors.⁴⁹⁻⁵¹ Alkaline chemicals, *e.g.*, CaO, $Ca(OH)_2$, NaOH, $NaHCO_3$, Na_2CO_3 are often used to remove major scale forming precursors including Ca^{2+} , Ba^{2+} , Mg^{2+} , and SiO_2 .⁵¹⁻⁵⁴ NaOH softening and lime softening using CaO, $Ca(OH)_2$, $NaHCO_3$ or Na_2CO_3 would be beneficial, because these methods only require simple chemical addition; as a result, it allows for the recovery of relatively pure minerals from the sludge of the CDM process. Nonetheless, the kinetics and mechanisms of CDM after antiscalant degradation via UV/PS remain unknown, and the impact of UV/PS and CDM processes on system water recovery needs to be answered.

The objectives of this research were to: (1) evaluate the applicability of the UV/PS coupled with CDM to degrade antiscalant and remove scale-forming precursors from brackish water desalination brine; (2) determine operating conditions of the UV/PS process (*i.e.*, persulfate dose and UV irradiation time) to degrade antiscalant in the feed

water; (3) identify the kinetics and mechanisms of calcium precipitation and calcium removal efficiency by NaOH softening and lime softening methods in the presence and absence of UV/PS pre-treatment at the CDM process; (4) investigate the solid/liquid separation performance of the MF process after CDM in the absence and presence of the UV/PS process, and (5) assess the water recovery potential at RO after UV/PS-CDM process. The performance of the UV/PS-CDM process was evaluated based on a few technical evaluation metrics, including the settling rate of mineral precipitates at the CDM process, product water quality, and the extent of MF membrane fouling.

Materials and Methods

Chemicals and Solutions

Stock solutions and synthetic brine feed water were prepared using Milli-Q water. All chemicals are reagent grade or higher and obtained from JT Baker, Sigma-Aldrich, or Fisher Scientific. Synthetic brine solutions were prepared to simulate the chemical composition of inland brackish groundwater RO concentrate at the Inland Empire Brine Line in Riverside, California, USA.⁵⁵ The brine water quality, based on the actual brine quality from Arlington Desalter (DWTP #1, discussed in Chapter 2), is detailed in Table 1. The use of synthetic feed water allowed a fundamental investigation of the calcium carbonate precipitation, which is a major supersaturated solid in inland desalination brines.^{41,56} Diethylenetriamine pentamethylene phosphonic acid (DTPMP) was chosen as a representative phosphonate-based antiscalant to prepare the synthetic brine, because DTPMP is a widely used antiscalant in membrane treatment and exhibits a strong scaling inhibition effect.^{33,35} The chemical structure of DTPMP is shown in Fig. S1.

Experimental Setup

The brine treatment process consisted of a UV/PS pre-treatment to degrade antiscalant, a CDM step to remove scaling components, and a microfiltration (MF) step to separate scaling minerals from the treated brine (Fig. 1). For UV/PS experiments, a 4-L beaker UV reactor equipped with a 450-W medium pressure UV immersion lamp (Ace Glass, Inc.) was utilized (Fig. S2A). To start an experiment, a 3.5-L synthetic brine solution containing 2-5 mM persulfate and 0.1 mM DTPMP (equivalent to 15.5 mg/L as organic phosphorus) was exposed to UV irradiation that last up to 60 minutes. The initial and final pH of the brine solutions was 7.8 and 6.7, respectively. The chosen concentration of DTPMP was at the higher end of typical phosphonate-based antiscalant concentration observed in RO brine.^{39,57} During UV/PS experimentation, 3-mL samples were withdrawn by pipette from the experimental reservoirs at each targeted reaction time interval. Additional details on the UV/PS experiment can be found in Text S1 of the Supporting Information.

Following the UV/PS experiment, 1L of the UV/PS treated brine underwent a CDM process in a 2-L stirred rectangular batch reactor (Fig. S2B). For the UV/PS pre-treatment prior to the CDM process, 4 mM persulfate and 5, 10, or 20 minutes of UV irradiation time were employed. In addition, two control CDM experiments were conducted using a synthetic brine without UV/PS pre-treatment (control – no UV/PS pre-treatment), and a synthetic brine in the absence of antiscalant without UV/PS pre-treatment (control – no antiscalant). Two chemical demineralization methods were evaluated for the CDM process, *i.e.*, NaOH softening and lime softening. For the NaOH

softening method, a targeted amount of NaOH was added to adjust the pH of the UV/PS-treated brine to either 7.8, 9.0 or 10.2 with prior to CDM process. pH 7.8 is synthetic RO brine feedwater pH (Table 1), pH 10.2 is where the plateau of the calcium carbonate saturation index in the brine started (Fig. S3), and pH 9 is the middle point of those two pHs. For the lime softening method, a requisite amount of $\text{Ca}(\text{OH})_2$ and NaHCO_3 in combination was added to the UV/PS-treated brine. Immediately after chemical addition, the brine was rapid-mixed at 700 rpm for 1 minute to allow chemical mixing, followed by 29 minutes of sedimentation (*i.e.*, a total of 30 mins of CDM process). At targeted time intervals during the CDM process, 3-mL samples were withdrawn from the batch reactor at 3 cm below the water-air interface using a pipette, which minimized the stirring impact on the reactor (Fig. S2B). All samples were immediately acidified with 100 μL of concentrated HNO_3 and preserved for total calcium analysis.

Following the CDM process, a MF step was conducted to evaluate the impact of the UV/PS-CDM treatment on the solid/liquid separation process from the treated brine. Specifically, the CDM treated brine further underwent a dead-end microfiltration (MF) process to separate residual particles in the supernatant.⁵⁸⁻⁶¹ Based on the CDM process results, the solid/liquid separation was performed 3 minutes of the lime softening CDM process and 5 minutes after the start point of NaOH softening CDM process with different UV/PS pre-treated brines. The experimental setup consisted of 0.1- μm polyvinylidene fluoride membrane (Millipore Sigma, Burlington, MA), pressurizing equipment (nitrogen gas tank, pressure gauge, and pressure control valve), a 200 mL stirred cell (Millipore Sigma, Burlington, MA), and a permeate collection line (Fig.S4

and Text S2). The permeate flux was measured continuously by a digital mass balance. Membrane permeate flux and relative permeate flux were calculated using Equations 1-2, respectively:

$$J = \frac{M}{At} \quad (\text{E1})$$

$$\text{Relative permeate flux} = \frac{J}{J_0} \quad (\text{E2})$$

Where J is the permeate flux ($\text{g cm}^{-2} \text{sec}^{-1}$), M is total mass of permeate (g), A is membrane area (cm^2), t is experimental time (sec), and J_0 is initial permeate flux ($\text{g cm}^{-2} \text{sec}^{-1}$).

Analytical Methods for Water Samples

During the UV/PS pre-treatment, the concentration of persulfate in the brine was determined by a colorimetric method using potassium iodide.⁶² The concentration of DTPMP in the brine was calculated by measuring orthophosphate concentration using Standard method 4500-P E,⁶³ since orthophosphate is the final phosphorus oxidation product.^{46,58} During the CDM experimental step, the solid precipitation and sedimentation were monitored by measuring the change of total calcium concentration at pre-determined time intervals. The concentrations of total calcium and sodium in the initial synthetic brine and sampled product solutions were determined using an Inductively Coupled Plasma Mass Spectroscopy (ICP-MS, Agilent Technologies, Palo Alto, CA). Alkalinity was measured by titration based on standard method 2320B and the concentration of chloride was determined following Standard Methods 4110B by ion chromatography (Dionex ICS-1100, Thermo Scientific, Sunnyvale, CA).⁶³

Results and Discussion

Antiscalant DTPMP Degradation by UV/persulfate

DTPMP was successfully degraded in synthetic brine as the brine was irradiated in the UV/persulfate system (Fig. 2A). The degradation of DTPMP followed a *pseudo* first-order kinetics model (all $R^2 > 0.95$). The observed *pseudo* first-order rates of DTPMP degradation increased from 5.9×10^{-2} to $9.6 \times 10^{-2} \text{ min}^{-1}$ as the persulfate dosage increased from 2 to 5 mM (Fig. 2B). Persulfate photolysis generates $\text{SO}_4^{\bullet-}$ (Reaction 1), which further hydrolyzes to HO^\bullet (Reaction 2; $k_2 = 6.5 \times 10^7 \text{ M}^{-1}\text{s}^{-1}$):^{64,65}



A persulfate dosage equal or higher than 4 mM completely degraded DTPMP in 30 minutes UV irradiation time; however, a persulfate dosage less than 4 mM were not enough to completely degrade 0.1 mM DTPMP (Fig. 2A), due to an insufficient generation of reactive radicals via persulfate photolysis (R1 - R2).

$\text{SO}_4^{\bullet-}$ and HO^\bullet can be scavenged by persulfate (Reactions 3-4; $k_3 = 5.5 \times 10^5 \text{ M}^{-1}\text{s}^{-1}$; $k_4 = 1.4 \times 10^7 \text{ M}^{-1}\text{s}^{-1}$), respectively,^{46,66} and generate non-reactive persulfate radical $\text{S}_2\text{O}_8^{\bullet-}$:^{67,68}



This scavenging impeded the degradation of DTPMP with increasing persulfate dosage; therefore, the rate constant of DTPMP degradation increased at a slower pace as the persulfate dosage increased beyond 4 mM (Fig. 2B). Because more than 90% of DTPMP

was degraded after 20 minutes of persulfate photolysis with 4 mM persulfate dosage (Fig. 2B), 4 mM dosage of persulfate was chosen for subsequent UV/PS-CDM experiments.

Chemical Demineralization by NaOH Softening

Calcium carbonate is a major precipitate from the brine, and the precipitation of calcium carbonate is dictated by pH of the solution as a result of carbonate speciation.⁶⁹ The saturation index (SI, the logarithm value of the saturation state) of calcium carbonate of the brine was approximately 1.8 (Fig. S3), indicating precipitation is thermodynamically favorable (SI > 0). When NaOH is added to the brine to increase pH, chemical demineralization occurs via calcium carbonate precipitation (Reactions 5-7):



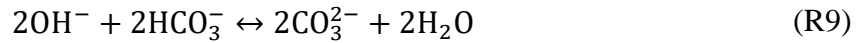
Therefore, the saturation index of calcium carbonate mineral increases as pH increases (Fig. S3). Experimental data showed that total calcium residual in the brine exhibited the biggest decrease when the brine pH was adjusted to 10.2 during the CDM process (Fig. 3A). When the brine pH increased from pH 7.8 to pH 10.2, the dominant carbonate species switches from HCO_3^- to CO_3^{2-} and promoted calcium precipitation (R5 - R7). In comparison with the control without UV/PS pre-treatment, the UV/PS pre-treatment was shortening the settling time of calcium precipitates during the CDM process and achieved the lowest final calcium concentration (Fig. 3B). In addition, the total calcium removal from the UV/PS pre-treated brine during the CDM process exhibited similar reaction kinetics in comparison to the CDM control without antiscalant (Fig. 3B). These

trends strongly suggested that the degradation of DTPMP during the UV/PS pre-treatment promoted calcium removal during the CDM process. The presence of DTPMP has a detrimental effect on the calcium removal and delayed the sedimentation of calcium precipitates during the CDM (Control without UV/PS pre-treatment in Fig. 3A).

Antiscalants interfere with the complete particle growth by adsorbing onto nucleating crystals and blocking the crystal growth sites.^{70,71}

Chemical Demineralization by Lime Softening

Chemical demineralization via lime softening introduces additional calcium in the form of hydrated lime Ca(OH)_2 into the system and induces calcium carbonate precipitation (Reactions 8-10):



Since additional calcium was added for demineralization, total calcium concentration increased initially during the first one minute and then decreased as reactions took place (Fig. 4). During the lime softening CDM process, total calcium concentration in the UV/PS pre-treated brine exhibited the fastest removal in comparison to controls (Fig. 4). The settling of calcium precipitates mostly took place during the first 3 minutes of the CDM process. In contrast, no calcium removal was achieved after 15 minutes of CDM process in the two control experiments.

In addition, as DTPMP was degraded to orthophosphate during the UV/PS pre-treatment, the formation of orthophosphate accelerated total calcium removal during the CDM

process. In a separate control experiment by adding orthophosphate to the brine prior to the CDM process, the effects of orthophosphate addition on the kinetics of total calcium removal were similar to UV/PS pre-treatment. This behavior was observed for both NaOH softening (Fig. S5A) and lime softening (Fig. S5B). The formation of orthophosphate resulted in the supersaturation and precipitation of hydroxyapatite $\text{Ca}_5(\text{PO}_4)_3\text{OH}_{(s)}$ in the brine (saturation index > 14.4), which could accelerate the nucleation and precipitation of calcium solids. Therefore, the UV/PS pre-treatment both removed the inhibitive effect of DTPMP on calcium precipitation and accelerated additional calcium phosphate mineral nucleation, both of which contributed to the total calcium removal during the CDM process.

The effect of varying UV irradiation time during the UV/PS pre-treatment on total calcium removal via the CDM process was also investigated. Results showed that an increase in the UV irradiation time led to better total calcium removal during the NaOH softening CDM process (Fig. 5A). For the lime softening CDM process, notably a faster settling was achieved with UV/PS pre-treatment regardless of the UV irradiation time (Fig. 5B), indicating that a partial degradation of DTPMP also accelerated the demineralization process.

Microfiltration Performance Following Chemical Demineralization

The CDM-treated brine further underwent an MF process and the effect of UV/PS pre-treatment on the MF performance was evaluated. Results showed that the MF permeate flux maintained at a high level and exhibited little decline when the brine was pre-treated with the UV/PS as the first step (Fig. 6). This trend suggested that the UV/PS pre-

treatment significantly alleviated particle scaling on the MF membrane surface. Because the UV/PS pre-treated brine exhibited a fast settling of calcium solids and a majority of the solids were removed during the first 5 minutes of the CDM process, the combined UV/PS-CDM treated brine feeding into the MF step had minimal suspended solids. Consequently, the MF permeate fluxes showed a minimal decline. In contrast, the brine without UV/PS pre-treatment exhibited a severe flux decline (50% -80% decrease) during the MF separation (Fig. 6). Without antiscalant degradation by the UV/PS pre-treatment, a significant amount of precipitates remained after the CDM process in the solution due to slow settling rate, which induced fouling on the MF membrane by precipitates and promotes a denser fouling cake.³⁵ The less fouling on the MF membrane indicates that increase in product water yield, less frequent membrane backwashing and replacement, and reduced MF operation cost.

Engineering Implications on Freshwater Recovery

The application of the UV/PS pre-treatment followed by a CDM process improves the permeate flux during the MF step due to a low calcium concentration in the MF permeate (Table S1). The MF permeate can further undergo an additional RO step to recover freshwater from the sequential UV/PS-CDM-MF treated brine. The extent of water recovery via this additional RO step is limited by calcite mineral scaling on the RO membrane, which can be predicted based on the theoretical calculations on the saturation index (SI) of calcite in the UV/PS-CDM-MF treated brine (*i.e.*, RO feed brine). Details on the SI calculations are provided in Text S3 and Table S1. Calcite is oversaturated in the untreated brackish desalination brine and its oversaturation leads to membrane scaling

during the RO step and limits water recovery. Specifically, water recovery can be continuously achieved via the additional RO system in the absence of antiscalant when the calcite SI of the feed brine is below zero, *i.e.*, the sequential UV/PS-CDM-MF treated brine is undersaturated with respect to calcite. Furthermore, additional antiscalant can be added to the UV/PS-CDM-MF treated brine to alleviate calcite scaling. For a conservative RO system design, the upper operating limit of calcite SI is recommended to be 1.8 for the RO feed water with phosphonate-based antiscalants to avoid extreme operating conditions or system failure.⁷²

Calculations show that the calcite SI of the untreated brine (control without treatment), UV/PS-CDM-MF treated brine (via lime softening during the CDM process) and UV/PS-CDM-MF treated brine (via NaOH softening during the CDM process) was 1.8, 0.3 and -0.2, respectively (Fig. 7). This suggests that the untreated brine is an unfavorable condition for additional water recovery. When an antiscalant is added during the additional RO step to recover freshwater from the treated brine, the NaOH softening based UV/PS-CDM-MF treatment train can achieve more than 90% freshwater recovery until the SI limit (*i.e.*, a value of 1.8) of antiscalant inhibition is reached (Fig. 7). Similarly, the lime softening based UV/PS-CDM-MF treatment train can achieve more than 85% freshwater recovery until the SI limit is reached (Fig. 7).

Conclusions

The performance of the sequential UV/PS-CDM-MF treatment train process was evaluated and compared to control experiments. The results show that the UV/PS-CDM-MF in combination is a promising inland desalination brine treatment technology to

remove oversaturated calcium and increase the freshwater recovery potential via an additional RO step. UV/persulfate process effectively degraded phosphonate-based antiscalant. In addition, the CDM process after UV/PS pre-treatment achieved faster settling rate of calcium precipitates due to antiscalant degradation by the UV/PS pre-treatment. Both NaOH- and lime-softening based CDM methods prevent flux decline during the subsequent microfiltration step and extend the duration of operation during the calcium solid/treated brine separation process. The application of the UV/PS-CDM-MF treatment train process has the potential to remove more than 90% calcium from inland desalination brine. As a result, a very high-water recovery (>90%) by an additional RO process is expected. Future work will evaluate the applicability of the UV/PS-CDM-MF-RO treatment train for freshwater recovery and hardness mineral recoveries from inland desalination brine.

Supporting information

Please refer to Appendix B for Supporting Information.

Table 3-1. Chemical composition of brackish water desalination brine solutions.

Parameter	Synthetic Brine water quality in this study	Brine water quality of Inland Empire Brine Line	Unit
Total Dissolved Solids	5900	5100	mg/L
Calcium	660	660	mg/L
Sodium	1260	800	mg/L
Bicarbonate	1300	1300	mg/L
Chloride	2200	2200	mg/L
Antiscalant	15.5	1	mg P/L
pH	7.8	7.8	--
Ionic strength	98*	98	mM
Calcite Saturation Index	1.8	1.8	--
Temperature	23	23	°C

*NaClO₄ was added to the synthetic brine to reach the targeted ionic strength value.

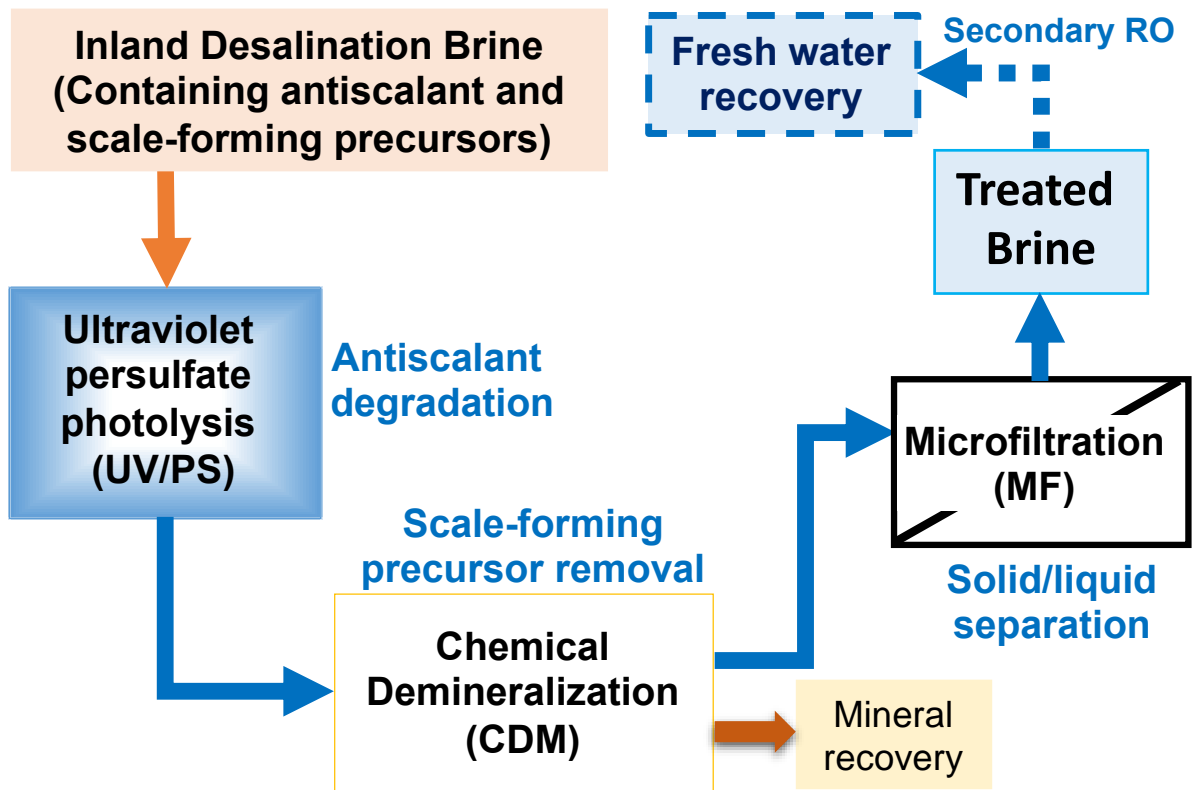


Figure 3-1. A schematic of the UV/PS-CDM-MF brine pre-treatment developed in this study.

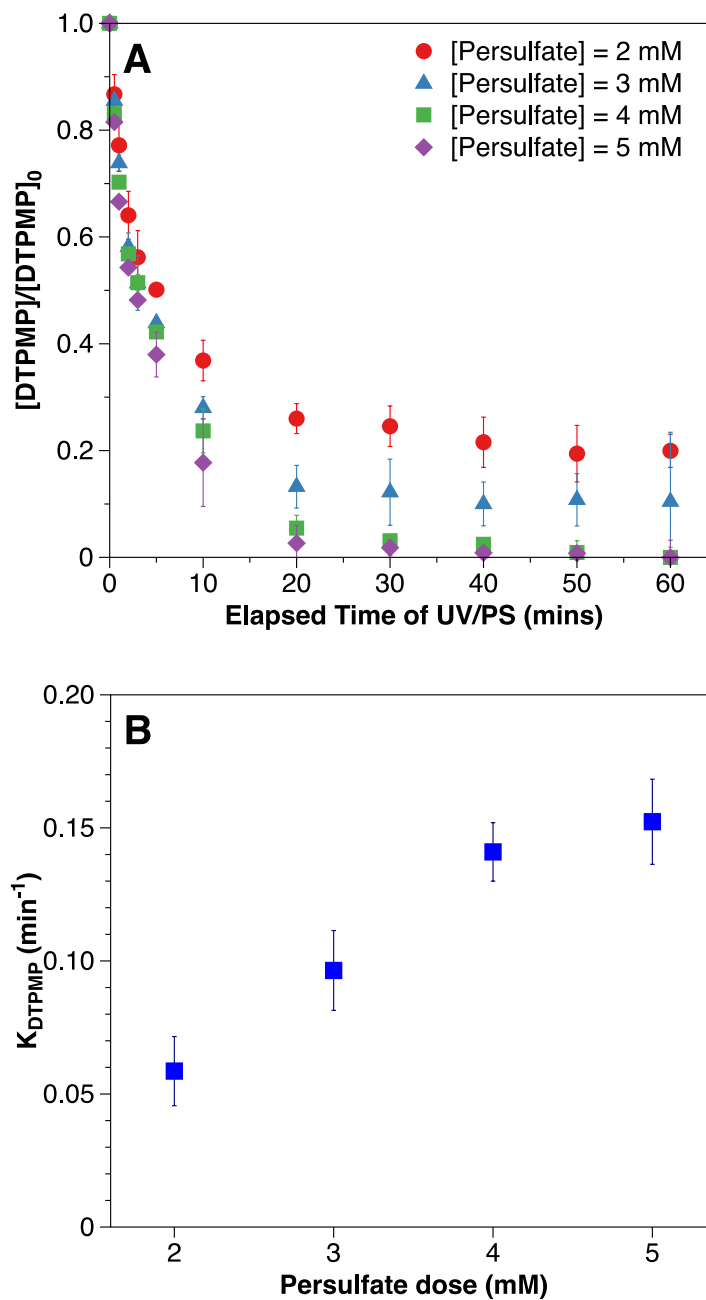


Figure 3-2. Contribution of persulfate dose to DTPMP degradation (A) effect of UV/persulfate on DTPMP degradation and (B) observed pseudo first-order rates of DTPMP degradation. Experimental condition: Synthetic brine, [Ionic strength] = 98 mM; [DTPMP]₀ = 0.1 mM; [Persulfate]₀ = 2.0 - 5.0 mM; initial pH = 7.8; Error bars represent the range of values for triplicate tests.

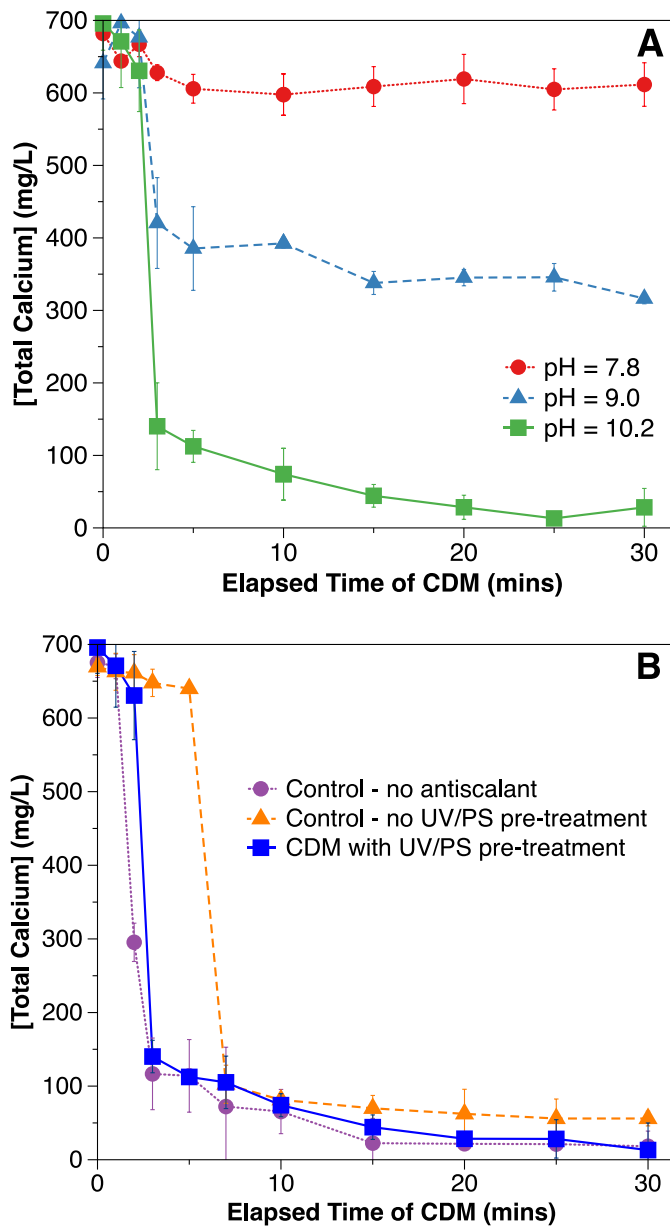


Figure 3-3. Total calcium concentration of CDM process by NaOH softening with 5 M NaOH. (A) the CDM process with UV/PS pre-treatment at pH 7.8, pH 9, and pH 10.2; (B) The CDM process for controls and CDM process with UV/PS pre-treatment at pH 10.2. Note: after chemical addition (time zero), each solution was rapid-mixed at 700 rpm for 1 minute to allow chemical mixing and precipitation to occur and then sit for 29 mins for sedimentation (that is, a total elapsed time of 30 mins); Error bars represent the range of values for triplicate tests.

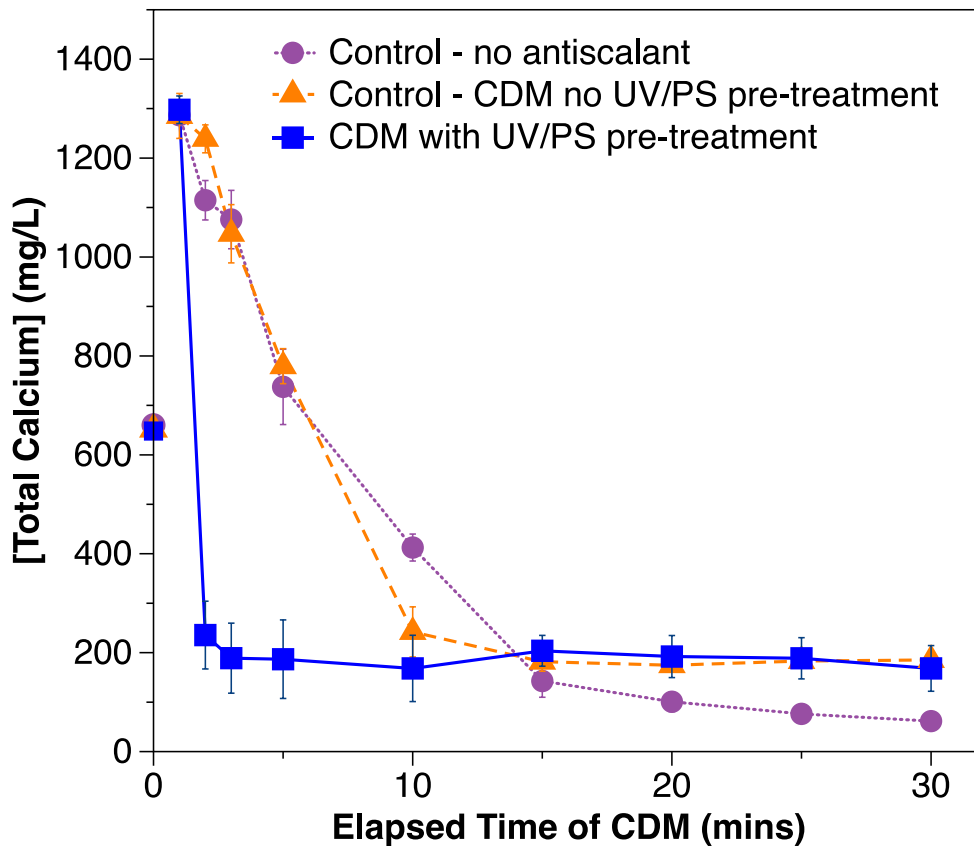


Figure 3-4. Total calcium concentration of the CDM process by lime softening (16.5 mM of $\text{Ca}(\text{OH})_2$ and 11.7 mM of NaHCO_3). Note: after chemical addition (time zero), each solution was rapid-mixed at 700 rpm for 1 minute to allow chemical mixing and precipitation to occur and then sit for 29 mins for sedimentation (that is, a total elapsed time of 30 mins); Error bars represent the range of values for triplicate tests.

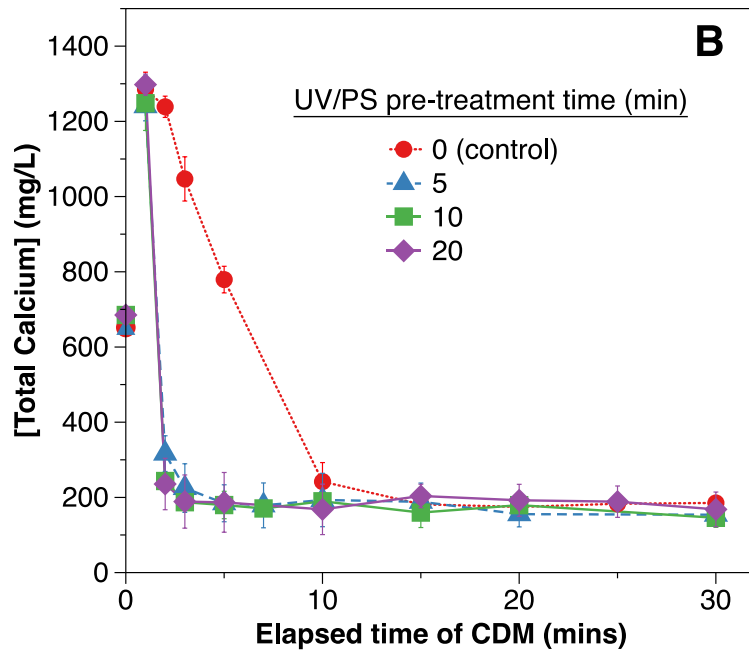
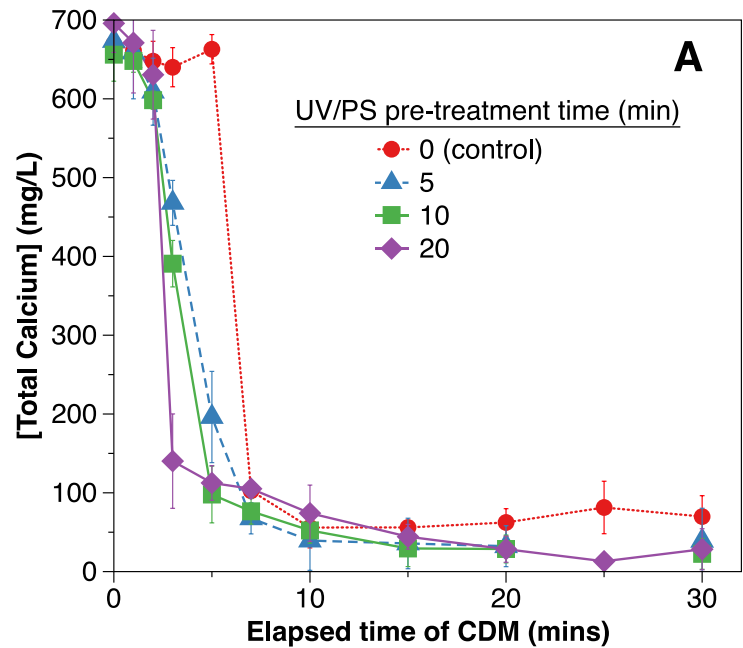


Figure 3-5. Total calcium concentration change during the CDM process after 0, 5, 10, and 20 minutes UV/PS pre-treatment, (A) NaOH softening at pH 10.2; (B) lime softening (16.5 mM of $\text{Ca}(\text{OH})_2$ and 11.7 mM of NaHCO_3). Note: after chemical addition (time zero), each solution was rapid-mixed at 700 rpm for 1 minute to allow chemical mixing and precipitation to occur and then sit for 29 mins for sedimentation (Total 30 mins); Error bars represent the range of values for triplicate tests.

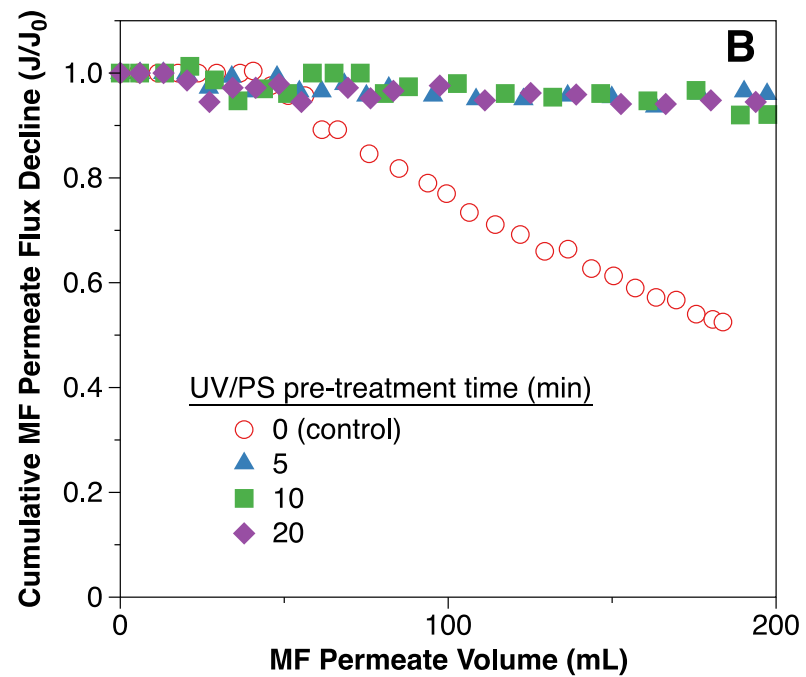
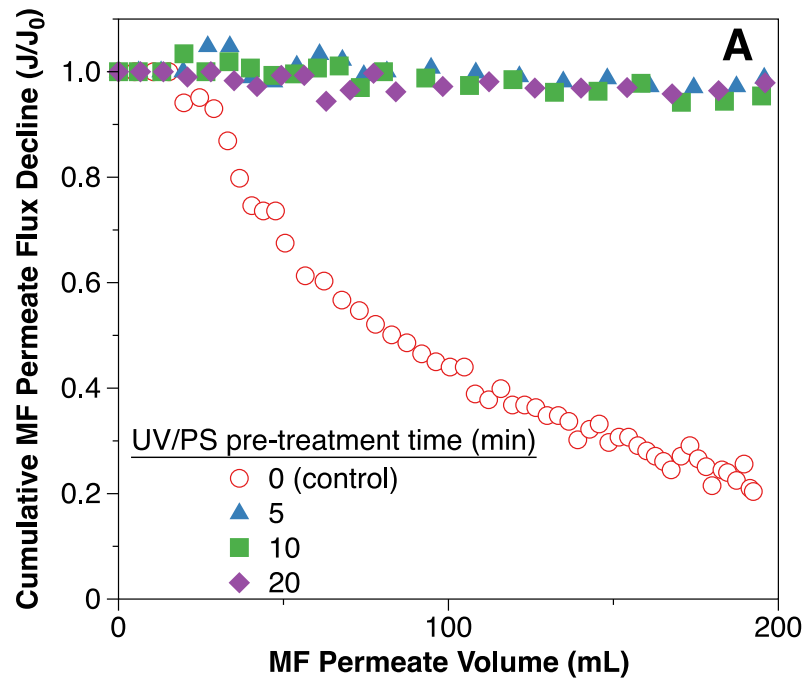


Figure 3-6. Normalized permeate flux decline as a function of cumulative normalized volume throughput in the solutions of (A) NaOH softening (5 M NaOH, pH 10.2) and (B) lime softening demineralization without and with UV/PS pre-treatment.

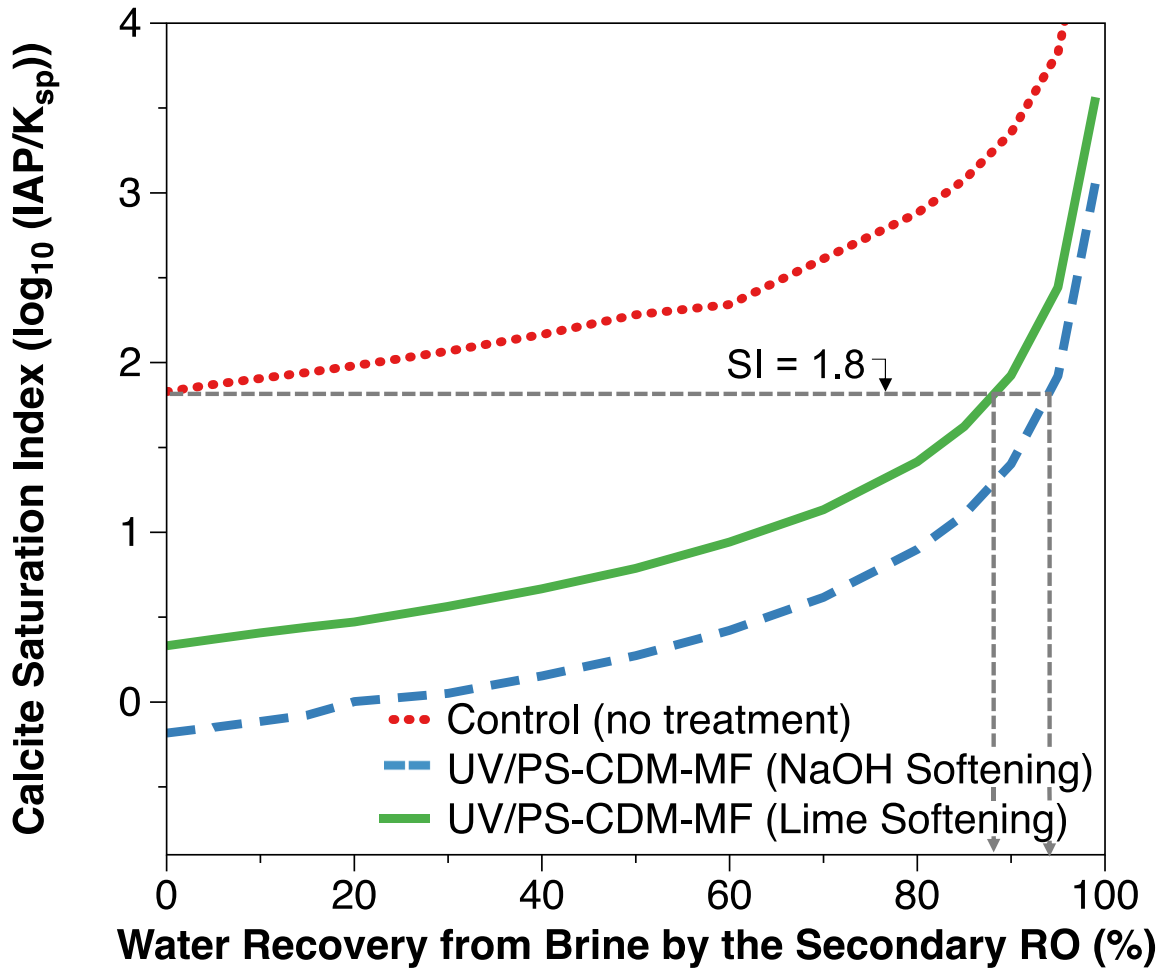


Figure 3-7. Calcite saturation index calculations for calcite in the treated brine after UV/PS-CDM (NaOH softening) and UV/PS-CDM (lime softening). Control stands for no UV/PS-CDM treatment (direct use of brine). Saturation index calculations were performed through Visual Minteq (Version 3.1) for a pH of 7.8 with 100% salts rejection rate at the additional RO process, and input water quality parameters are in Table S1. Note: the ordinate is a saturation index, and it is a logarithmic number.

References

- (1) Mekonnen, M. M.; Hoekstra, A. Y. Sustainability: Four Billion People Facing Severe Water Scarcity. *Science Advances* **2016**, *2* (2), 1–7. <https://doi.org/10.1126/sciadv.1500323>.
- (2) Schwabe, K.; Nemati, M.; Landry, C.; Zimmerman, G. Water Markets in the Western United States: Trends and Opportunities. *Water (Switzerland)* **2020**, *12* (1), 1–15. <https://doi.org/10.3390/w12010233>.
- (3) Yoon, J. H.; Wang, S. Y. S.; Gillies, R. R.; Kravitz, B.; Hipps, L.; Rasch, P. J. Increasing Water Cycle Extremes in California and in Relation to ENSO Cycle under Global Warming. *Nature Communications* **2015**, *6*. <https://doi.org/10.1038/ncomms9657>.
- (4) Khanzada, N. K.; Khan, S. J.; Davies, P. A. Performance Evaluation of Reverse Osmosis (RO) Pre-Treatment Technologies for in-Land Brackish Water Treatment. *Desalination* **2017**, *406*, 44–50. <https://doi.org/10.1016/j.desal.2016.06.030>.
- (5) Greenlee, L. F.; Lawler, D. F.; Freeman, B. D.; Marrot, B.; Moulin, P. Reverse Osmosis Desalination: Water Sources, Technology, and Today's Challenges. *Water Res* **2009**, *43* (9), 2317–2348. <https://doi.org/10.1016/j.watres.2009.03.010>.
- (6) Landsman, M. R.; Sujanani, R.; Brodfuehrer, S. H.; Cooper, C. M.; Darr, A. G.; Davis, R. J.; Kim, K.; Kum, S.; Nalley, L. K.; Nomaan, S. M.; Oden, C. P.; Paspureddi, A.; Reimund, K. K.; III, L. S. R.; Yeo, S.; Lawler, D. F.; Freeman, B. D.; Katz, L. E. Water Treatment: Are Membranes the Panacea? *Annual Review in Chemical and Biomolecular Engineering* **2020**, *11*, 559–585. <https://doi.org/https://doi.org/10.1146/annurev-chembioeng-111919-091940>.
- (7) McCool, B. C.; Rahardianto, A.; Faria, J. I.; Cohen, Y. Evaluation of Chemically-Enhanced Seeded Precipitation of RO Concentrate for High Recovery Desalting of High Salinity Brackish Water. *Desalination* **2013**, *317*, 116–126. <https://doi.org/10.1016/j.desal.2013.01.010>.
- (8) Mickley, M. *Updated and Extended Survey of U.S. Municipal Desalination Plants*; 2018.
- (9) Almulla, A.; Eid, M.; Côté, P.; Coburn, J. Developments in High Recovery Brackish Water Desalination Plants as Part of the Solution Yp Water Quantity Problems. *Desalination* **2003**, *153* (1–3), 237–243. [https://doi.org/10.1016/S0011-9164\(02\)01142-6](https://doi.org/10.1016/S0011-9164(02)01142-6).

- (10) Malmrose, P.; Lozier, J.; Mickley, M.; Reiss, R.; Russell, J.; Schaefer, J.; Sethi, S.; Manuszak, J.; Bergman, R.; Atasi, K. Z. Committee Report: Current Perspectives on Residuals Management for Desalting Membranes. *J Am Water Works Assoc* **2004**, *96* (12). <https://doi.org/10.1002/j.1551-8833.2004.tb10760.x>.
- (11) National Research Council. *Desalination: A National Perspective*; National Academies Press: Washington, DC, 2008. <https://doi.org/10.17226/12184>.
- (12) Morillo, J.; Usero, J.; Rosado, D.; El Bakouri, H.; Riaza, A.; Bernaola, F. J. Comparative Study of Brine Management Technologies for Desalination Plants. *Desalination* **2014**, *336* (1), 32–49. <https://doi.org/10.1016/j.desal.2013.12.038>.
- (13) Bond, P.; Veerapaneni, S. Zeroing in on ZLD Technologies for Inland Desalination. *Journal (American Water Works Association)* **2008**, *100* (9), 76–89. <https://doi.org/10.1002/j.1551-8833.2008.tb09722.x>.
- (14) Ahmed, M.; Shayya, W. H.; Hoey, D.; Al-Handaly, J. Brine Disposal from Inland Desalination Plants. *Water International* **2002**, *27* (2), 194–201. <https://doi.org/10.1080/02508060208686992>.
- (15) Jensen, V. B.; Darby, J. L. Brine Disposal Options for Small Systems in California’s Central Valley. *J Am Water Works Assoc* **2016**, *108* (5), 276–289. <https://doi.org/10.5942/jawwa.2016.108.0045>.
- (16) U.S. Department of the Interior Bureau of Reclamation. *Brine-Concentrate Treatment and Disposal Options Report*; 2009.
- (17) Tang, X.; Kum, S.; Liu, H. Inland Desalination Brine Disposal : A Baseline Study from Southern California on Brine Transport Infrastructure and Treatment Potential. *ACS ES&T Engineering* **2021**. <https://doi.org/10.1021/acsestengg.1c00276>.
- (18) Ahmed, M.; Shayya, W. H.; Hoey, D.; Al-Handaly, J. Brine Disposal from Reverse Osmosis Desalination Plants in Oman and the United Arab Emirates. *Desalination* **2001**, *133* (2), 135–147. [https://doi.org/10.1016/S0011-9164\(01\)80004-7](https://doi.org/10.1016/S0011-9164(01)80004-7).
- (19) Leitner and Associates, Inc. *Survey of U.S. Costs and Water Rates for Desalination and Membrane Softening Plants*; Denver, CO, 1997.
- (20) Xu, P.; Cath, T. Y.; Robertson, A. P.; Reinhard, M.; Leckie, J. O.; Drewes, J. E. Critical Review of Desalination Concentrate Management, Treatment and Beneficial Use. *Environ Eng Sci* **2013**, *30* (8), 502–514. <https://doi.org/10.1089/ees.2012.0348>.

- (21) Mezher, T.; Fath, H.; Abbas, Z.; Khaled, A. Techno-Economic Assessment and Environmental Impacts of Desalination Technologies. *Desalination* **2011**, *266* (1–3), 263–273. <https://doi.org/10.1016/j.desal.2010.08.035>.
- (22) Pramanik, B. K.; Shu, L.; Jegatheesan, V. A Review of the Management and Treatment of Brine Solutions. *Environ Sci (Camb)* **2017**, *3* (4), 625–658. <https://doi.org/10.1039/c6ew00339g>.
- (23) Malek, A.; Hawlader, M. N. A.; Ho, J. C. Design and Economics of RO Seawater Desalination. *Desalination* **1996**, *105* (3), 245–261. [https://doi.org/10.1016/0011-9164\(96\)00081-1](https://doi.org/10.1016/0011-9164(96)00081-1).
- (24) Alghoul, M. A.; Poovanaesvaran, P.; Sopian, K.; Sulaiman, M. Y. Review of Brackish Water Reverse Osmosis (BWRO) System Designs. *Renewable and Sustainable Energy Reviews* **2009**, *13* (9), 2661–2667. <https://doi.org/10.1016/j.rser.2009.03.013>.
- (25) Liu, Q.; Xu, G.-R.; Das, R. Inorganic Scaling in Reverse Osmosis (RO) Desalination: Mechanisms, Monitoring, and Inhibition Strategies. *Desalination* **2019**, *468* (June), 114065. <https://doi.org/10.1016/j.desal.2019.07.005>.
- (26) Lyster, E.; Kim, M. man; Au, J.; Cohen, Y. A Method for Evaluating Antiscalant Retardation of Crystal Nucleation and Growth on RO Membranes. *Journal of Membrane Science* **2010**, *364* (1–2), 122–131. <https://doi.org/10.1016/j.memsci.2010.08.020>.
- (27) Subramani, A.; Cryer, E.; Liu, L.; Lehman, S.; Ning, R. Y.; Jacangelo, J. G. Impact of Intermediate Concentrate Softening on Feed Water Recovery of Reverse Osmosis Process during Treatment of Mining Contaminated Groundwater. *Separation and Purification Technology* **2012**, *88*, 138–145. <https://doi.org/10.1016/j.seppur.2011.12.010>.
- (28) Greenlee, L. F.; Freeman, B. D.; Lawler, D. F. Ozonation of Phosphonate Antiscalants Used for Reverse Osmosis Desalination: Parameter Effects on the Extent of Oxidation. *Chemical Engineering Journal* **2014**, *244*, 505–513. <https://doi.org/10.1016/j.cej.2014.02.002>.
- (29) McCool, B. C.; Rahardianto, A.; Cohen, Y. Antiscalant Removal in Accelerated Desupersaturation of RO Concentrate via Chemically-Enhanced Seeded Precipitation (CESP). *Water Research* **2012**, *46* (13), 4261–4271. <https://doi.org/10.1016/j.watres.2012.04.045>.

- (30) Ruiz-García, A.; Nuez, I.; Carrascosa-Chisvert, M. D.; Santana, J. J. Simulations of BWRO Systems under Different Feedwater Characteristics. Analysis of Operation Windows and Optimal Operating Points. *Desalination* **2020**, *491* (May), 114582. <https://doi.org/10.1016/j.desal.2020.114582>.
- (31) Ruiz-García, A.; Feo-García, J. Antiscalant Cost and Maximum Water Recovery in Reverse Osmosis for Different Inorganic Composition of Groundwater. *Desalination and Water Treatment* **2017**, *73* (May 2016), 46–53. <https://doi.org/10.5004/dwt.2017.20806>.
- (32) Hasson, D.; Drak, A.; Semiat, R. Induction Times Induced in an RO System by Antiscalants Delaying CaSO₄ Precipitation. *Desalination* **2003**, *157* (1–3), 193–207. [https://doi.org/10.1016/S0011-9164\(03\)00399-0](https://doi.org/10.1016/S0011-9164(03)00399-0).
- (33) Jain, T.; Sanchez, E.; Owens-Bennett, E.; Trussell, R.; Walker, S.; Liu, H. Impacts of Antiscalants on the Formation of Calcium Solids: Implication on Scaling Potential of Desalination Concentrate. *Environ Sci (Camb)* **2019**, *5* (7), 1285–1294. <https://doi.org/10.1039/c9ew00351g>.
- (34) Yu, W.; Song, D.; Chen, W.; Yang, H. Antiscalants in RO Membrane Scaling Control. *Water Research* **2020**, *183* (July), 115985. <https://doi.org/10.1016/j.watres.2020.115985>.
- (35) Greenlee, L. F.; Testa, F.; Lawler, D. F.; Freeman, B. D.; Moulin, P. The Effect of Antiscalant Addition on Calcium Carbonate Precipitation for a Simplified Synthetic Brackish Water Reverse Osmosis Concentrate. *Water Res* **2010**, *44* (9), 2957–2969. <https://doi.org/10.1016/j.watres.2010.02.024>.
- (36) Istirokhatun, T.; Dewi, M. N.; Ilma, H. I.; Susanto, H. Separation of Antiscalants from Reverse Osmosis Concentrates Using Nanofiltration. *Desalination* **2018**, *429* (December 2017), 105–110. <https://doi.org/10.1016/j.desal.2017.12.018>.
- (37) Boels, L.; Tervahauta, T.; Witkamp, G. J. Adsorptive Removal of Nitriilotris(Methylenephosphonic Acid) Antiscalant from Membrane Concentrates by Iron-Coated Waste Filtration Sand. *Journal of Hazardous Materials* **2010**, *182* (1–3), 855–862. <https://doi.org/10.1016/j.jhazmat.2010.06.123>.
- (38) Boels, L.; Keesman, K. J.; Witkamp, G. J. Adsorption of Phosphonate Antiscalant from Reverse Osmosis Membrane Concentrate onto Granular Ferric Hydroxide. *Environmental Science and Technology* **2012**, *46* (17), 9638–9645. <https://doi.org/10.1021/es302186k>.

- (39) Chen, Y.; Baygents, J. C.; Farrell, J. Removing Phosphonate Antiscalants from Membrane Concentrate Solutions Using Granular Ferric Hydroxide. *Journal of Water Process Engineering* **2017**, *19* (June), 18–25.
<https://doi.org/10.1016/j.jwpe.2017.07.002>.
- (40) Comstock, S. E. H.; Boyer, T. H.; Graf, K. C. Treatment of Nanofiltration and Reverse Osmosis Concentrates: Comparison of Precipitative Softening, Coagulation, and Anion Exchange. *Water Research* **2011**, *45* (16), 4855–4865.
<https://doi.org/10.1016/j.watres.2011.06.035>.
- (41) Azadi Aghdam, M.; Zraick, F.; Simon, J.; Farrell, J.; Snyder, S. A. A Novel Brine Precipitation Process for Higher Water Recovery. *Desalination* **2016**, *385*, 69–74.
<https://doi.org/10.1016/j.desal.2016.02.007>.
- (42) Yang, Q.; Lisitsin, D.; Liu, Y.; David, H.; Semiat, R. Desupersaturation of RO Concentrates by Addition of Coagulant and Surfactant. *Journal of Chemical Engineering of Japan* **2007**, *40* (9), 730–735.
<https://doi.org/10.1252/jcej.07WE035>.
- (43) Kim, M. M.; Au, J.; Rahardianto, A.; Glater, J.; Cohen, Y.; Geringer, F. W.; Gabelich, C. J. Impact of Conventional Water Treatment Coagulants on Mineral Scaling in RO Desalting of Brackish Water. *Ind Eng Chem Res* **2009**, *48* (6), 3126–3135. <https://doi.org/10.1021/ie800937c>.
- (44) Baudequin, C.; Mai, Z.; Rakib, M.; Deguerry, I.; Severac, R.; Pabon, M.; Couallier, E. Removal of Fluorinated Surfactants by Reverse Osmosis - Role of Surfactants in Membrane Fouling. *J Memb Sci* **2014**, *458*, 111–119.
<https://doi.org/10.1016/j.memsci.2014.01.063>.
- (45) Rott, E.; Minke, R.; Bali, U.; Steinmetz, H. Removal of Phosphonates from Industrial Wastewater with UV/FeII, Fenton and UV/Fenton Treatment. *Water Res* **2017**, *122*, 345–354. <https://doi.org/10.1016/j.watres.2017.06.009>.
- (46) Wang, Z.; Chen, G.; Patton, S.; Ren, C.; Liu, J.; Liu, H. Degradation of Nitrilotris-Methylenephosphonic Acid (NTMP) Antiscalant via Persulfate Photolysis: Implications on Desalination Concentrate Treatment. *Water Res* **2019**, *159*, 30–37.
<https://doi.org/10.1016/j.watres.2019.04.051>.
- (47) Xu, Z. Bin; Wang, W. L.; Huang, N.; Wu, Q. Y.; Lee, M. Y.; Hu, H. Y. 2-Phosphonobutane-1,2,4-Tricarboxylic Acid (PBTCA) Degradation by Ozonation: Kinetics, Phosphorus Transformation, Anti-Precipitation Property Changes and Phosphorus Removal. *Water Res* **2019**, *148*, 334–343.
<https://doi.org/10.1016/j.watres.2018.10.038>.

- (48) Li, W.; Patton, S.; Gleason, J. M.; Mezyk, S. P.; Ishida, K. P.; Liu, H. UV Photolysis of Chloramine and Persulfate for 1,4-Dioxane Removal in Reverse-Osmosis Permeate for Potable Water Reuse. *Environ Sci Technol* **2018**, *52* (11), 6417–6425. <https://doi.org/10.1021/acs.est.7b06042>.
- (49) Rioyo, J.; Aravinthan, V.; Bundschuh, J.; Lynch, M. Research on ‘High-PH Precipitation Treatment’ for RO Concentrate Minimization and Salt Recovery in a Municipal Groundwater Desalination Facility. *Desalination* **2018**, *439* (April), 168–178. <https://doi.org/10.1016/j.desal.2018.04.020>.
- (50) Rahardianto, A.; McCool, B. C.; Cohen, Y. Accelerated Desupersaturation of Reverse Osmosis Concentrate by Chemically-Enhanced Seeded Precipitation. *Desalination* **2010**, *264* (3), 256–267. <https://doi.org/10.1016/j.desal.2010.06.018>.
- (51) Gabelich, C. J.; Williams, M. D.; Rahardianto, A.; Franklin, J. C.; Cohen, Y. High-Recovery Reverse Osmosis Desalination Using Intermediate Chemical Demineralization. *J Memb Sci* **2007**, *301* (1–2), 131–141. <https://doi.org/10.1016/j.memsci.2007.06.007>.
- (52) Wang, Z.; Sun, P.; Li, Y.; Meng, T.; Li, Z.; Zhang, X.; Zhang, R.; Jia, H.; Yao, H. SI: Reactive Nitrogen Species Mediated Degradation of Estrogenic Disrupting Chemicals by Biochar/Monochloramine in Buffered Water and Synthetic Hydrolyzed Urine. *Environmental Science and Technology* **2019**, *53* (21), 12688–12696. <https://doi.org/10.1021/acs.est.9b04704>.
- (53) Yin, Y.; Wang, W.; Kota, A. K.; Zhao, S.; Tong, T. Elucidating Mechanisms of Silica Scaling in Membrane Distillation: Effects of Membrane Surface Wettability. *Environmental Science: Water Research and Technology* **2019**, *5* (11), 2004–2014. <https://doi.org/10.1039/c9ew00626e>.
- (54) Greenlee, L. F.; Testa, F.; Lawler, D. F.; Freeman, B. D.; Moulin, P. Effect of Antiscalants on Precipitation of an RO Concentrate: Metals Precipitated and Particle Characteristics for Several Water Compositions. *Water Res* **2010**, *44* (8), 2672–2684. <https://doi.org/10.1016/j.watres.2010.01.034>.
- (55) Owens-Bennett, E. L.; Trussell, B.; Monroy, I. *TECHNICAL MEMORANDUM - Proposed Solids Formation Recovery Formula for the Inland Empire Brine Line*; 2016.
- (56) Yang, H. L.; Huang, C.; Pan, J. R. Characteristics of RO Foulants in a Brackish Water Desalination Plant. *Desalination* **2008**, *220* (1–3), 353–358. <https://doi.org/10.1016/j.desal.2007.01.040>.

- (57) Xu, Z. Bin; Wang, W. L.; Huang, N.; Wu, Q. Y.; Lee, M. Y.; Hu, H. Y. 2-Phosphonobutane-1,2,4-Tricarboxylic Acid (PBTCA) Degradation by Ozonation: Kinetics, Phosphorus Transformation, Anti-Precipitation Property Changes and Phosphorus Removal. *Water Research* **2019**, *148*, 334–343. <https://doi.org/10.1016/j.watres.2018.10.038>.
- (58) Greenlee, L. F.; Testa, F.; Lawler, D. F.; Freeman, B. D.; Moulin, P. Effect of Antiscalant Degradation on Salt Precipitation and Solid/Liquid Separation of RO Concentrate. *J Memb Sci* **2011**, *366* (1–2), 48–61. <https://doi.org/10.1016/j.memsci.2010.09.040>.
- (59) Howe, K. J.; Marwah, A.; Chiu, K. P.; Adham, S. S. Effect of Membrane Configuration on Bench-Scale MF and UF Fouling Experiments. *Water Research* **2007**, *41* (17), 3842–3849. <https://doi.org/10.1016/j.watres.2007.05.025>.
- (60) Wadekar, S. S.; Hayes, T.; Lokare, O. R.; Mittal, D.; Vidic, R. D. Laboratory and Pilot-Scale Nanofiltration Treatment of Abandoned Mine Drainage for the Recovery of Products Suitable for Industrial Reuse. *Industrial and Engineering Chemistry Research* **2017**, *56* (25), 7355–7364. <https://doi.org/10.1021/acs.iecr.7b01329>.
- (61) Mosqueda-Jimenez, D. B.; Narbaitz, R. M.; Matsuura, T. Membrane Fouling Test: Apparatus Evaluation. *Journal of Environmental Engineering-Asce* **2004**, *130* (1), 90–99. [https://doi.org/Doi 10.1061/\(Asce\)0733-9372\(2004\)130:1\(90\)](https://doi.org/Doi%2010.1061/(Asce)0733-9372(2004)130:1(90)).
- (62) Liang, C.; Huang, C. F.; Mohanty, N.; Kurakalva, R. M. A Rapid Spectrophotometric Determination of Persulfate Anion in ISCO. *Chemosphere* **2008**, *73* (9), 1540–1543. <https://doi.org/10.1016/j.chemosphere.2008.08.043>.
- (63) American Public Health Association; American Water Works Association; Water Environment Foundation. *Standard Methods for the Examination of Water and Wastewater*, 23rd Ed.; Baird, R. B., Eaton, A. D., Rice, E. W., Eds.; American Public Health Association; American Water Works Association; Water Environment Foundation, 2017.
- (64) Li, W.; Jain, T.; Ishida, K.; Liu, H. A Mechanistic Understanding of the Degradation of Trace Organic Contaminants by UV/Hydrogen Peroxide, UV/Persulfate and UV/Free Chlorine for Water Reuse. *Environ Sci (Camb)* **2017**, *3* (1), 128–138. <https://doi.org/10.1039/c6ew00242k>.
- (65) Neta, P.; Huie, R. E.; Ross, A. B. Rate Constants for Reactions of Aliphatic Carbon-Centered Radicals in Aqueous Solution. *J Phys Chem Ref Data* **1988**, *17*, 1027. <https://doi.org/doi.org/10.1063/1.555808>.

- (66) Wang, Z.; Shao, Y.; Gao, N.; Lu, X.; An, N. Degradation of Diethyl Phthalate (DEP) by UV/Persulfate: An Experiment and Simulation Study of Contributions by Hydroxyl and Sulfate Radicals. *Chemosphere* **2018**, *193*, 602–610. <https://doi.org/10.1016/j.chemosphere.2017.11.075>.
- (67) Buxton, G. V.; Greenstock, C. L.; Helman, W. P.; Ross, A. B. Critical Review of Rate Constants for Reactions of Hydrated Electrons, Hydrogen Atoms and Hydroxyl Radicals in Aqueous Solution. *J Phys Chem Ref Data* **1988**, *17* (2), 513–886. <https://doi.org/10.1063/1.555805>.
- (68) Yu, X. Y.; Bao, Z.-C.; Barker, J. R. Free Radical Reactions Involving Cl \cdot , Cl $_2$ \cdot^- , and SO $_4$ \cdot^- in the 248 Nm Photolysis of Aqueous Solutions Containing S $_2$ O $_8^{2-}$ and Cl \cdot . *Journal of Physical Chemistry Association* **2004**, *108* (2), 295–308. <https://doi.org/10.1021/jp036211i>.
- (69) Benjamin, M. M. *Water Chemistry*, 2nd ed.; Waveland Press, Inc, 2014.
- (70) Lin, Y. P.; Singer, P. C. Inhibition of Calcite Crystal Growth by Polyphosphates. *Water Research* **2005**, *39* (19), 4835–4843. <https://doi.org/10.1016/j.watres.2005.10.003>.
- (71) Reddy, M. M.; Hoch, A. R. Calcite Crystal Growth Rate Inhibition by Polycarboxylic Acids. *Journal of Colloid and Interface Science* **2001**, *235* (2), 365–370. <https://doi.org/10.1006/jcis.2000.7378>.
- (72) Hydranautics. *Chemical Pretreatment For RO and NF*. Technical Application Bulletin No. 111, Rev. B. <https://membranes.com/wp-content/uploads/2017/06/TAB-111.pdf> (accessed 2020-03-27).

Chapter 4

Recovery of Fresh Water and Minerals from Inland Brackish Desalination Brine via Persulfate-based Photochemical Treatment and Demineralization

Previously published in *Separation and Purification Technology*

Kum, S., Tang, X., & Liu, H. (2024). Recovery of fresh water and minerals from inland brackish desalination brine via persulfate-based photochemical treatment and demineralization. *Separation and Purification Technology*, 342, 126994.
<https://doi.org/10.1016/j.seppur.2024.126994>.

Abstract

Managing inland brackish desalination brine is challenging but critical to future water security. This study investigated the use of a treatment train with an ultraviolet persulfate (UV/PS) oxidative pre-treatment followed by chemical demineralization (CDM), microfiltration (MF) and secondary reverse osmosis (RO) to achieve antiscalant degradation, scale-forming constituent removal, mineral recovery, and fresh water recovery from an inland brackish RO brine. Results showed that the UV/PS pre-treatment efficiently degraded the phosphonate antiscalant ubiquitously present in the brine within 20 min of UV irradiation and improved mineral resource recovery from the brine in a subsequent CDM process. Analyses of the recovered minerals revealed that calcium, magnesium, and silica were the major chemical components, and calcite was a major crystallized mineral. The MF process successfully separated solid and liquid from the CDM process, and MF membrane fouling potential was significantly reduced with UV/PS-CDM treatment. The CDM process, coupled with UV/PS pre-treatment, mitigated membrane fouling and improved fresh water recovery during a subsequent RO step due to the lower magnesium and silica concentrations and the removal of phosphonate antiscalant. Over 40% of total dissolved solids in the raw brine ($> 2.1 \text{ g} \cdot \text{L}^{-1}$) were recovered as mineral resources from the raw brine, and over 75% fresh water recovery was achieved. The results demonstrated the benefits and applicability of a persulfate-based photochemical treatment followed by CDM, MF, and RO for inland brackish water brine treatment and recovery of additional water.

Introduction

Climate impact and population growth lead to severe fresh water scarcity worldwide.¹⁻³ In arid inland areas, including the Middle East and the Southwestern U.S., brackish groundwater has become an alternative water source to produce potable water via reverse osmosis (RO) membrane processes.⁴⁻⁷ However, inland brackish water desalination inevitably generates a large quantity of membrane concentrate, also known as brine, which accounts for 15% to 60% of the feed water that needs disposal.⁸⁻¹¹ The disposal of inland brine is challenging due to the lack of direct access to ocean outfall, therefore bearing a high cost and big environmental footprint.¹²⁻¹⁴ Conventional options for inland brine treatment include deep well injection, evaporation pond, land application, ocean discharge via pipeline, and advanced brine treatment. Deep well injection and land application can induce adverse environmental impacts by increasing salinity and inducing secondary pollution.¹⁴⁻¹⁶ Evaporation pond is feasible in regions where solar energy is abundant but requires a large land that prohibits its application in densely populous urban areas.^{13,17} The use of a brine pipeline connected to ocean outfall bears a high infrastructure cost and faces severe pipeline scaling issues.^{18,19} Advanced brine treatment includes membrane-based (*e.g.*, RO and electrodialysis) and thermal-based processes (*e.g.*, crystallizer and evaporator). The RO process can be applied to feed salinity up to 70 g · L⁻¹ and achieve up to 50% water recovery with 2 – 6 kWh · m⁻³ energy consumption, but it is not effective as a stand-alone technology, and membrane fouling is a major obstacle.²⁰ Electrodialysis (ED) uses an electrical driving force to separate dissolved ions through ion exchange membranes. ED has been widely

used for RO concentrate treatment and is able to concentrate feed waters to over $100 \text{ g} \cdot \text{L}^{-1}$ salinity with $7 - 15 \text{ kWh} \cdot \text{m}^{-3}$ energy consumption.²¹ However, high concentrations of antiscalants and fine organics could lead to fouling.^{22,23} Evaporators, such as multi-stage flash, multi-effect distillation, and mechanical vapor compression, evaporate saline water and recondense vapors as fresh water. These thermal processes are effective technologies to achieve zero liquid disposal for up to $180 \text{ g} \cdot \text{L}^{-1}$ salinity but require a high specific energy consumption ($7 - 39 \text{ kWh} \cdot \text{m}^{-3}$).^{21,24,25} Brine crystallizer can be applicable to feed salinity up to $300 \text{ g} \cdot \text{L}^{-1}$ and may recover up to 99% of water but requires high capital and operation costs as well as high energy input ($52 - 70 \text{ kWh} \cdot \text{m}^{-3}$).²⁶ Membrane distillation (MD) process, a thermally driven membrane separation process, can treat feedwater salinity up to $350 \text{ g} \cdot \text{L}^{-1}$ and achieve 90% fresh water recovery with $39 - 67 \text{ kWh} \cdot \text{m}^{-3}$ energy consumption.²⁷ But it requires multi-stage processing to achieve near-zero discharge.^{21,28,29} Therefore, a more sustainable brine treatment is needed for inland brine treatment.

Inland brackish RO brine has a unique chemistry – containing a high level of various scale-forming ions, including calcium and magnesium, and an elevated level of salinity, with the total dissolved solids (TDS) concentration ranging from 5 to $15 \text{ g} \cdot \text{L}^{-1}$. More importantly, the inland brine is often oversaturated with respect to calcium and magnesium hardness minerals. This is due to the presence of antiscalants that are added to the feedwater during the RO process to prevent membrane scaling of hardness minerals. Antiscalants are typically composed of phosphonate, which has a significant inhibition effect on the hardness of mineral precipitation. The typical dosage of

phosphonate antiscalant in RO feedwater ranges from 1–10 mg·L⁻¹. The concentration of antiscalants in the brine can be several times higher than that in the RO feed due to the concentration effects via the RO process. The existence of a high concentration of residual antiscalants in the brine not only inhibits the removal of scale-forming ions and recovery of hardness minerals during the treatment, but also increases the risk of biofouling during the secondary RO process for additional water recovery.^{19,30–32}

Therefore, future sustainable brine treatment needs to consider the fate and removal of antiscalants for hardness mineral recovery.

Additionally, fresh water recovery from inland brine can be achieved by secondary membrane separation processes subsequent to the removal of scaling hardness minerals. For example, chemical precipitation and crystallization can recover minerals from RO brine. Prior studies investigated combined treatment trains to achieve both water and resource recovery from RO brine, including electrodialysis reversal with a crystallizer^{33,34} membrane distillation crystallization³⁵ and RO with chemically enhanced seeded precipitation.^{8,36} However, the effects of the removal of antiscalants from RO brine on water and resource recovery remain largely unknown.

Advanced oxidation processes (AOPs) have been recently investigated to degrade phosphonate-based antiscalants. Among various AOPs, an ultraviolet-driven persulfate oxidation process (UV/PS) has attracted significant scientific interest for the destruction of organic compounds in the aquatic system and shown the potential to remove phosphonate antiscalants effectively.^{37–40} UV photolysis of persulfate (S₂O₈²⁻) generates a strong oxidant — a sulfate radical (SO₄^{•-}) — similar in oxidizing power (E⁰ = 2.5–3.1 V)

to HO• ($E^0 = 1.9\text{--}2.7\text{ V}$), and more selective than HO• toward organic pollutants. Once the antiscalants are degraded via UV/PS, precipitation of scale-forming ions including calcium and magnesium can be enhanced via a chemical demineralization (CDM) process.⁴¹ Precipitation of calcium and magnesium (major cations in brine) is primarily controlled by solution pH.^{42,43} During the CDM process, supersaturation levels of scale-forming ions decrease by increasing the solution pH to the alkaline pH, and precipitates are recovered as mineral resources. Benefitting from hardness ions removal, the RO brine will have a significantly less scaling potential and, therefore, can undergo a secondary RO for additional fresh water recovery. Until now, the application of the CDM process with UV/PS pre-treatment on real inland brackish desalination brine has not been investigated.

Accordingly, the objectives of this study were to: (1) develop a treatment train by a sequential combination of UV/PS pre-treatment, a CDM process, microfiltration (MF) and RO to achieve antiscalant degradation, hardness mineral recovery, and fresh water recovery from an inland brackish desalination brine; (2) optimize the UV/PS pre-treatment to degrade antiscalant in real brine, including the persulfate dosage and UV irradiation time; (3) evaluate the effects of UV/PS pre-treatment on the subsequent CDM process with respect to mineral resource recovery; and (4) maximize fresh water recovery from the RO brine.

Materials and Methods

Sampling of Brackish RO Brine

Inland brackish RO brine samples were collected from the Arlington Desalter (DWTP #1, discussed in Chapter 2) in Riverside, California via six sampling events from September 2020 to January 2021. The brine sample contains a phosphonate antiscalant (Pretreat Plus[®] Y2K, King Lee Technologies, San Diego, CA) enriched from the primary RO desalination process. A 40-L fresh brine sample sealed without headspace was collected and used for experiments within three days. Water quality parameters were measured, including pH, alkalinity, cation and anion concentrations. Based on the measured water quality of RO brine, thermodynamic calculations using Visual Minteq were performed to predict the oversaturated minerals of the raw brine and brine at pH 10.2 in the absence of antiscalants. Specifically, the chemical composition of the brine was the input parameter to the chemical model in a closed system. The predicted oversaturated solids were subsequently selected and the theoretical type and amount of solid formation in the brine at equilibrium were calculated.

Experimental Details on Brine Treatment

UV/PS experiments were conducted in a 4-L UV reactor equipped with a 450W medium pressure UV immersion lamp (Ace Glass Inc.). All chemical solutions were prepared using Milli-Q water (18 M Ω -cm resistivity at 25°C). To start an experiment, 0.5 – 4 mM persulfate was added into 3.5-L brine in the UV reactor. 3-mL samples were withdrawn by pipette from the reactor at designated UV irradiation time intervals for chemical analysis that lasted up to 30 min.

CDM experiments were conducted using a 3.5-L brine that had been treated for 20 min by UV/PS with 1 mM persulfate. In addition, CDM control experiments were conducted using the raw brine without UV/PS pre-treatment. To start a CDM experiment, the UV/PS treated brine or raw brine was transferred to a 4-L reactor. The brine pH was first increased to 10.2 with 5 M NaOH, note that pH 10.2 is where the plateau of the calcium carbonate saturation index in the brine started. The brine was then rapidly mixed for 1 minute at 700 rpm with a stir bar to promote chemical mixing and mineral precipitation, followed by a 30-min stagnation period to facilitate the settling of precipitates. At targeted time intervals during the stagnation period, 3-mL aliquots of the supernatant were withdrawn 3 cm below the water surface with a pipette, immediately acidified with concentrated HNO₃, and analyzed for the major hardness ions. At the end of the stagnation period, all supernatant from the reactor was collected and filtered with a 0.45- μ m polyvinylidene fluoride membrane (MF process). The filter-retained precipitates were dried at 105 °C for 24 hours and preserved for further characterization.

A 3.5-L of the filtered solution (defined as CDM treated brine) was subsequently used as feedwater to the subsequent secondary RO process. Before the RO step, the pH of the CDM treated brine was adjusted with 5 M HCl to pH 7.8 which is the same pH of raw RO brine or pH 5, which is the lowest allowable pH for antiscalant application.⁴⁴ CDM treatment brine without pH adjustment (pH 10.2) was also used as feedwater. In addition, a RO control experiment was conducted using the raw brine (pH 7.8). A crossflow system with brackish desalination RO membranes (BW30LE, DuPont FilmTec, Edina, MN) was used and operated at a constant pressure of 150 psi for 24 hours in partial

recycling mode (details provided in Text S1). The RO permeate was collected and its mass was continuously measured by an electronic balance and converted to normalized permeate water flux and fresh water recovery rate (details provided in Text S2). In addition, 3-mL samples of feedwater and permeate were collected at targeted time intervals during the RO step and acidified with HNO₃ for analysis of calcium, magnesium, sodium, and TDS. Fig. 1 shows the schematic diagram of the suggested system (UV/PS-CDM-MF-RO).

Analytical Methods

Alkalinity of the raw brine was measured by titration based on Standard Method 2320B. The concentrations of chloride, nitrate, ammonium, and sulfate ions in the RO brine were determined using an ion chromatography (Dionex ICS-1100, Thermo Scientific, Sunnyvale, CA) following Standard Methods 4110B. The concentration of persulfate was determined by a standard colorimetric method using potassium iodide. The phosphonate antiscalant concentration in the brine sample was quantified by converting it to orthophosphate via persulfate photolysis and measuring the product of orthophosphate (Fig. S2). The concentration of orthophosphate was measured by Standard method 4500-P E. Calcium, magnesium, and silica were measured using an inductively coupled plasma mass spectrometry (ICP-MS, Agilent 7700 Series, Santa Clara, CA). Triplicate measurements of each sample were conducted for all chemical parameters. TDS was measured using a TDS meter (3200, YSI Inc., Yellow Spring, OH). The weight of dried precipitates collected from the CDM experiment was measured by a precision balance. The crystal structure of recovered minerals was determined by X-ray

diffraction analysis (XRD) with Cu K α radiation (Empyrean Series 2, Malvern Panalytical, United Kingdom), and chemical composition was evaluated by surface-sensitive X-ray photoelectron spectroscopy (XPS, Kratos AXIS Ultra DLD, Shimadzu, Japan). Detailed information on the XRD and XPS measurements are provided in Texts S3. In addition, 50 mg of the minerals were digested by Standard Method 3005A. Concentrations of calcium, magnesium and silica in the digested solution were measured by ICP-MS.

Results and Discussion

Phosphonate Antiscalant Degradation by UV/persulfate

The major chemical constituents of the raw inland brackish RO brine used in this study are displayed in Table 1. The brine pH was 7.8 with an average TDS of 5250 ± 246 mg·L⁻¹ and alkalinity of 1560 ± 34 mg·L⁻¹ as CaCO₃. The major cations were calcium, magnesium, and sodium. The major anions were bicarbonate, sulfate, nitrate, and chloride. Sources of the hardness ions and bicarbonate were from mineral dissolution and equilibration with the groundwater in the aquifer. Historical agricultural activity and long-term fertilizer application in the region of this study also introduced nitrate to the groundwater and, consequently, to the brine. The average concentration of phosphonate antiscalant in the brine was 23 mg·L⁻¹, corresponding to 1 mg P·L⁻¹ (Fig. S2).

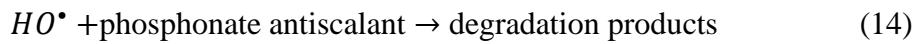
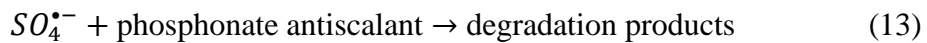
Thermodynamic calculations based on the chemical composition of the RO brine indicated that calcite (CaCO_{3(s)}), dolomite (CaMg(CO₃)_{2(s)}), and Silica (SiO_{2(s)}) were supersaturated (Table S2).

UV/PS pre-treatment degraded phosphonate antiscalant to orthophosphate and exhibited distinct kinetics with different persulfate dosages (Fig. 2A). For example, a persulfate dosage >1 mM degraded 100% of phosphonate within 20 min of UV irradiation; however, 0.5 mM persulfate was not sufficient to fully degrade the residual antiscalant in the RO brine. The generation of orthophosphate followed a pseudo-first-order kinetics model with rate constants between 0.18 and 0.39 min⁻¹ that increased non-linearly with the increase of persulfate dosage indicating that the degradation rate decreased at higher persulfate dosage (Fig. 2B).

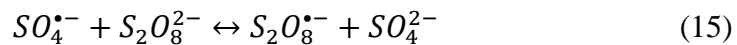
Persulfate is photolyzed directly to sulfate radicals ($SO_4^{\bullet-}$) (Eq. 1), which further undergo hydrolysis to form hydroxyl radical (HO^{\bullet}) (Eq. 2, $k = 6.5 \times 10^7 \text{ M}^{-1}\text{s}^{-1}$).^{39,45}

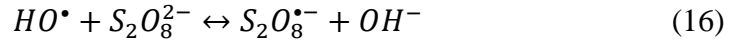


Both $SO_4^{\bullet-}$ and HO^{\bullet} degrade phosphonate antiscalants with second-order reaction rate constants of $(2.9 \pm 0.6) \times 10^7 \text{ M}^{-1}\text{s}^{-1}$ (Eq. 3) and $(1.1 \pm 0.1) \times 10^8 \text{ M}^{-1}\text{s}^{-1}$ (Eq. 4), respectively.³¹



Both $SO_4^{\bullet-}$ and HO^{\bullet} can be scavenged by persulfate and generate a non-reactive persulfate radical ($S_2O_8^{\bullet-}$). The second-order rate constant is $5.5 \times 10^5 \text{ M}^{-1}\text{s}^{-1}$ and $1.4 \times 10^7 \text{ M}^{-1}\text{s}^{-1}$ for sulfate radical and persulfate reaction (Eq. 5) and hydroxyl radical and persulfate reaction (Eq. 6), respectively.^{46,47}

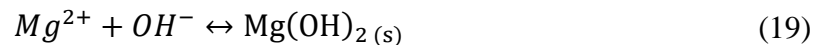


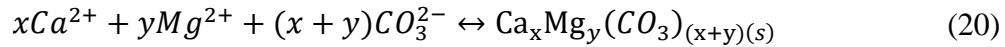


An increase in persulfate dosage promotes the scavenging of the reactive radicals (Eq. 5 and 6); therefore, the correlation between the antiscalant degradation rate constant and the persulfate dosage deviated from linearity at a dosage higher than 2 mM (Fig. 2B). Therefore, 1 mM persulfate with 20 min of UV irradiation was employed to achieve the highest efficiency and the most efficient utilization of persulfate, leaving only 5% persulfate residual in the UV/PS treated brine (Fig. S3).

Removal of Hardness Ions from the Brine by Chemical Demineralization

During the CDM process, the pH of the UV/persulfate pretreated RO brine was raised from 7.8 to 10.2 with NaOH, leading to a shift in the bicarbonate equilibrium to carbonate (Eq. 7). As a result, calcium carbonate precipitation actively occurred (Eq. 8, $K_{sp} = 8.7 \times 10^{-9}$ at 25 °C) and magnesium also interacted with carbonate to form magnesium carbonate ($K_{sp} = 1 \times 10^{-5}$ at 25°C). In addition, carbonate and hydroxide ions react with magnesium and calcium to form magnesium hydroxide (Eq. 9, $K_{sp} = 8.9 \times 10^{-12}$ at 25°C) and calcium-magnesium carbonate (Eq. 10, $K_{sp} = 2.9 \times 10^{-17}$ at 25°C). Among possible magnesium precipitates, magnesium carbonate is highly soluble under the experimental condition.⁴⁸ Therefore, magnesium hydroxide and calcium-magnesium carbonate precipitates were expected in UV/PS-treated brine at pH 10.2.





UV/PS pre-treatment improved the removal of hardness ions from the brine when the CDM process was conducted at a pH of 10.2. When applied, calcium removal was approximately 16% more effective during the first 5 mins of the CDM process (Fig. 3A), and the overall magnesium removal improved by 13% (Fig. 3B). UV/PS pre-treatment degraded phosphonate antiscalant and removed its inhibitive effect on hardness ion precipitation. As a result, more magnesium precipitation occurred in the CDM process with UV/PS pre-treatment. In addition, there was no persulfate residual in the UV/PS-CDM treated process, indicating residual persulfate from the UV/PS pre-treatment is completely utilized during the CDM process.

Mineral Recovery after Chemical Demineralization

CDM with UV/PS pre-treatment resulted in the mineral recovery of over 40% of total dissolved solids (over $2.1 \text{ g} \cdot \text{L}^{-1}$) and 5% more mineral resource recovery than the control without UV/PS pre-treatment (Fig. 4), which was consistent with the removal efficiencies of calcium and magnesium during the CDM step in Fig. 3. Thermodynamics calculations show that $\text{CaCO}_{3(s)}$, $\text{CaMg}(\text{CO}_3)_2(s)$, and $\text{SiO}_{2(s)}$ were the projected minerals from brine in the absence of phosphonate antiscalant (Table S2). Based on thermodynamics calculations, calcite accounted for more than 50% of the dry mass in the recovered minerals and dolomite and silica were second and third major precipitates (Fig. 4). The percentage of magnesium and silica in the recovered mineral increased by approximately 40% and 25%, respectively, when the CDM process was coupled with a UV/PS pre-treatment in comparison to without UV/PS pre-treatment (Fig. 4). Other minor

compositions were expected as sodium chloride and carbonate salts. XRD analysis also confirmed the existence of calcite as the major mineral recovered from the CDM process both with and without UV/PS pre-treatment (Fig. S4). XPS analysis confirmed that calcium, magnesium, silica, sodium, carbon, and oxygen were the major elements in the precipitates recovered from the CDM process (Fig. S5). Degradation of phosphonate antiscalant via UV/PS likely affected the precipitation kinetics of magnesium and silica solids to a larger extent than calcium solids, and consequently resulted in more magnesium and silica removal from the brine.

Fresh Water Recovery from the Brine Following UV/PS and CDM

The supernatant of the treated brine after the CDM step was subject to a sequential combination of MF and RO membrane separation to recover additional fresh water. Results showed that the CDM process with UV/PS pre-treatment was most effective in recovering fresh water from the brine while experiencing the least membrane flux decline at the same water recovery rate (Fig. 5). At the start of RO operation, the permeate flux without any pre-treatment (control, raw brine) decreased immediately, indicating that the presence of scale-forming ions in the untreated brine led to mineral scaling of the membrane. In contrast, the application of UV/PS pre-treatment with the CDM process prior to RO showed less permeate flux decline than control at all pHs and even less permeate flux decline than only CDM pre-treatment at pH 7.8 and pH 10.2 (Fig. 5). The CDM process removed the scale-forming ions and induced slower mineral scaling on the membrane surface.

For the RO feed solution from the CDM process with UV/PS pre-treatment, overall water recovery was 59%, 77%, and 75% at feedwater pH of 10.2, pH 7.8 and pH 5, respectively (Fig. 5). On the other hand, the CDM process without UV/PS pre-treatment, overall water recovery was much lower at 44%, 56% and 74% at pH of 10.2, pH 7.8, and pH 5, respectively. More water recovery was achieved when the RO feedwater pH was lowered to 5, mainly due to the absence of carbonate ions, which is a major scaling inducer. However, the RO feed solution from the CDM process with UV/PS pre-treatment achieved similar overall water recovery at pH 7.8 and pH 5, suggesting it is less sensitive to pH (Fig. 5); therefore, pH 7.8 will be desirable for UV/PS-CDM treated brine and fewer acid consumption is expected for pH adjustment of the RO feed water.

Calcium, magnesium, and sodium removal efficiencies and permeate TDS achieved by RO with UV/PS-CDM pre-treatment or CDM-only pre-treatment are shown in Table S3. TDS of the RO permeate was below $500 \text{ mg}\cdot\text{L}^{-1}$, which meets the secondary drinking water quality standards of the U.S. EPA. The removal efficiencies of calcium, magnesium, and sodium were similar regardless of UV/PS pre-treatment. Under the laboratory setup, membrane fouling increased with time and the feed water became concentrated; however, the measured removal rates were consistent throughout the RO operation, suggesting that the fouling layer and feed concentration had little impact on the efficiency of ion removal.

Implications

A treatment train with UV/PS pre-treatment-CDM-MF-RO achieved antiscalant degradation, resource recovery and fresh water recovery from an inland brackish

desalination brine. The estimated specific energy consumption for the whole system is 16.7 – 18.7 kWh · m⁻³ (details provided in Text S5), which is lower than the energy consumption of thermal brine treatment processes, such as evaporator, brine crystallizer, and membrane distillation. The experimental results confirmed that the brine treatment system is a promising technology to recover additional water and mineral resources. The CDM process with UV/PS pre-treatment resulted in greater magnesium and silica removal efficiencies due to phosphonate antiscalant degradation and mitigated membrane fouling in the secondary RO process due to the lower concentration of magnesium, silica, and phosphonate antiscalant in the RO feed solution. In addition, the UV/PS pre-treatment and CDM produced an RO feed water that resulted in high water recovery at neutral pH; therefore, less acid is needed for pH adjustment of the feed water and to add additional base to the RO permeate to bring the pH to between 6.5 and 8.5, the recommended pH range by the United States Environmental Protection Agency and World Health Organization. Collectively, the suggested system in this study can help achieve a near zero liquid discharge goal in the inland brackish water treatment plant and improve the sustainability of the desalination plant.

Supporting Information

Details of bench-scale reverse osmosis system, normalized permeate water flux calculation, chemical analysis on the recovered minerals from the brine, and XPS and XRD results of recovered resources from the CDM process are provided in the Supporting Information (Appendix C).

Table 4-12. Major chemical constituents of the inland brackish RO brine.

Chemical Parameter	Values	Unit
Ca ²⁺	830 ± 20	mg/L
Mg ²⁺	310 ± 10	mg/L
Na ⁺	580 ± 50	mg/L
Ba ²⁺	0.2 ± 0.04	mg/L
H ₄ SiO ₄	51 ± 2	mg Si/L
SO ₄ ²⁻	709 ± 13	mg/L
Cl ⁻	816 ± 19	mg/L
NO ₃ ⁻	81 ± 2	mg N/L
PO ₄ ³⁻	0.1±0.04	mg P/L
Phosphonate antiscalant	1	mg P/L
Alkalinity	1560 ± 34	mg/L as CaCO ₃
TDS*	5250 ± 246	mg/L
DOC	5.9 ± 0.1	mg C/L
pH	7.8 ± 0.1	--
Conductivity	7.53 ± 0.34	mS/cm

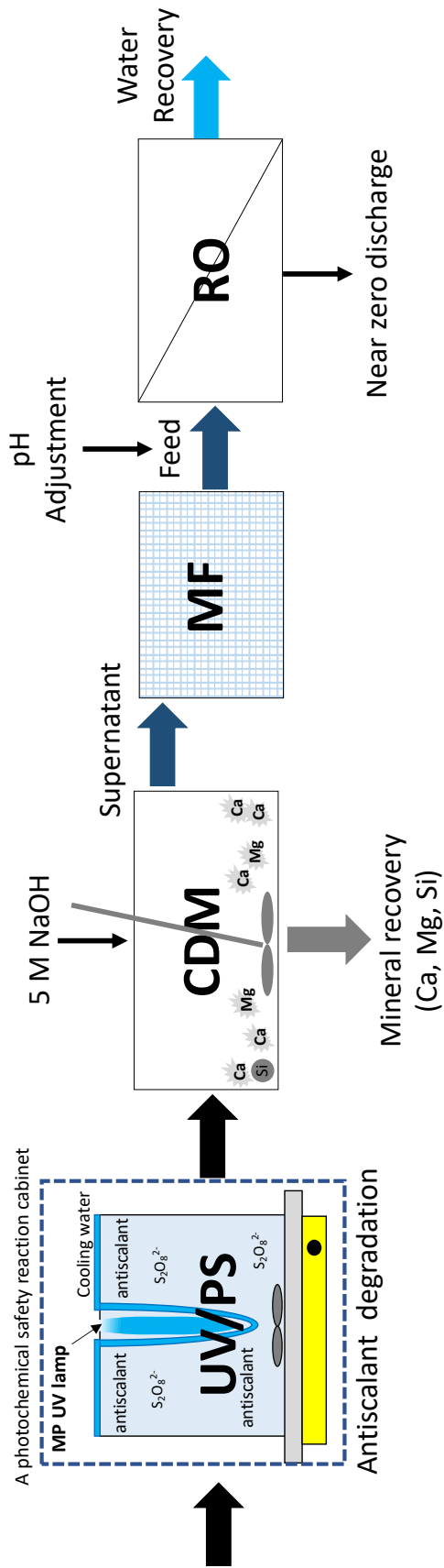


Figure 4-1. Schematic of sequential persulfate-based photochemical pre-treatment, chemical demineralization, microfiltration, and reverse osmosis (UV/PS-CDM-MF-RO) system.

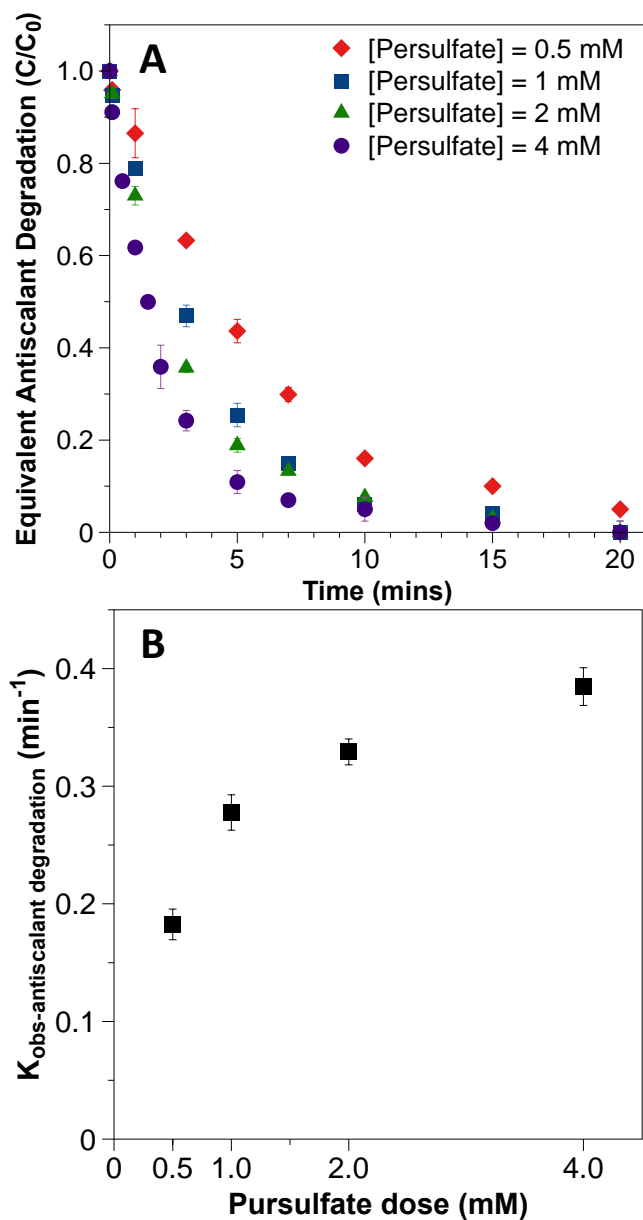


Figure 4-2. Antiscalant degradation by UV/persulfate treatment (A) effect of UV irradiation time and (B) observed pseudo-first-order rates of antiscalant degradation. Experimental condition: [Persulfate]₀ = 0 – 4.0 mM; initial pH = 7.8. Note: Final orthophosphate concentration \cong 1 mg/L and orthophosphate concentration was measured as an indicator of phosphonate antiscalant degradation.^{31,49} Error bars represent the range of values for triplicate tests.

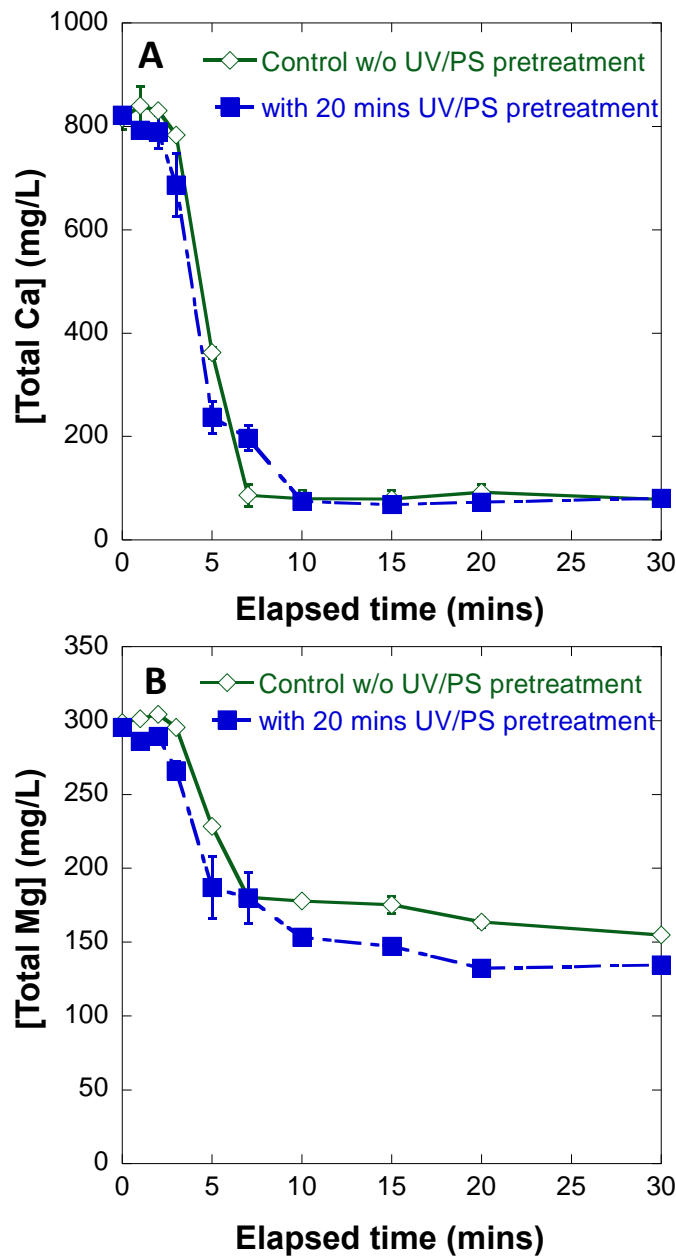


Figure 4-3. Total calcium and magnesium concentration of CDM process after adjustment to pH 10.2 with 5 M NaOH: (A) calcium and (B) magnesium. Note: after chemical addition (time zero), each solution was rapid-mixed at 700 rpm for 1 min to allow chemical mixing and precipitation to occur and then sit for 29 min for sedimentation (that is, a total elapsed time of 30 mins); Error bars represent the range of values for triplicate tests.

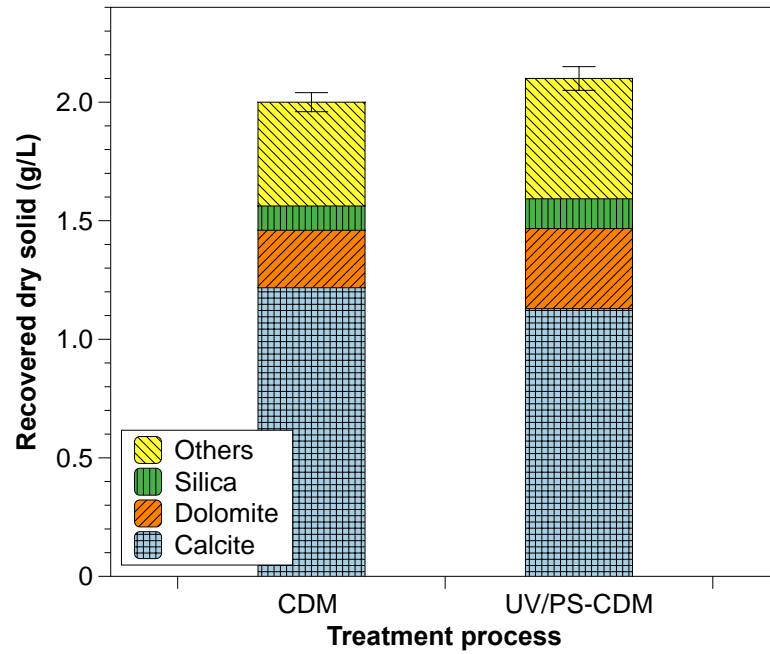


Figure 4-4. The amount of recovered minerals from the brine after the CDM process. Note: error bars are for the total recovered dry solid amount. Detailed explanation of the recovered mineral amount calculation procedure is described in Text S4.

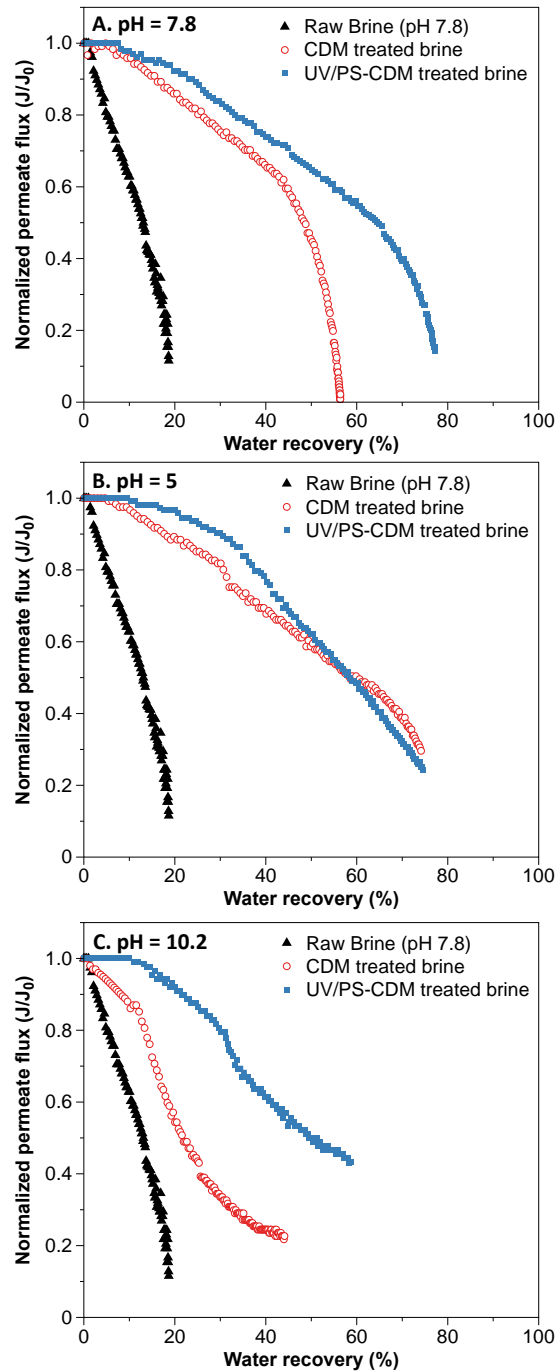


Figure 4-5. Normalized permeate flux decline as a function of water recovery for RO feed solutions: (A) pH 7.8, (B) pH 5, and (C) pH 10.2. Note: CDM indicates the CDM process without UV/PS pre-treatment and UV/PS-CDM indicates the CDM process with UV/PS pre-treatment. The RO process was operated for 24 hours in a closed-loop recirculation mode.

References

- (1) UN-Water. *2021: Summary Progress Update 2021 – SDG 6 – Water and Sanitation for All*; Geneva, Switzerland, 2021.
- (2) Ma, T.; Sun, S.; Fu, G.; Hall, J. W.; Ni, Y.; He, L.; Yi, J.; Zhao, N.; Du, Y.; Pei, T.; Cheng, W.; Song, C.; Fang, C.; Zhou, C. Pollution Exacerbates China's Water Scarcity and Its Regional Inequality. *Nat Commun* **2020**, *11* (1), 1–9. <https://doi.org/10.1038/s41467-020-14532-5>.
- (3) van Vliet, M. T. H.; Jones, E. R.; Flörke, M.; Franssen, W. H. P.; Hanasaki, N.; Wada, Y.; Yearsley, J. R. Global Water Scarcity Including Surface Water Quality and Expansions of Clean Water Technologies. *Environmental Research Letters* **2021**, *16* (2). <https://doi.org/10.1088/1748-9326/abbfc3>.
- (4) Greenlee, L. F.; Lawler, D. F.; Freeman, B. D.; Marrot, B.; Moulin, P. Reverse Osmosis Desalination: Water Sources, Technology, and Today's Challenges. *Water Res* **2009**, *43* (9), 2317–2348. <https://doi.org/10.1016/j.watres.2009.03.010>.
- (5) Landsman, M. R.; Sujanani, R.; Brodfuehrer, S. H.; Cooper, C. M.; Darr, A. G.; Davis, R. J.; Kim, K.; Kum, S.; Nalley, L. K.; Nomaan, S. M.; Oden, C. P.; Paspureddi, A.; Reimund, K. K.; III, L. S. R.; Yeo, S.; Lawler, D. F.; Freeman, B. D.; Katz, L. E. Water Treatment: Are Membranes the Panacea? *Annual Review in Chemical and Biomolecular Engineering* **2020**, *11*, 559–585. <https://doi.org/https://doi.org/10.1146/annurev-chembioeng-111919-091940>.
- (6) Jones, E.; Qadir, M.; van Vliet, M. T. H.; Smakhtin, V.; Kang, S. mu. The State of Desalination and Brine Production: A Global Outlook. *Science of the Total Environment* **2019**, *657*, 1343–1356. <https://doi.org/10.1016/j.scitotenv.2018.12.076>.
- (7) Honarparvar, S.; Zhang, X.; Chen, T.; Alborzi, A.; Afroz, K.; Reible, D. Frontiers of Membrane Desalination Processes for Brackish Water Treatment: A Review. *Membranes (Basel)* **2021**, *11* (4). <https://doi.org/10.3390/membranes11040246>.
- (8) McCool, B. C.; Rahardianto, A.; Faria, J. I.; Cohen, Y. Evaluation of Chemically-Enhanced Seeded Precipitation of RO Concentrate for High Recovery Desalting of High Salinity Brackish Water. *Desalination* **2013**, *317*, 116–126. <https://doi.org/10.1016/j.desal.2013.01.010>.
- (9) Mickley, M. *Updated and Extended Survey of U.S. Municipal Desalination Plants*; 2018.

- (10) Almulla, A.; Eid, M.; Côté, P.; Coburn, J. Developments in High Recovery Brackish Water Desalination Plants as Part of the Solution to Water Quantity Problems. *Desalination* **2003**, *153* (1–3), 237–243. [https://doi.org/10.1016/S0011-9164\(02\)01142-6](https://doi.org/10.1016/S0011-9164(02)01142-6).
- (11) Malmrose, P.; Lozier, J.; Mickley, M.; Reiss, R.; Russell, J.; Schaefer, J.; Sethi, S.; Manuszak, J.; Bergman, R.; Atasi, K. Z. Committee Report: Current Perspectives on Residuals Management for Desalting Membranes. *J Am Water Works Assoc* **2004**, *96* (12). <https://doi.org/10.1002/j.1551-8833.2004.tb10760.x>.
- (12) National Research Council. *Desalination: A National Perspective*; National Academies Press: Washington, DC, 2008. <https://doi.org/10.17226/12184>.
- (13) Ahmed, M.; Shayya, W. H.; Hoey, D.; Al-Handaly, J. Brine Disposal from Inland Desalination Plants Research Needs Assessment. *Water Int* **2002**, *27* (2), 194–201. <https://doi.org/10.1080/02508060208686992>.
- (14) Pramanik, B. K.; Shu, L.; Jegatheesan, V. A Review of the Management and Treatment of Brine Solutions. *Environ Sci (Camb)* **2017**, *3* (4), 625–658. <https://doi.org/10.1039/c6ew00339g>.
- (15) Xu, P.; Cath, T. Y.; Robertson, A. P.; Reinhard, M.; Leckie, J. O.; Drewes, J. E. Critical Review of Desalination Concentrate Management, Treatment and Beneficial Use. *Environ Eng Sci* **2013**, *30* (8), 502–514. <https://doi.org/10.1089/ees.2012.0348>.
- (16) Mezher, T.; Fath, H.; Abbas, Z.; Khaled, A. Techno-Economic Assessment and Environmental Impacts of Desalination Technologies. *Desalination* **2011**, *266* (1–3), 263–273. <https://doi.org/10.1016/j.desal.2010.08.035>.
- (17) Kim, M. S.; Cha, D.; Lee, S. M.; Jeong, H.; Lee, C. Prediction of Brine Evaporation Rate in a Pond: Development of Different Models under Controlled Meteorological Conditions and Comparative Evaluation. *Desalination* **2023**, *551* (November 2022), 116415. <https://doi.org/10.1016/j.desal.2023.116415>.
- (18) Jensen, V. B.; Darby, J. L. Brine Disposal Options for Small Systems in California's Central Valley. *J Am Water Works Assoc* **2016**, *108* (5), 276–289. <https://doi.org/10.5942/jawwa.2016.108.0045>.
- (19) Tang, X.; Kum, S.; Liu, H. Inland Desalination Brine Disposal : A Baseline Study from Southern California on Brine Transport Infrastructure and Treatment Potential. *ACS ES&T Engineering* **2021**. <https://doi.org/10.1021/acsestengg.1c00276>.

- (20) Panagopoulos, A.; Giannika, V. Comparative Techno-Economic and Environmental Analysis of Minimal Liquid Discharge (MLD) and Zero Liquid Discharge (ZLD) Desalination Systems for Seawater Brine Treatment and Valorization. *Sustainable Energy Technologies and Assessments* **2022**, 53 (PA), 102477. <https://doi.org/10.1016/j.seta.2022.102477>.
- (21) Tong, T.; Elimelech, M. The Global Rise of Zero Liquid Discharge for Wastewater Management: Drivers, Technologies, and Future Directions. *Environ Sci Technol* **2016**, 50 (13), 6846–6855. <https://doi.org/10.1021/acs.est.6b01000>.
- (22) Zhao, D.; Lee, L. Y.; Ong, S. L.; Chowdhury, P.; Siah, K. B.; Ng, H. Y. Electrodialysis Reversal for Industrial Reverse Osmosis Brine Treatment. *Sep Purif Technol* **2019**, 213, 339–347. <https://doi.org/10.1016/j.seppur.2018.12.056>.
- (23) Hansima, M. A. C. K.; Makehelwala, M.; Jinadasa, K. B. S. N.; Wei, Y.; Nanayakkara, K. G. N.; Herath, A. C.; Weerasooriya, R. Fouling of Ion Exchange Membranes Used in the Electrodialysis Reversal Advanced Water Treatment: A Review. *Chemosphere* **2021**, 263, 127951. <https://doi.org/10.1016/j.chemosphere.2020.127951>.
- (24) Wang, R.; Lin, S. Thermodynamics and Energy Efficiency of Zero Liquid Discharge. *ACS ES&T Engineering* **2022**. <https://doi.org/10.1021/acsestengg.2c00013>.
- (25) Al-Karaghoul, A.; Kazmerski, L. L. Energy Consumption and Water Production Cost of Conventional and Renewable-Energy-Powered Desalination Processes. *Renewable and Sustainable Energy Reviews* **2013**, 24, 343–356. <https://doi.org/doi.org/10.1016/j.rser.2012.12.064>.
- (26) Panagopoulos, A. Techno-Economic Assessment of Zero Liquid Discharge (ZLD) Systems for Sustainable Treatment, Minimization and Valorization of Seawater Brine. *J Environ Manage* **2022**, 306 (January), 114488. <https://doi.org/10.1016/j.jenvman.2022.114488>.
- (27) Panagopoulos, A.; Haralambous, K. J.; Loizidou, M. Desalination Brine Disposal Methods and Treatment Technologies - A Review. *Science of the Total Environment* **2019**, 693, 133545. <https://doi.org/10.1016/j.scitotenv.2019.07.351>.
- (28) Balis, E.; Griffin, J. C.; Hiibel, S. R. Membrane Distillation-Crystallization for Inland Desalination Brine Treatment. *Sep Purif Technol* **2022**, 290 (January), 120788. <https://doi.org/10.1016/j.seppur.2022.120788>.

- (29) Sharan, P.; Yoon, T. J.; Thakkar, H.; Currier, R. P.; Singh, R.; Findikoglu, A. T. Optimal Design of Multi-Stage Vacuum Membrane Distillation and Integration with Supercritical Water Desalination for Improved Zero Liquid Discharge Desalination. *J Clean Prod* **2022**, *361* (November 2021), 132189. <https://doi.org/10.1016/j.jclepro.2022.132189>.
- (30) Greenlee, L. F.; Testa, F.; Lawler, D. F.; Freeman, B. D.; Moulin, P. The Effect of Antiscalant Addition on Calcium Carbonate Precipitation for a Simplified Synthetic Brackish Water Reverse Osmosis Concentrate. *Water Res* **2010**, *44* (9), 2957–2969. <https://doi.org/10.1016/j.watres.2010.02.024>.
- (31) Wang, Z.; Chen, G.; Patton, S.; Ren, C.; Liu, J.; Liu, H. Degradation of Nitrilotris-Methylenephosphonic Acid (NTMP) Antiscalant via Persulfate Photolysis: Implications on Desalination Concentrate Treatment. *Water Res* **2019**, *159*, 30–37. <https://doi.org/10.1016/j.watres.2019.04.051>.
- (32) Jain, T.; Sanchez, E.; Owens-Bennett, E.; Trussell, R.; Walker, S.; Liu, H. Impacts of Antiscalants on the Formation of Calcium Solids: Implication on Scaling Potential of Desalination Concentrate. *Environ Sci (Camb)* **2019**, *5* (7), 1285–1294. <https://doi.org/10.1039/c9ew00351g>.
- (33) Oren, Y.; Korngold, E.; Daltrophe, N.; Messalem, R.; Volkman, Y.; Aronov, L.; Weismann, M.; Bouriakov, N.; Glueckstern, P.; Gilron, J. Pilot Studies on High Recovery BWRO-EDR for near Zero Liquid Discharge Approach. *Desalination* **2010**, *261* (3), 321–330. <https://doi.org/10.1016/j.desal.2010.06.010>.
- (34) Loganathan, K.; Chelme-Ayala, P.; Gamal El-Din, M. Treatment of Basal Water Using a Hybrid Electrodialysis Reversal-Reverse Osmosis System Combined with a Low-Temperature Crystallizer for near-Zero Liquid Discharge. *Desalination* **2015**, *363*, 92–98. <https://doi.org/10.1016/j.desal.2015.01.020>.
- (35) Jiang, X.; Tuo, L.; Lu, D.; Hou, B.; Chen, W.; He, G. Progress in Membrane Distillation Crystallization: Process Models, Crystallization Control and Innovative Applications. *Front Chem Sci Eng* **2017**, *11* (4), 647–662. <https://doi.org/10.1007/s11705-017-1649-8>.
- (36) Gabelich, C. J.; Williams, M. D.; Rahardianto, A.; Franklin, J. C.; Cohen, Y. High-Recovery Reverse Osmosis Desalination Using Intermediate Chemical Demineralization. *J Memb Sci* **2007**, *301* (1–2), 131–141. <https://doi.org/10.1016/j.memsci.2007.06.007>.
- (37) Yang, J.; Zhu, M.; Dionysiou, D. D. What Is the Role of Light in Persulfate-Based Advanced Oxidation for Water Treatment? *Water Res* **2021**, *189*. <https://doi.org/10.1016/j.watres.2020.116627>.

- (38) Yang, Y.; Lu, X.; Jiang, J.; Ma, J.; Liu, G.; Cao, Y.; Liu, W.; Li, J.; Pang, S.; Kong, X.; Luo, C. Degradation of Sulfamethoxazole by UV, UV/H₂O₂ and UV/Persulfate (PDS): Formation of Oxidation Products and Effect of Bicarbonate. *Water Res* **2017**, *118*, 196–207. <https://doi.org/10.1016/j.watres.2017.03.054>.
- (39) Li, W.; Jain, T.; Ishida, K.; Liu, H. A Mechanistic Understanding of the Degradation of Trace Organic Contaminants by UV/Hydrogen Peroxide, UV/Persulfate and UV/Free Chlorine for Water Reuse. *Environ Sci (Camb)* **2017**, *3* (1), 128–138. <https://doi.org/10.1039/c6ew00242k>.
- (40) Bao, Y.; Deng, S.; Jiang, X.; Qu, Y.; He, Y.; Liu, L.; Chai, Q.; Mumtaz, M.; Huang, J.; Cagnetta, G.; Yu, G. Degradation of PFOA Substitute: GenX (HFPO-DA Ammonium Salt): Oxidation with UV/Persulfate or Reduction with UV/Sulfite? *Environ Sci Technol* **2018**, *52* (20), 11728–11734. <https://doi.org/10.1021/acs.est.8b02172>.
- (41) Kum, S.; Tang, X.; Liu, H. Treatment of Brackish Water Inland Desalination Brine via Antiscalant Removal Using Persulfate Photolysis. *Environ Sci (Camb)* **2023**. <https://doi.org/https://doi.org/10.1039/D2EW00924B>.
- (42) Benjamin, M. M. *Water Chemistry*, 2nd ed.; Waveland Press, Inc, 2014.
- (43) Kedem, O.; Zalmon, G. Compact Accelerated Precipitation Softening (CAPS) as a Pretreatment for Membrane Desalination I. Softening by NaOH. *Desalination* **1997**, *113* (1), 65–71. [https://doi.org/10.1016/S0011-9164\(97\)00115-X](https://doi.org/10.1016/S0011-9164(97)00115-X).
- (44) King Lee Technologies. Pretreat Plus Y2K Inforsheet. King Lee Technologies: San Diego, CA 2020, p 1.
- (45) Neta, P.; Huie, R. E.; Ross, A. B. Rate Constants for Reactions of Aliphatic Carbon-Centered Radicals in Aqueous Solution. *J Phys Chem Ref Data* **1988**, *17*, 1027. <https://doi.org/doi.org/10.1063/1.555808>.
- (46) Buxton, G. V.; Greenstock, C. L.; Helman, W. P.; Ross, A. B. Critical Review of Rate Constants for Reactions of Hydrated Electrons, Hydrogen Atoms and Hydroxyl Radicals in Aqueous Solution. *J Phys Chem Ref Data* **1988**, *17* (2), 513–886. <https://doi.org/10.1063/1.555805>.
- (47) Yu, X. Y.; Bao, Z.-C.; Barker, J. R. Free Radical Reactions Involving Cl₂·, Cl₂·-, and SO₄·- in the 248 Nm Photolysis of Aqueous Solutions Containing S₂O₈²⁻ and Cl₂·-. *Journal of Physical Chemistry Association* **2004**, *108* (2), 295–308. <https://doi.org/10.1021/jp036211i>.

- (48) Davis, M. L. Lime-Soda Softening. In *Water and Wastewater Engineering: Design Principles and Practice*; McGraw-Hill Education: New York, 2020.
- (49) Greenlee, L. F.; Testa, F.; Lawler, D. F.; Freeman, B. D.; Moulin, P. Effect of Antiscalant Degradation on Salt Precipitation and Solid/Liquid Separation of RO Concentrate. *J Memb Sci* **2011**, *366* (1–2), 48–61.
<https://doi.org/10.1016/j.memsci.2010.09.040>.

Chapter 5

Mechanisms of Alleviating Gypsum Scaling by Antiscalants during Membrane Desalination: Implications on Agricultural Drainage Water Reuse

Previously published in *ACS ES&T Water*

Tang, X., & Liu, H. (2024). Mechanisms of Alleviating Gypsum Scaling by Antiscalants during Membrane Desalination: Implications on Agricultural Drainage Water Reuse. *ACS ES&T Water*, 4(8), 3486-3494. <https://doi.org/10.1021/acsestwater.4c00298>

Abstract

Agricultural drainage water has great potential as a freshwater supply via reverse osmosis (RO) membrane desalination. However, high calcium and sulfate concentrations in the drainage water lead to gypsum ($\text{CaSO}_{4(s)}$) scaling during the RO process. This study investigated the effects of three antiscalants, *i.e.*, two phosphonate-based (DTPMP and NTMP) and one polymer-based (PAA), as well as pH and natural organic matter (NOM) on alleviating gypsum scaling during RO desalination of drainage water and illustrated the gypsum inhibition mechanism of three antiscalants. Results showed that 1 μM of DTPMP was sufficient to prevent gypsum scaling within 24 hours of RO desalination, while both NTMP and PAA required 5 μM of dosage. At acidic pH 3, the permeate flux with 5 μM of DTPMP remained relatively stable, whereas the flux with NTMP and PAA decreased by 35% and 80% respectively. Furthermore, the presence of NOM did not significantly affect the antiscalant inhibitive capacity. The gypsum inhibition mechanism of DTPMP and NTMP was primarily contributed by negative charge repulsion, with higher pH increasing the total charge of antiscalant aqueous species, thereby strengthening the repulsive forces among calcium, sulfate, and gypsum nuclei. In contrast, PAA's gypsum inhibition mechanism involved both negative charge repulsion and crystal lattice distortion, which distorted gypsum crystals into irregular shapes and smaller sizes, preventing the formation of large-size gypsum precipitates under neutral and alkaline conditions, but deteriorating membrane scaling under acidic conditions. Ultimately, an ideal antiscalant for preventing gypsum scaling during RO desalination of

agricultural drainage water would preserve higher negative charges without changing precipitate morphology.

Keyword:

Desalination, agricultural drainage water, antiscalant, gypsum scaling, charge repulsion

Introduction

Fresh water scarcity has increasingly posed risks to agricultural irrigation and food production worldwide.¹⁻³ Meanwhile, agricultural irrigation accounts for up to 85% of total global water consumption and generates drainage wastewater from crop field irrigation.^{4,5} This drainage water can potentially be treated and reused as an alternative freshwater resource; however, it is chemically unique, characterized by high salinity and elevated hardness. High salinity is primarily contributed by interactions with saline soil and evaporation. The total dissolved solids (TDS) of agricultural drainage water ranges from 3000 to 30000 mg/L.⁶ Major chemical constituents include hardness ions, sodium, sulfate and chloride. The calcium concentration of hardness ions ranges from 200 to 600 mg/L, and the sulfate concentration ranges between 2000 to 20000 mg/L.⁶ Without appropriate treatment and reuse, the discharge of drainage water deteriorates soil productivity and creates environmental hazards.

Desalination of drainage water via reverse osmosis (RO) can produce fresh water,⁷⁻¹⁰ however, high concentrations of calcium and sulfate in the drainage water lead to oversaturation and precipitation of $\text{CaSO}_{4(s)}$, a mineral known as gypsum, on the membrane surface, inducing severe membrane scaling and paralyzing the desalination process.¹¹ To alleviate membrane scaling, antiscalants are added to the feedwater to delay mineral precipitation and increase RO permeate flux.¹²⁻¹⁶ There are two most common types of antiscalants based on the active functional groups: phosphonate and polymeric antiscalants.¹⁷⁻²¹ Phosphonate antiscalants contain $-\text{C-PO}(\text{OH})_2$ functional groups with a core covalent carbon-phosphorus (C-P) bond framework.²² Typical phosphonate

antiscalants include nitrilotri-methylphosphonic acid (NTMP) and diethylenetriaminepentakis-methylphosphonic acid (DTPMP). Polymeric antiscalants contain –R-COOH carboxylic functional groups on a polymeric backbone, with polyacrylic acid (PAA) being the most typical one.²¹ Different mechanisms of antiscalant inhibition have been reported. For example, both polymeric and phosphonate antiscalants were reported to complex with mineral cations, preventing it from forming crystals with anions.^{23–25} Carboxylate polymeric antiscalants were reported to strongly affect CaCO₃ crystallization and morphology.²⁶ Another study revealed that polyacrylate antiscalant adsorbed onto the calcite surface or complexed with calcium. This process generated negative charge and repulsive forces, facilitating the dispersion of small calcite crystals or the dissociation of calcium cations and carbonate anions.²⁷ Despite this, the inhibition mechanism of DTPMP, NTMP and PAA on gypsum scaling during drainage water desalination remains unclear.

The type and concentration of antiscalant directly affect its inhibitive performance on membrane scaling; however, the effects of phosphonate and polymeric antiscalants on gypsum scaling during the desalination of drainage water remain unexplored. Prior studies focused on different antiscalants, including commercial antiscalants whose compositions are confidential, and scaling of minerals not associated with agricultural drainage water, such as calcium carbonate, calcium phosphate or hydroxyapatite.^{28–32} In other instances, DTPMP was reported to exhibit the longest induction time to delay hydroxyapatite precipitation among phosphonate antiscalants,²⁸ but its effect on gypsum remains unknown. Therefore, it is important to comparatively investigate commonly used

phosphonate and polymeric antiscalant (DTPMP, NTMP and PAA) on gypsum scaling inhibition during the drainage water RO desalination.

Furthermore, feedwater pH affects the chemical speciation of antiscalant and consequently its inhibitive performance; however, the underlying mechanism of pH effect on antiscalant inhibitive capacity has not been fully evaluated. For example, one study found that with a commercial antiscalant (PermaTreat PC-504), flux decline at pH 5.5 is four times higher than that at pH 7.7 after 24 hours of drainage water desalination.³³ Another study suggested that acidic pH leads to protonation of commercial phosphonate antiscalant (PC-191) and increases the precipitation rate of gypsum.³⁴ Therefore, it is critical to quantitatively illustrate the mechanism of pH effect on the gypsum inhibitive capacity of antiscalants in drainage water RO desalination.

In addition, natural organic matter (NOM) up to several mg/L can exist in agricultural drainage water, but its interaction with antiscalants and its impact on the inhibitive capacity remain unknown. Prior studies mainly evaluated biologically derived organic matter such as alginate and bovine serum albumin on gypsum scaling. For example, alginate was reported to worsen RO flux decline during gypsum-dominated feedwater desalination.^{35,36} Contrarily, alginate was also reported to alleviate gypsum scaling at low concentration.^{37,38} The effect of terrestrial NOM remains unknown.

Accordingly, this study had several objectives. Firstly, it aimed to investigate the dosage effects of three most typical antiscalants (DTPMP, NTMP and PAA) with two most representative functional groups. Secondly, it examined the effect of feedwater pH and the presence of NOM on alleviating gypsum scaling during agricultural drainage water

RO desalination. Thirdly, it elucidated the mechanism of antiscalant inhibitive capacity on gypsum precipitation under different chemical conditions. At last, it established a chemical equilibrium model to quantify the antiscalant molecular speciation and its inhibitive capacity.

Methods and Materials

Chemicals and Materials

Three antiscalants - NTMP, DTPMP and PAA were purchased from Sigma-Aldrich. Their molecular structures were provided in Table S1 in the supporting information (SI). To evaluate the effects of antiscalants on membrane scaling, two types of synthetic agricultural drainage water were prepared based on previously reported drainage water chemistry from the Central Valley, Calif.⁶ The detailed chemical composition is listed in Table 1. Specifically, synthetic drainage water I was prepared using only CaCl₂ and Na₂SO₄ and used for experiments investigating the effects of antiscalant type and dosage, feedwater pH and NOM on gypsum scaling. Synthetic drainage water II was prepared using a comprehensive list of chemicals to examine the performance of optimized antiscalant condition during RO desalination of drainage water.⁶

Experimental Setup and Design

A lab-scale recirculation mode RO desalination unit was built for the experiments, with detailed components and preparation outlined in SI (Text S1 and Figure S1). A polyamide RO membrane (BW30XFRLE, FilmTec™) was selected for all RO experiments. This membrane is commercially available and widely used in the industry and using the same RO membrane with a negative surface charge offset the effect of the

membrane in the subsequent discussion of antiscalant effect.^{39,40} To understand the effect of antiscalant type and concentration, RO experiments were conducted in the recirculation mode, using synthetic drainage water I as the feedwater and dosed with one of the three antiscalants (DTPMP, NTMP or PAA) at a dosage ranging from 0.5 to 5 μM . This concentration range falls within the typical range of antiscalant concentrations used in RO applications.²⁸ To understand the effect of drainage water pH, additional RO experiments were conducted using synthetic drainage water I with pH ranging from 3 to 11. All antiscalant dosages were selected at 5 μM , which is the threshold concentration of NTMP and PAA, to exclude the effect of antiscalant concentration and to better illustrate the effect of acidic pH. The pH was adjusted before the RO experiments using 5 mM HCl or NaOH, and it remained relatively stable throughout the 24-hour RO desalination. To understand NOM effect, additional RO experiments were conducted using synthetic drainage water I with 5 mg C/L Suwannee River NOM (IHSS, 2R101N) as the feedwater, and the DTPMP dosage was controlled at 1 μM . Furthermore, to investigate the effectiveness of optimized antiscalant conditions, RO experiments were conducted using synthetic drainage water II with a DTPMP dosage of 1 μM .

Each desalination experiment was conducted for a duration of 24 hours. 3 mL of RO feedwater and permeate samples was collected at 0 and 24 hours, filtered through 0.22- μm filters to measure dissolved calcium concentrations. In selected PAA experiments, unfiltered feedwater samples were withdrawn using a syringe from the feedwater reservoir after 12 hours of desalination for particle size measurement. All aqueous samples were prepared in duplicate and analyzed within 24 hours. At the end of the RO

experiments, the RO membrane was preserved and dried in a desiccator at 25 °C, and the scaling layer was analyzed through membrane surface characterization within 24 hours.

Analytical Methods

Real-time RO permeate flux was calculated by continuously measuring the weight of RO permeate and converting it to volume-based values. The normalized permeate flux was calculated by dividing the permeate flux at any given time during the RO experiment by the flux at the beginning of the experiment. The dissolved calcium concentration in the permeate and feedwater samples was measured using Inductively Coupled Plasma Mass Spectrometry (ICP-MS, Agilent 7700 series). The concentration of precipitated calcium as solid was calculated as the difference between the initial total calcium concentration in the feedwater and the total dissolved calcium concentration at any given time during the RO experiment. The particle size of gypsum precipitates in the feedwater after 12 hours of desalination was measured using Dynamic Light Scattering (DLS, Malvern Zetasizer Nano ZS90). The membrane surface scaling layer was characterized by Scanning Electron Microscopy (SEM) and Energy Dispersive X-ray Spectroscopy (EDS) (TESCAN Vega3 SBH).

Results and Discussions

Effect of Different Antiscalant on Gypsum Scaling

Among the three antiscalants, DTPMP exhibited the strongest inhibitive capacity on gypsum scaling, while NTMP demonstrated the weakest inhibitive capacity. In the recirculation mode of the desalination process, flux will naturally decline due to increasing ionic strength of feedwater. Figure 1A showed that, in the presence of 1 μM

DTPMP, the desalination of drainage water exhibited the smallest flux decline rate among the three antiscalants. In contrast, NTMP and PAA demonstrated unique flux decline due to the onset of gypsum precipitation, as the flux decline rate dramatically increased during the 24 hours of desalination. The flux with PAA started to drop significantly at a much later time than that with NTMP, indicating that PAA has a stronger ability to delay gypsum precipitation than NTMP. Furthermore, the flux decline with PAA was more rapid than that with NTMP after 15 hours of desalination when gypsum started to precipitate. Ultimately, the flux with both NTMP and PAA reached a stable low level, similar to the antiscalant-free scenario.

To evaluate the effectiveness of different antiscalants, a normalized permeate flux percentage was calculated as the normalized flux with different antiscalants after 24 hours of desalination with respect to the flux with DTPMP. A low percentage indicates weaker antiscalant inhibitive capacity compared to DTPMP at the same concentration. Figure 1B showed that at 5 μM antiscalant concentration, all three antiscalant exhibited similar inhibitive capacity. When antiscalant concentration decreased to 1 μM , the normalized permeate flux percentage with PAA or NTMP declined to around 75%, which was much lower compared to that with DTPMP. When antiscalant concentration further decreased to 0.5 μM , the normalized permeate flux percentage with NTMP slightly decreased to 70% while that with PAA decreased to approximately 55%. Although the permeate flux performance with 0.5 μM DTPMP is similar to that with 1 μM DTPMP, approximately 5% calcium precipitation was observed after 24 hours (Figure S2D). Therefore, the threshold concentration of DTPMP was determined as 1 μM due to a

complete inhibition of gypsum scaling. This value is the lowest compared to that of the other two antiscalants (5 μM). The results confirmed that DTPMP has the strongest inhibitive capacity on gypsum scaling among the three antiscalants, and PAA at low concentrations can induce a more severe permeate flux decline compared to the others.

Membrane Scaling Surface Characterization

Membrane scaling surface characterization showed that the addition of 1 μM DTPMP during drainage water desalination prevented the formation of membrane scaling layer, while the addition of 1 μM NTMP or PAA was unable to prevent scaling layer formation. Specifically, no gypsum scaling layer was observed after 24 hours of desalination in the presence of 1 μM DTPMP (Figure 2A). In contrast, the gypsum scaling layer observed with 1 μM NTMP was dominated by large and long prismatic gypsum precipitates with sizes of 100-150 μm (Figure 2B), while the scaling layer observed with 1 μM PAA mostly consisted of condensed small particles with sizes of 5-15 μm (Figure 2C). The morphology of the gypsum scaling layer formed in the control without antiscalant addition is similar to that in the presence of 1 μM NTMP (Figure 2D). Elements of calcium, sulfur, and oxygen were identified by EDS in the membrane scaling layer formed in the presence of 1 μM NTMP or PAA, while no calcium element was detected on the membrane surface with 1 μM DTPMP (Figure S3). The chemical composition of the surface scaling layer further confirmed gypsum as the main precipitates on the membrane scaling layer (Table S2). The results confirmed that DTPMP was the most effective antiscalant, and PAA promoted the formation of a more condensed scaling

layer, which was consistent with the observed higher flux decline in the presence of PAA when gypsum precipitation started (Figure 1A).

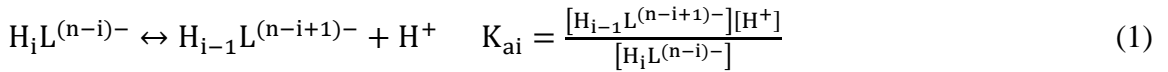
Effect of pH on Gypsum Scaling

Experimental results showed that an increase in pH was beneficial to antiscalant inhibitive capacity and enhanced RO performance, while an extremely acidic pH lower than 4 compromised antiscalant effectiveness and desalination performance. Specifically, among the three antiscalants, the inhibitive capacity of DTPMP exhibited the strongest resistance to pH changes, while PAA inhibitive capacity was the most sensitive one to feedwater pH. Figure 3A showed, in the presence of 5 μ M DTPMP, the normalized RO permeate flux after 12 hours of desalination did not change significantly as pH decreased from 11 to 3. In contrast, in the presence of 5 μ M NTMP or PAA, the normalized permeate flux was stable when the feedwater pH decreased from pH 11 to 4 but exhibited a dramatic decrease when the feedwater pH further decreased from 4 to 3. Normalized RO permeate flux after 24 hours showed a similar trend (Figure S4). Specifically, the flux at 12 hours of desalination declined approximately 35% from pH 4 to 3 in the presence of NTMP and declined approximately 80% in the presence of PAA. In addition, 24-hour flux decline with DTPMP did not significantly change from pH 11 to 3 while both NTMP and PAA showed much stronger flux decline when pH decreased to 3 (Figure S5).

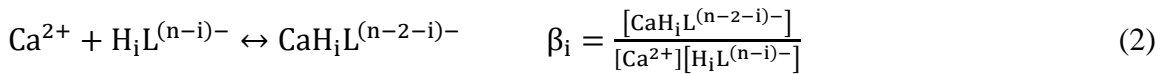
Mechanisms of Antiscalant Inhibition on Gypsum Scaling

Our evaluation discovered that the inhibitive capacity of antiscalants on gypsum precipitation was closely associated with the total charges of antiscalant aqueous species. A higher total charge led to a stronger dispersion of cations, anions, and precipitate

nuclei, resulting in a stronger inhibitive capacity. Specifically, all antiscalants are protic acids that undergo equilibrium speciation. DTPMP and NTMP are multiprotic phosphonic acids with 10 and 6 pK_a values, respectively (pK_a values of DTPMP are 1.04, 2.08, 3.11, 4.15, 5.19, 6.23, 7.23, 8.3, 11.18, 12.58; pK_a values of NTMP are 0.3, 1.5, 4.64, 5.86, 7.3, 12.1).^{24,25} In contrast, PAA is a monoprotic acid with a pK_a value of 3.5.⁴¹ The acid-base equilibrium of antiscalants is expressed as:



where L symbolizes the deprotonated antiscalant molecular structure, K_{ai} is the equilibrium constant of antiscalant speciation in its ith step of deprotonation, and n is the maximal protonation number. For NTMP, n equals 6 and i ranges from 1 to 6. For DTPMP, n equals 10 and i ranges from 1 to 10. For PAA, n and i equal to 1 (Text S2). In calcium-rich drainage water, different protonated antiscalant acids-base species can react with calcium to form Ca-antiscalant complexes.^{24,25} Complexation reactions between antiscalants aqueous species and calcium are:



For NTMP, there are 5 complexation equations and i ranges from 0 to 4. For DTPMP, there are 8 complexation equations and i ranges from 2 to 9. For PAA, there are 2 complexation equations and i ranges from 0 to 1. The equilibrium constants available in the current literature only include the complexation between one mole of calcium and one mole of an antiscalant. In the case of inorganic anions, chloride and sulfate exhibit monodentate complexation with calcium.⁴² Therefore, only the complexation between

one mole of calcium and one mole of either antiscalant or inorganic anions was considered in the theoretical calculation. (detailed reactions and calculations are listed in Text S2).

Consequently, the total value of negative charge of antiscalant aqueous species (denoted as Φ) is calculated by adding the charges of all conjugate acid/base species and calcium complexes at a specific feedwater pH:

$$\Phi = \sum \left([H_i L^{(n-i)-}] (n - i) + [CaH_i L^{(n-2-i)-}] (n - 2 - i) \right) \quad (3)$$

The negative charge repulsion mechanism plays an important role in gypsum inhibition.

Calculations showed that the total charges of DTPMP or NTMP aqueous species gradually increased with the increase of pH, while the total charges of PAA aqueous species increased dramatically with pH increasing from 3 to 4 but remained stable with pH increasing from 4 to 11 (Figure 3B). In addition, for DTPMP and NTMP, the total negative charge contributed by Ca-antiscalants species dramatically increased when the pH increased above 4 (Figure S6A, S6B). In contrast, the total negative charge of PAA species was only contributed by the deprotonated PAA species from pH 3 to 11 (Figure S6C), which indicated that the pH-charge profile shares a similar trend with the pH-concentration profile of deprotonated PAA. When the total negative charge was mainly contributed by Ca-antiscalant species, negatively charged antiscalant species complexed with calcium while repelling negative sulfate anions, preventing the formation of gypsum nuclei.^{43,44} When the total negative charge was mainly contributed by deprotonated antiscalant species, small gypsum nuclei would be wrapped by negatively charged antiscalant species through adsorption. Then the negative surface charge of gypsum

nuclei would provide strong repulsive force against other negatively charged wrapped gypsum nuclei, maintaining dispersion of small gypsum nuclei and delaying its aggregation in solution.^{43–45}

Threshold concentration is a boundary value which represents the minimum total negative charge to prevent gypsum scaling within 24 hours of RO desalination of drainage water. When the total negative charge exceeds this threshold concentration, negative charge-driven repulsive interactions are sufficient to inhibit gypsum scaling within 24 hours of RO desalination. As a result, further increases in negative charge repulsion do not improve flux. Conversely, when the total negative charge is below the threshold concentration, the permeate flux increases with the enhancement of negative charge repulsion. For DTPMP, the total negative charge increased, and the negative charge repulsion effect was strengthened as the pH increased from 3 to 11; however, the flux with DTPMP remained relatively stable. In contrast, for NTMP, the flux increased with the total negative charge when the pH increased from 3 to 4 but became relatively stable when the pH increased above 4 (Figure 3). This was because the total negative charge of DTPMP species at pHs 3 to 11, and NTMP species at pHs 4 to 11, were all higher than the threshold concentration, which was determined as approximately 5×10^{-4} mol/L total charge per mol/L of Ca^{2+} in the feedwater (Figure 3B). Therefore, even though the total charge of both NTMP and DTPMP species continued to increase as the pH increased from 4 to 11, the permeate flux could no longer be improved as the charge repulsion was already strong enough to inhibit gypsum precipitation.

In addition, compared to DTPMP and NTMP, the concentration of total negative charge of PAA species was significantly lower while maintaining high permeate flux (Figure 3), which cannot be explained solely by the negative charge repulsion mechanism. Crystal lattice distortion was likely to contribute as an additional mechanism, which led to PAA inhibition on gypsum scaling at neutral and alkaline pHs, while deteriorated membrane scaling at acidic pHs. Membrane surface characterization showed that the addition of 1 μM PAA resulted in a distinctly more condensed scaling layer, composed of small, irregularly shaped gypsum particles, compared to large and long prismatic gypsum particles of 1 μM NTMP under neutral pH (Figure 2C vs. Figure 2B). This indicated that, under neutral and alkaline conditions, PAA can distort precipitated minerals into irregular shapes and smaller sizes, likely due to its adsorption onto the active surface sites of gypsum crystals.^{21,45,46} Consequently, these small, irregularly shaped crystals are less likely to collide, grow, deposit onto the membrane surface and form a condense scaling layer, contributing to gypsum inhibition mechanism of PAA. When the dosage of PAA exceeded its threshold concentration (5 μM), the formation of large, cohesive scale deposits was prevented within 24-hour RO desalination (Figure S2), despite the lower total negative charge of PAA species compared to other antiscalants. However, when the concentration of PAA was below the threshold, both charge repulsion and morphology distortion were weakened, leading to earlier gypsum precipitation and the formation of small, irregularly shaped crystals (Figure 2).

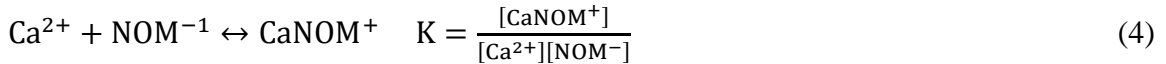
To better understand the dramatic decline in normalized flux and the role of the two PAA inhibition mechanisms under acidic pH, the particle size of gypsum crystals and the

percentage of total calcium as gypsum after 12 hours of drainage water desalination were measured. With 5 μM of PAA, when the pH increased from 3 to 4, the particle size of gypsum crystals increased from 180 to 370 nm. Meanwhile, both the precipitated calcium fraction and the flux decline slope decreased (Figure 4 and S7). This result indicated that at pH 3, weaker negative charge repulsion was less effective in maintaining the dispersion of small gypsum crystals. Simultaneously, stronger PAA-induced morphology distortion made the irregular-shaped gypsum crystals harder to grow. These two mechanisms collectively resulted in faster precipitation of irregular-shaped gypsum with smaller size, forming a much more condensed gypsum scaling layer on the membrane surface, and inducing a severe flux decline and poorer desalination performance. In contrast, at pH 4, stronger negative charge repulsion was more effective at maintaining dispersion of relatively larger gypsum crystals, while weaker morphology distortion by PAA allowed the formation of larger, irregular-shaped gypsum crystals. This caused slower precipitation of larger, irregular-shaped gypsum crystals, resulting in a relatively less condensed scaling layer, leading to improved permeate flux and better desalination performance.

Effect of NOM on Gypsum Scaling

The effect of NOM on the gypsum inhibitive capacity of the most effective antiscalant, *i.e.*, DTPMP was evaluated. Results showed that the presence of NOM did not compromise DTPMP inhibitive capacity. When dosed with 1 μM DTPMP, the presence of NOM did not affect the flux decline trend. In the control without DTPMP, the addition of 5 mg C/L NOM led to a much faster flux decline than that without NOM (Figure 5A).

Membrane surface characterization further confirmed NOM did not induce membrane scaling with DTPMP addition. Without DTPMP addition, condensed small gypsum particles depositing on the membrane surface were observed with the addition of NOM (Figure 5B), indicating NOM has a similarity compared to PAA as they both can change the gypsum crystal morphology. In contrast, with the addition of DTPMP, only a small amount of large and long prismatic crystals was observed on the membrane surface (Figure 5C), and nearly no calcium precipitation at 24 hours was detected (Figure S8). NOM mostly consists of humic acid and fulvic acid. In drainage water pH, NOM exists in a deprotonated form (NOM^{-1}), which complexes with calcium as:



The pK value was obtained from a previous study (Text S2).⁴⁷ Calculation showed that complexation between calcium and up to 10 mg C/L NOM was negligible as it did not change the concentration of the total negative charge of DTPMP species (Figure S9) and thus did not affect DTPMP speciation and complexation with calcium. This result confirmed that NOM in drainage water did not affect the negative charges of antiscalant species and its inhibitive capacity.

Engineering Implications

To further evaluate the engineering application of desalination of drainage water with complex chemistry, an additional proof-of-concept experiment was conducted using a synthetic drainage water with comprehensive chemical compositions. Results showed that the addition of 1 μM DTPMP effectively inhibited gypsum precipitation in RO desalination of agricultural drainage water. With the addition of 1 μM DTPMP, the flux

decline was minimal after 7 hours of RO desalination (Figure S10). In contrast, without the addition of DTPMP, the flux dropped rapidly within the first hour of desalination. From the aspect of engineering application, DTPMP is the optimal antiscalant for gypsum-dominated drainage water desalination compared to NTMP and PAA. Aqueous acid-base speciation and calcium complexation with DTPMP leads to a high concentration of total negative charges, resulting in a stronger ability to maintain dispersion of calcium, sulfate, and gypsum nuclei in the solution. It is less sensitive to extreme pH conditions and remains effective even if NOM and other inorganic anions are present in the feedwater.

Results from this study also provide insight into the selection and development of future antiscalants for desalination applications. Specifically, antiscalants with multiple functional groups that can lead to a high negative charge are a better choice as they can maintain stronger electrostatic repulsion between hardness ions and nuclei. In addition, antiscalants that can distort precipitate morphology into irregular shapes and smaller sizes should be used with caution, especially under acidic conditions, as the formation of small, irregularly shaped scaling particles can worsen membrane scaling issues.

Conclusions

This study evaluated the inhibitive capacity of three antiscalants, DTPMP, NTMP and PAA, on gypsum-dominated drainage water RO desalination under varying conditions of antiscalant dosage, feedwater pH, and the presence of NOM. The underlying inhibition mechanisms were illustrated for the first time. At the same antiscalant concentration, DTPMP was the most effective antiscalant in inhibiting gypsum precipitation. In addition,

acidic pH conditions compromised antiscalant inhibitive capacity, while neutral and alkaline conditions did not. The sensitivity ranking to acidic pH conditions was PAA > NTMP > DTPMP. Furthermore, the presence of NOM did not negatively affect the effectiveness of DTPMP on gypsum inhibition.

The gypsum inhibition mechanism for DTPMP and NTMP was attributed to negative charge repulsion. When the total negative charge exceeded the threshold concentration, optimal permeate flux performance was maintained. In contrast, PAA's gypsum inhibition mechanism involved both negative charge repulsion and crystal lattice distortion. This led to the formation of a condensed scaling layer composed of small, irregularly shaped gypsum particles, which caused a significant decline in permeate flux under acidic pH conditions. Ultimately, an antiscalant that can preserve higher negative charges without changing precipitate morphology, such as DTPMP, is ideal for preventing gypsum scaling during RO desalination of agricultural drainage water.

Supporting information

Please refer to Appendix D for Supporting Information.

Table 5-1. Chemical compositions of two types of synthetic drainage water.

Parameters	Drainage water I*	Drainage water II**	Unit
Na⁺	225	374	mM
Ca²⁺	20	35	mM
Cl⁻	39	91	mM
SO₄²⁻	112	202	mM
K⁺	—	0.4	mM
Mg²⁺	—	36	mM
H₃BO₃	—	6.6	mM
HCO₃⁻	—	13	mM
F⁻	—	1.6	mM
NO₃⁻	—	2.3	mM
SiO₃²⁻	—	1.6	mM
PO₄³⁻	—	0.01	mM
TOC	—	5	mg/L
pH	7.6	7.6	—
TDS	18123	34669	mg/L
Ionic strength	0.3	0.5	M

*: Type I feedwater ionic strength was set at median level, 0.3M, to study effect of antiscalant type and concentration, effect of pH and NOM.

** : Type II feedwater ionic strength was set at the upper range level, 0.5M, to evaluate optimized antiscalant condition

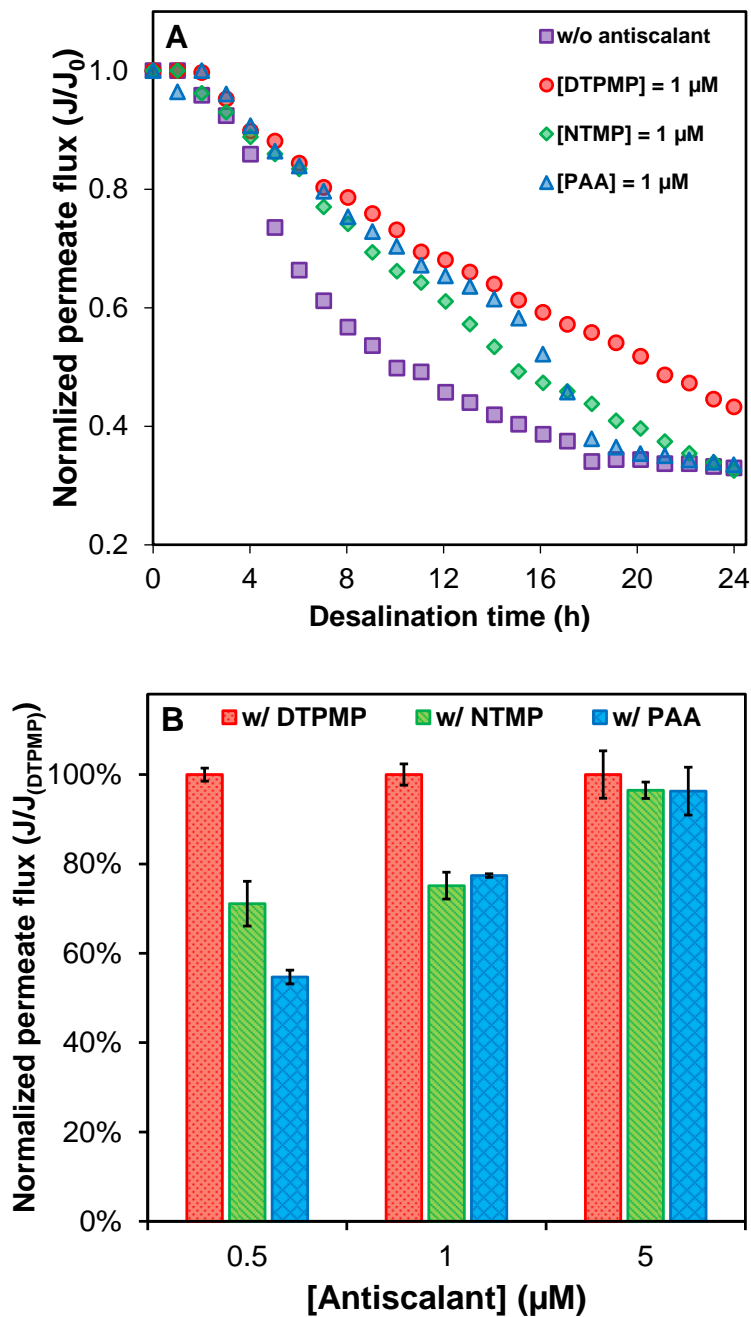


Figure 5-1. Effect of antiscalant type and concentration on RO permeate flux. (A) Effect of different antiscalants on RO permeate flux. Value of y-axis was calculated as permeate flux (time t) divided by permeate flux (time 0). (B) Comparison of permeate flux with different antiscalant types and concentration at 24 hours desalination. Value of y-axis was calculated as permeate flux (24h, with different antiscalants) divided by permeate flux (24h, with DTPMP). Feedwater using synthetic drainage water I.

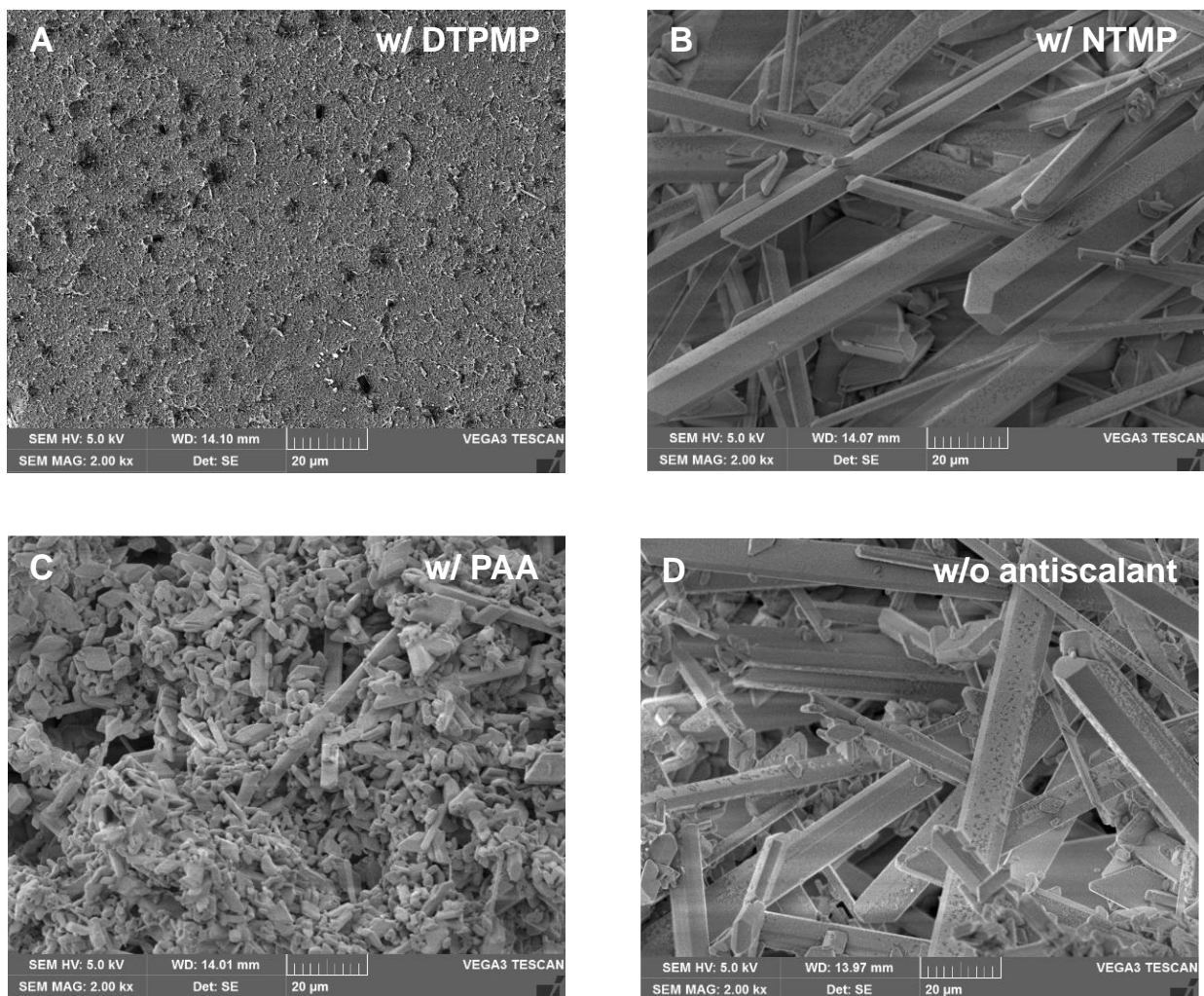


Figure 5-2. Effects of different antiscalants on the scaling layer of RO membrane surface after 24 hours of RO desalination using synthetic drainage water I as the feedwater. (A) [DTPMP]=1 μM; (B) [NTMP]=1 μM; (C) [PAA]=1 μM; (D) without any antiscalant.

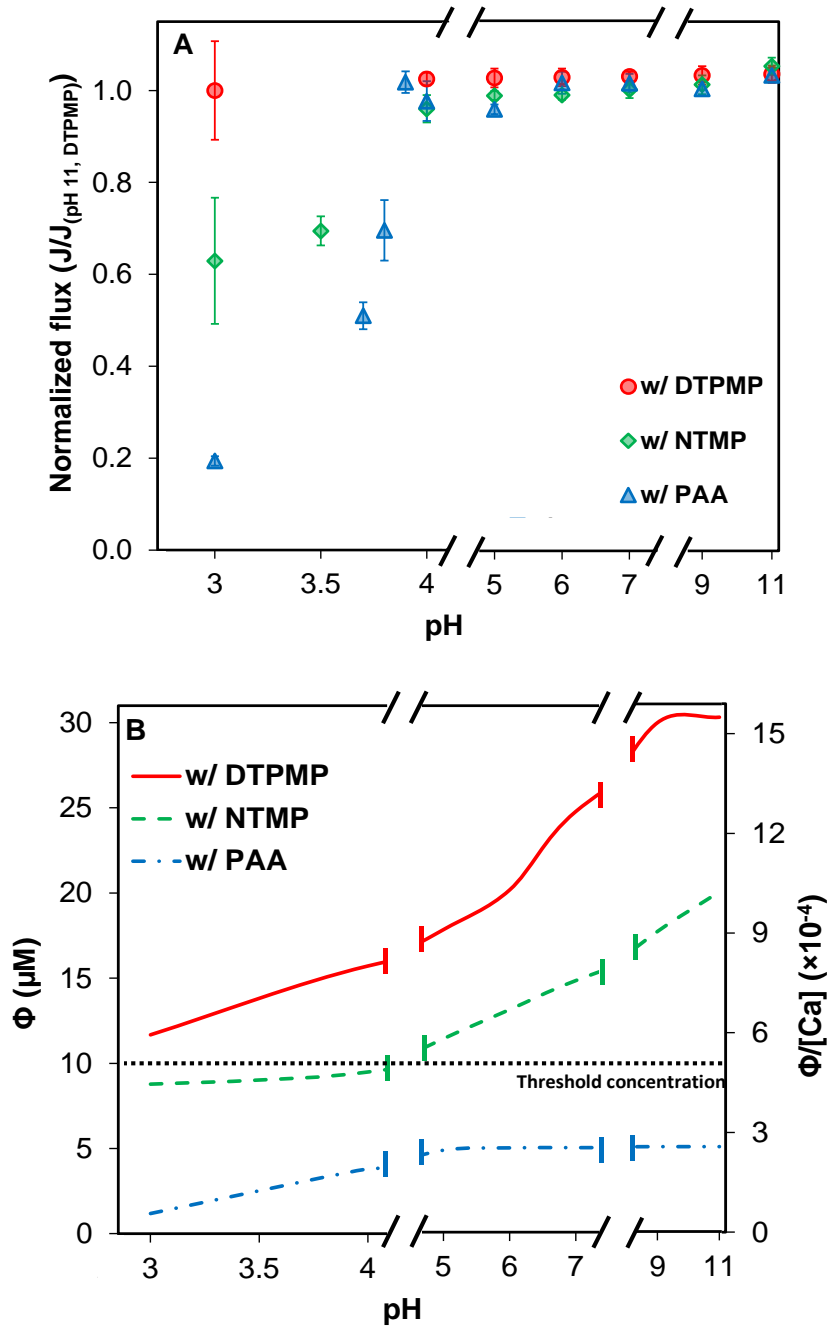


Figure 5-3. (A) Effect of pH on normalized flux (flux / flux (pH 11, 5 μM DTPMP)) at 12 hours with different antiscalants. (B) Effect of pH on concentration of total charges of antiscalants species (Φ). Feedwater using synthetic drainage water I with 5 μM NTMP or DTPMP or PAA under various pH.

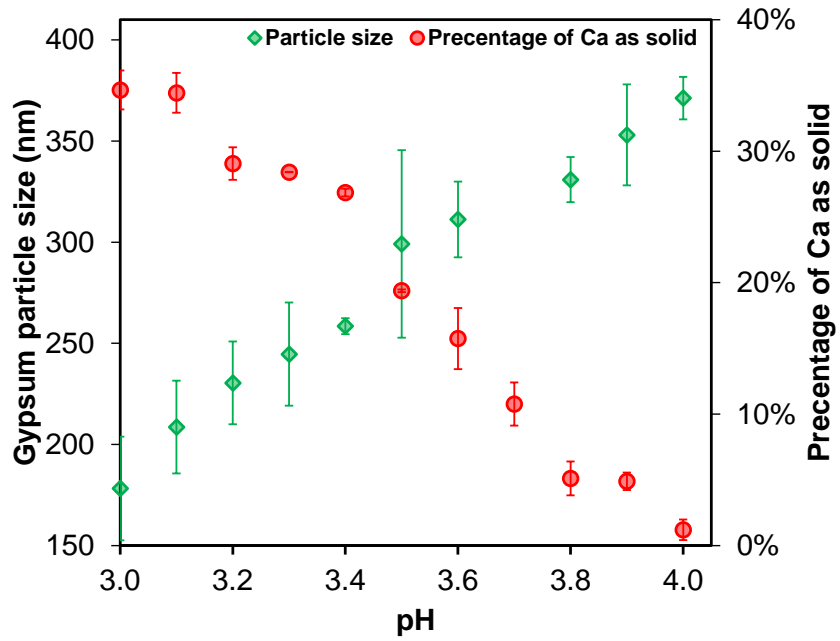


Figure 5-4. Effect of acidic pH on particle size of gypsum precipitates and percentage of calcium as solid at 12 hours of RO desalination. Feedwater using synthetic drainage water I with 5 μ M PAA.

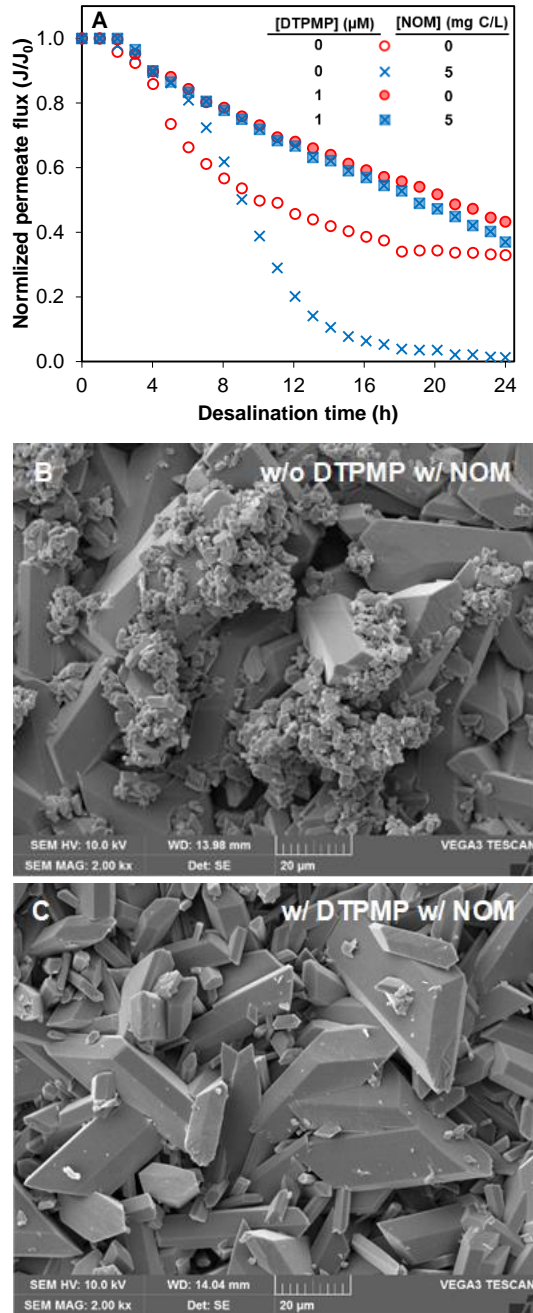


Figure 5-5. Effect of NOM on RO permeate flux and membrane surface characteristics. (A) Effect of NOM on permeate flux with or without DTPMP. (B) Membrane surface characteristics after 24 hours RO desalination with NOM but without DTPMP addition, (C) with both NOM and DTPMP addition. Feedwater using synthetic drainage water I with or without 1 μM DTPMP or 5 mg C/L NOM.

Reference

- (1) Vallino, E.; Ridolfi, L.; Laio, F. Measuring Economic Water Scarcity in Agriculture: A Cross-Country Empirical Investigation. *Environ Sci Policy* **2020**, *114*, 73–85. <https://doi.org/10.1016/J.ENVSCI.2020.07.017>.
- (2) Booker, J. F.; Trees, W. S. Implications of Water Scarcity for Water Productivity and Farm Labor. *Water* **2020**, *Vol. 12*, Page 308 **2020**, *12* (1), 308. <https://doi.org/10.3390/W12010308>.
- (3) Hristov, J.; Barreiro-Hurle, J.; Salputra, G.; Blanco, M.; Witzke, P. Reuse of Treated Water in European Agriculture: Potential to Address Water Scarcity under Climate Change. *Agric Water Manag* **2021**, *251*. <https://doi.org/10.1016/J.AGWAT.2021.106872>.
- (4) Danilo Chiarelli, D.; Rosa, L.; Bini, A.; Zilberman, D.; Cristina Rulli, M. The Global Value of Water in Agriculture. *PNAS* **2020**, *117* (36), 21985–21993. <https://doi.org/10.1073/pnas.2005835117/-/DCSupplemental>.
- (5) Hejase, C. A.; Weitzel, K. A.; Stokes, S. C.; Graubeger, B. M.; Young, R. B.; Arias-Paic, M. S.; Kong, M.; Chae, S.; Bandhauer, T. M.; Tong, T.; Herber, D. R.; Stout, S.; Miara, A.; Huang, Z.; Evans, A.; Kurup, P.; Talmadge, M.; Kandt, A.; Stokes-Draut, J. R.; Macknick, J.; Borch, T.; Dionysiou, D. D. Opportunities for Treatment and Reuse of Agricultural Drainage in the United States. *ACS ES&T Engineering* **2021**, acsestengg.1c00277. <https://doi.org/10.1021/ACSESTENGG.1C00277>.
- (6) Cohen, Y. *Membrane Desalination of Agricultural Drainage Water: Water Recovery Enhancement and Brine Minimization*; 2008.
- (7) Shih, W. Y.; Rahardianto, A.; Lee, R. W.; Cohen, Y. Morphometric Characterization of Calcium Sulfate Dihydrate (Gypsum) Scale on Reverse Osmosis Membranes. *J Memb Sci* **2005**, *252* (1–2), 253–263. <https://doi.org/10.1016/j.memsci.2004.12.023>.
- (8) Gabelich, C. J.; Yun, T. I.; Coffey, B. M.; Suffet, I. H. Pilot-Scale Testing of Reverse Osmosis Using Conventional Treatment and Microfiltration. *Desalination* **2003**, *154* (3), 207–223. [https://doi.org/10.1016/S0011-9164\(03\)80036-X](https://doi.org/10.1016/S0011-9164(03)80036-X).
- (9) Afonso, M. D.; Jaber, J. O.; Mohsen, M. S. Brackish Groundwater Treatment by Reverse Osmosis in Jordan. *Desalination* **2004**, *164* (2), 157–171. [https://doi.org/10.1016/S0011-9164\(04\)00175-4](https://doi.org/10.1016/S0011-9164(04)00175-4).

- (10) Agashichev, S. P.; El-Dahshan, M. E. Reverse Osmosis Incorporated into Existing Cogenerating Systems as a Sustainable Technological Alternative for United Arab Emirates. *Desalination* **2003**, *157* (1–3), 33–49. [https://doi.org/10.1016/S0011-9164\(03\)00381-3](https://doi.org/10.1016/S0011-9164(03)00381-3).
- (11) Le Gouellec, Y. A.; Elimelech, M. Calcium Sulfate (Gypsum) Scaling in Nanofiltration of Agricultural Drainage Water. *J Memb Sci* **2002**, *205* (1–2), 279–291. [https://doi.org/10.1016/S0376-7388\(02\)00128-X](https://doi.org/10.1016/S0376-7388(02)00128-X).
- (12) Xiao, J. (Alan); and, A. T. K.; Tomson, M. B. Prediction of BaSO₄ Precipitation in the Presence and Absence of a Polymeric Inhibitor: Phosphino-Polycarboxylic Acid. *Langmuir* **2001**, *17* (15), 4668–4673. <https://doi.org/10.1021/LA001721E>.
- (13) Öner, M.; Doğan, Ö.; Öner, G. The Influence of Polyelectrolytes Architecture on Calcium Sulfate Dihydrate Growth Retardation. *J Cryst Growth* **1998**, *186* (3), 427–437. [https://doi.org/10.1016/S0022-0248\(97\)00518-6](https://doi.org/10.1016/S0022-0248(97)00518-6).
- (14) Ghafour, E. E. A. Enhancing RO System Performance Utilizing Antiscalants. *Desalination* **2003**, *153* (1–3), 149–153. [https://doi.org/10.1016/S0011-9164\(02\)01117-7](https://doi.org/10.1016/S0011-9164(02)01117-7).
- (15) Amjad, Z. Applications of Antiscalants to Control Calcium Sulfate Scaling in Reverse Osmosis Systems. *Desalination* **1985**, *54* (C), 263–276. [https://doi.org/10.1016/0011-9164\(85\)80022-9](https://doi.org/10.1016/0011-9164(85)80022-9).
- (16) Le Gouellec, Y. A.; Elimelech, M. Control of Calcium Sulfate (Gypsum) Scale in Nanofiltration of Saline Agricultural Drainage Water. *Environ Eng Sci* **2004**, *19* (6), 387–397. <https://doi.org/10.1089/109287502320963382>.
- (17) Zhang, Y.; Yin, H.; Zhang, Q.; Li, Y.; Yao, P. Synthesis and Characterization of Novel Polyaspartic Acid/Urea Graft Copolymer with Acylamino Group and Its Scale Inhibition Performance. *Desalination* **2016**, *395*, 92–98. <https://doi.org/10.1016/J.DESAL.2016.05.020>.
- (18) Yang, L.; Yang, W.; Xu, B.; Yin, X.; Chen, Y.; Liu, Y.; Ji, Y.; Huan, Y. Synthesis and Scale Inhibition Performance of a Novel Environmental Friendly and Hydrophilic Terpolymer Inhibitor. *Desalination* **2017**, *416*, 166–174. <https://doi.org/10.1016/J.DESAL.2017.05.010>.
- (19) Gryta, M. Polyphosphates Used for Membrane Scaling Inhibition during Water Desalination by Membrane Distillation. **2011**. <https://doi.org/10.1016/j.desal.2011.09.051>.

- (20) Lin, Y.-P. ã.; Singer, P. C. Inhibition of Calcite Crystal Growth by Polyphosphates. *Water Res* **2005**, *39*, 4835–4843. <https://doi.org/10.1016/j.watres.2005.10.003>.
- (21) Yu, W.; Song, D.; Chen, W.; Yang, H. Antiscalants in RO Membrane Scaling Control. *Water Res* **2020**, *183*. <https://doi.org/10.1016/J.WATRES.2020.115985>.
- (22) Nowack, B. Environmental Chemistry of Phosphonates. *Water Res* **2003**, *37* (11), 2533–2546. [https://doi.org/10.1016/S0043-1354\(03\)00079-4](https://doi.org/10.1016/S0043-1354(03)00079-4).
- (23) Miyajima, T.; Mori, M.; Ishiguro, S. I. Analysis of Complexation Equilibria of Polyacrylic Acid by a Donnan-Based Concept. *J Colloid Interface Sci* **1997**, *187* (1), 259–266. <https://doi.org/10.1006/JCIS.1996.4694>.
- (24) Tomson, B.; Kan, A. T.; Oddo, J. E. Acid/Base and Metal Complex Solution Chemistry of the Polyphosphonate DTPMP versus Temperature and Ionic Strength. *Langmuir* **1994**, *10*, 1442–1449.
- (25) Deluchat, V.; Bollinger, J. C.; Serpaud, B.; Caullet, C. Divalent Cations Speciation with Three Phosphonate Ligands in the PH-Range of Natural Waters. *Talanta* **1997**, *44* (5), 897–907. [https://doi.org/10.1016/S0039-9140\(96\)02136-4](https://doi.org/10.1016/S0039-9140(96)02136-4).
- (26) Neira-Carrillo, A.; Acevedo, D. F.; Miras, M. C.; Barbero, C. A.; Gebauer, D.; Cölfen, H.; Arias, J. L. Influence of Conducting Polymers Based on Carboxylated Polyaniline on In Vitro CaCO₃ Crystallization. <https://doi.org/10.1021/la802231s>.
- (27) Eriksson, R.; Merta, J.; Rosenholm, J. B. The Calcite/Water Interface I. Surface Charge in Indifferent Electrolyte Media and the Influence of Low-Molecular-Weight Polyelectrolyte. *J Colloid Interface Sci* **2007**, *313*, 184–193. <https://doi.org/10.1016/j.jcis.2007.04.034>.
- (28) Jain, T.; Sanchez, E.; Owens-Bennett, E.; Trussell, R.; Walker, S.; Liu, H. Impacts of Antiscalants on the Formation of Calcium Solids: Implication on Scaling Potential of Desalination Concentrate. *Environ Sci (Camb)* **2019**, *5* (7), 1285–1294. <https://doi.org/10.1039/c9ew00351g>.
- (29) Shih, W.-Y.; Albrecht, K.; Glater, J.; Cohen, Y. A Dual-Probe Approach for Evaluation of Gypsum Crystallization in Response to Antiscalant Treatment. *Desalination* **2004**, *169* (3), 213–221. <https://doi.org/10.1016/j.desal.2003.12.008>.

- (30) Nasir Mangal, M.; Salinas-Rodriguez, S. G.; Dusseldorp, J.; Kemperman, A. J. B.; Schippers, J. C.; Kennedy, M. D.; Van Der Meer, W. G. J. Effectiveness of Antiscalants in Preventing Calcium Phosphate Scaling in Reverse Osmosis Applications. *J Memb Sci* **2021**, *623*, 119090. <https://doi.org/10.1016/j.memsci.2021.119090>.
- (31) Yu, W.; Song, D.; Li, A.; Yang, H. Control of Gypsum-Dominated Scaling in Reverse Osmosis System Using Carboxymethyl Cellulose. *J Memb Sci* **2019**, *577* (February), 20–30. <https://doi.org/10.1016/j.memsci.2019.01.053>.
- (32) Oshchepkov, M.; Golovesov, V.; Ryabova, A.; Tkachenko, S.; Redchuk, A.; Rönkkömäki, H.; Rudakova, G.; Pervov, A.; Popov, K. Visualization of a Novel Fluorescent-Tagged Bisphosphonate Behavior during Reverse Osmosis Desalination of Water with High Sulfate Content. *Sep Purif Technol* **2021**, *255*, 117382. <https://doi.org/10.1016/J.SEPPUR.2020.117382>.
- (33) Rahardianto, A.; Mccool, B. C.; Cohen, Y. Reverse Osmosis Desalting of Inland Brackish Water of High Gypsum Scaling Propensity: Kinetics and Mitigation of Membrane Mineral Scaling. *Environ Sci Technol* **2008**, *42* (12), 4292–4297. <https://doi.org/10.1021/es702463a>.
- (34) Rosenberg, Y. O.; Reznik, I. J.; Zmora-Nahum, S.; Ganor, J. The Effect of PH on the Formation of a Gypsum Scale in the Presence of a Phosphonate Antiscalant. *Desalination* **2012**, *284*, 207–220. <https://doi.org/10.1016/J.DESAL.2011.08.061>.
- (35) Wang, J.; Wang, L.; Miao, R.; Lv, Y.; Wang, X.; Meng, X.; Yang, R.; Zhang, X. Enhanced Gypsum Scaling by Organic Fouling Layer on Nanofiltration Membrane: Characteristics and Mechanisms. *Water Res* **2016**, *91*, 203–213. <https://doi.org/10.1016/J.WATRES.2016.01.019>.
- (36) Benecke, J.; Rozova, J.; Ernst, M. Anti-Scale Effects of Select Organic Macromolecules on Gypsum Bulk and Surface Crystallization during Reverse Osmosis Desalination. *Sep Purif Technol* **2018**, *198*, 68–78. <https://doi.org/10.1016/J.SEPPUR.2016.11.068>.
- (37) Karabelas, A. J.; Karanasiou, A.; Sioutopoulos, D. C. Experimental Study on the Effect of Polysaccharides on Incipient Membrane Scaling during Desalination. *Desalination* **2017**, *416*, 106–121. <https://doi.org/10.1016/J.DESAL.2017.04.009>.
- (38) Lee, S.; Choi, J. S.; Lee, C. H. Behaviors of Dissolved Organic Matter in Membrane Desalination. *Desalination* **2009**, *238* (1–3), 109–116. <https://doi.org/10.1016/J.DESAL.2008.01.041>.

- (39) Kwon, Y. N.; Hong, S.; Choi, H.; Tak, T. Surface Modification of a Polyamide Reverse Osmosis Membrane for Chlorine Resistance Improvement. *J Memb Sci* **2012**, *415–416*, 192–198. <https://doi.org/10.1016/J.MEMSCI.2012.04.056>.
- (40) Coday, B. D.; Luxbacher, T.; Childress, A. E.; Almaraz, N.; Xu, P.; Cath, T. Y. Indirect Determination of Zeta Potential at High Ionic Strength: Specific Application to Semipermeable Polymeric Membranes. *J Memb Sci* **2015**, *478*, 58–64. <https://doi.org/10.1016/J.MEMSCI.2014.12.047>.
- (41) Khan, M. A.; Azad, A. K.; Safdar, M.; Nawaz, A.; Akhlaq, M.; Paul, P.; Hossain, M. K.; Rahman, M. H.; Baty, R. S.; El-Kott, A. F.; Kamel, M.; Bungau, S. G.; Abdel-Daim, M. M. Synthesis and Characterization of Acrylamide/Acrylic Acid Co-Polymers and Glutaraldehyde Crosslinked PH-Sensitive Hydrogels. *Gels* **2022**, *8* (1). <https://doi.org/10.3390/GELS8010047>.
- (42) Mark M. Benjamin. *Water Chemistry*; 2015.
- (43) Al-Roomi, Y. M.; Hussain, K. F. Potential Kinetic Model for Scaling and Scale Inhibition Mechanism. *Desalination* **2016**, *393*, 186–195. <https://doi.org/10.1016/J.DESAL.2015.07.025>.
- (44) Darton, E. G. Membrane Chemical Research: Centuries Apart. *Desalination* **2000**, *132* (1–3), 121–131. [https://doi.org/10.1016/S0011-9164\(00\)00141-7](https://doi.org/10.1016/S0011-9164(00)00141-7).
- (45) Li, H.; Hsieh, M. K.; Chien, S. H.; Monnell, J. D.; Dzombak, D. A.; Vidic, R. D. Control of Mineral Scale Deposition in Cooling Systems Using Secondary-Treated Municipal Wastewater. *Water Res* **2011**, *45* (2), 748–760. <https://doi.org/10.1016/J.WATRES.2010.08.052>.
- (46) Liu, Q.; Xu, G. R.; Das, R. Inorganic Scaling in Reverse Osmosis (RO) Desalination: Mechanisms, Monitoring, and Inhibition Strategies. *Desalination* **2019**, *468*, 114065. <https://doi.org/10.1016/J.DESAL.2019.07.005>.
- (47) KIRISHIMA, A.; OHNISHI, T.; SATO, N.; TOCHIYAMA, O. Simplified Modelling of the Complexation of Humic Substance for Equilibrium Calculations. *J Nucl Sci Technol* **2010**, *47* (11), 1044–1054. <https://doi.org/10.1080/18811248.2010.9711669>.

Chapter 6

Conclusions and Broader Impacts

Brine Line Scaling Case Study in Inland Desalination Systems

Chapter 2 of this dissertation focused on the scaling challenges faced by inland desalination brine transport infrastructure, specifically within a 116-km brine line in Southern California. This study examined brine composition, identified theoretical solid precipitation from the brine, including calcite, dolomite, silica, and hydroxyapatite, and evaluated the impact of flow conditions and antiscalants on scaling. Both primary and secondary antiscalants can effectively delay the formation of solids. However, solids already present in the discharge from desalination plants may accumulate in the brine line, potentially causing scaling problems over time. To mitigate these issues, strategies for active brine pretreatment were recommended, such as removing antiscalants and hardness ions prior to transport and implementing real-time flow monitoring to control turbulence. These findings emphasize the importance of infrastructure improvements to support sustainable brine management and reduce scaling-related costs.

Enhancing Brine Treatment through Antiscalant Removal via UV/PS

In Chapter 3, the research developed a UV-driven persulfate (UV/PS) oxidation process to degrade phosphonate-based antiscalants from brackish inland desalination brine. The removal of antiscalants, which hinder subsequent treatment stages, was crucial for facilitating effective calcium removal through chemical demineralization. This study assessed the impacts of persulfate dose and UV irradiation time on the degradation efficiency of antiscalants, showing that UV/PS pretreatment significantly enhanced the kinetics of calcium precipitation during demineralization. Notably, UV/PS pretreatment with NaOH- or lime-softening based demineralization methods all decreased fouling

potential in downstream microfiltration (MF) processes, demonstrating that UV/PS-CDM-MF treatment process could be highly effective in improving brine quality for secondary water recovery stages. This UV/PS-CDM-MF method presents a viable pre-treatment option to enhance brine treatment efficacy, offering a sustainable and efficient approach to inland brine management.

Integrated Multi-Stage Brine Treatment for Water and Mineral Recovery

Building upon the UV/PS pretreatment method, Chapter 4 introduced an integrated treatment sequence—combining UV/PS, chemical demineralization (CDM), microfiltration (MF), and secondary reverse osmosis (RO) to maximize water and mineral recovery from brackish inland desalination brine. This multi-stage approach was designed to degrade antiscalants, remove scale-forming ions, and facilitate resource recovery. Results demonstrated that this system achieved substantial freshwater recovery (over 75%) at neutral pH, resulting in much less usage of acid and base for pH adjustment. It also achieved dramatic mineral crystallization, particularly for magnesium and silica, while also reducing membrane fouling during the RO process. In addition, this system achieved lower energy consumption compared to conventional thermal brine treatment systems. The UV/PS-CDM-MF-RO treatment train underscores the potential for inland desalination brine to be not only treated but also repurposed as a valuable source of water and minerals. By optimizing conditions for each treatment step, this integrated system could be adapted to meet varying brine compositions and operational needs, paving the way for a more sustainable and economically feasible inland brine management framework.

Gypsum Scaling Control in Agricultural Drainage Water Desalination

In Chapter 5, the dissertation shifts focus to a related but distinct area: managing gypsum scaling in the RO desalination of agricultural drainage water. High concentrations of calcium and sulfate in drainage water create a unique challenge, as they lead to gypsum (CaSO_4) scaling on membrane surfaces. This study evaluated the inhibitive capacity of three widely used antiscalants—DTPMP, NTMP, and PAA—on gypsum scaling under varying conditions of antiscalant dosage, feedwater pH, and the presence of natural organic matter (NOM). At equivalent dosages, DTPMP emerged as the most effective antiscalant, demonstrating a strong inhibitory mechanism involving negative charge repulsion. This mechanism maintained optimal permeate flux by stabilizing flux and mitigating scaling over extended operational times, even in the presence of NOM. The study also revealed that acidic pH conditions compromised the antiscalant inhibitory capacity, with the sensitivity to acidic pH ranked as $\text{PAA} > \text{NTMP} > \text{DTPMP}$. In particular, PAA presented an added risk under acidic conditions, where its combined mechanisms of charge repulsion and crystal lattice distortion led to the formation of small, dense, irregularly shaped gypsum crystals, which ultimately caused a significant decline in permeate flux. By contrast, DTPMP's charge repulsion mechanism preserved higher negative charges without altering precipitate morphology, thus optimizing gypsum inhibition across a wider pH range.

These insights into antiscalant selection, mechanisms, and performance provide practical guidance for optimizing RO desalination processes when treating agricultural drainage water, enhancing the potential for effective drainage water reuse in irrigation.

Future Work and Broader Implications

The studies presented in this dissertation collectively offer a foundation for developing scalable, efficient, and sustainable methods for inland brine management, brine treatment, and agricultural drainage water reuse. However, there are significant areas for further research.

A key next step involves a comprehensive economic analysis comparing the novel brine treatment process proposed in Chapters 3 and 4 of this dissertation with current brine disposal methods, including brine line discharge (Chapter 2), thermal crystallization, and evaporation ponds.

The major cost components of the proposed brine treatment process can be categorized into several key areas. First, capital expenditure (CapEx) encompasses the costs of infrastructure construction, permitting, and installation, including UV photochemical reactors for antiscalant degradation, chemical softening tanks for demineralization, and microfiltration and secondary RO units for brine treatment and water recovery. Land acquisition also contributes to CapEx, as sufficient space is needed for the integrated treatment system.

Operational expenditure (OpEx) includes electricity consumption to power UV lamps, pumps, and RO units, which are essential for continuous treatment operations. Skilled labor is required for safe and efficient operations. Regular maintenance is necessary to ensure the longevity and efficiency of the treatment system, such as periodic replacement and chemical cleaning of microfiltration and RO membranes and managing residuals or waste brine streams. Chemical inputs include persulfate for photochemical treatment,

acids for pH adjustment and scaling prevention, and bases, lime, and soda ash for chemical demineralization.

Brine line disposal typically incurs capital costs associated with constructing pipelines to transport brine to a disposal site or existing infrastructure. Operational costs include expenses for pumping, maintaining the pipelines, and brine disposal fees.

Thermal crystallizers involve a high initial capital investment for specialized equipment and significant electricity costs due to the energy-intensive process. Maintenance and waste disposal costs are also incurred for monitoring fouling, scaling, and corrosion, as well as managing the solid salts produced.

Evaporation ponds have substantial land acquisition costs and construction costs, particularly in areas with low evaporation rates, as large areas are required. Maintenance expenses arise from managing sedimentation, preventing leaks, and addressing algae or biological growth.

Future work should develop robust models to evaluate these cost components under varying scenarios. These models must account for:

1. Brine chemistry variability: the composition of brine significantly influences treatment requirements, scaling potential, and energy consumption.
2. Treatment scalability: the performance and cost-effectiveness of treatment technologies at different scales.
3. Site-specific factors: geographic and climatic conditions that impact the feasibility of evaporation ponds, transportation logistics for crystallizer outputs, and access to disposal brine lines.

4. Regulatory landscape: variations in discharge regulations and incentives for sustainable practices across regions.

By integrating these elements, a detailed cost-benefit analysis can guide stakeholders in selecting the most economically viable and environmentally sustainable disposal method. Additional research on energy-efficient methods for brine concentration and mineral recovery remains essential. Developing hybrid systems that combine renewable energy sources (e.g., solar, wind), with advanced brine treatment technologies could reduce the environmental footprint and operational costs. Exploring innovative mineral recovery processes that yield industrial- or agricultural-grade materials could unlock new economic incentives, offsetting the costs of brine treatment and disposal.

The broader implications of this work reach beyond inland desalination. Climate change and global population growth are increasing water scarcity pressures, particularly in arid regions where alternative water sources like brackish groundwater and agricultural drainage water are vital. The findings in this dissertation contribute to the development of sustainable water management practices that maximize water recovery, minimize waste, and promote the reuse of nontraditional water sources. Additionally, by addressing economic barriers through cost-effective disposal options, this research provides a roadmap for regions to adopt sustainable water management practices. With continued innovation, policy support and cross-sector collaboration, the methods explored here could provide significant benefits in regions facing water shortages, promoting environmental sustainability, economic resilience and resource equity.

Appendix A

Supporting Information for chapter 2

Previously published in *ACS ES&T Engineering*

Tang, X.; Kum, S.; Liu, H. Inland Desalination Brine Disposal: A Baseline Study from Southern California on Brine Transport Infrastructure and Treatment Potential. *ACS ES&T Engineering*. 2022, 2, 456-464 DOI: 10.1021/acsestengg.1c00276.

Text S1. Visual Minteq simulation procedures (Use brine from Site S1 as example)

Step A. Saturation indices calculation

Please supply a value for the alkalinity of the solution

mg/l CO32-
mg/l CaCO3
meq/l

32.5579536

pH Fixed at... 7.800

Ionic strength To be calculated

Concentration unit Molal

Temperature 22.2 deg C

Components in the present problem

Component name	Total concentration* Molal	Act guess?*
H+1	0	<input checked="" type="checkbox"/>
Ca+2	0.020967	<input checked="" type="checkbox"/>
Mg+2	0.012401	<input checked="" type="checkbox"/>
PO4-3	3.2285E-06	<input checked="" type="checkbox"/>
Na+1	0.020187	<input checked="" type="checkbox"/>
CO3-2****	0.0325579536	<input checked="" type="checkbox"/>
NO3-1	0.0046577	<input checked="" type="checkbox"/>
Cl-1	0.0497	<input checked="" type="checkbox"/>

1. Input pH, alkalinity, temperature and cation, anion concentration that measured by experiment and set ionic strength "To be calculated" (Chloride is calculated based on charge balance)



2. Click "Run" button and start the program

Distribution of components between dissolved,
(Concentrations in molal)

Component	Total dissolved	% dissolved	
Ca+2	2.0967E-02	100.000	
Cl-1	4.9700E-02	100.000	
CO3-2	3.2370E-02	100.000	
H+1	3.2187E-02	100.000	
Mg+2	1.2401E-02	100.000	
Na+1	2.0187E-02	100.000	
NO3-1	4.6577E-03	100.000	
PO4-3	3.2284E-06	100.000	

Mineral	log IAP	Sat. Index (=log IAP - log Ks)
Aragonite	-6.424	1.895
Artinite	6.527	-3.273
Bruoitite	13.178	-4.111
Ca3(PO4)2 (am1)	-28.665	-3.321
Ca3(PO4)2 (am2)	-28.665	-0.560
Ca3(PO4)2 (beta)	-28.665	0.344
Ca4H(PO4)3·3H2O(s)	-49.705	-1.929
CaCO3xH2O(s)	-6.425	0.699
CaHPO4(s)	-21.034	-1.708
CaHPO4·2H2O(s)	-21.038	-2.004
Calcite	-6.424	2.041
Dolomite (disordered)	-13.070	3.393
Dolomite (ordered)	-13.070	3.955
Halite	-3.244	-4.788
Huntite	-26.362	3.427
Hydromagnesite	-13.413	-5.010
Hydroxyapatite	-36.298	8.035
...

Red text - oversaturation Blue text - undersaturation **B**
Green - apparent equilibrium

- Record supersaturated solids and their saturation indices and total dissolved cation and anion concentration.

Step B. Theoretical solids amount and type simulation

pH

Ionic strength

1. Set pH “calculated from mass balance” and set ionic strength “To be calculated”.

Possible species in the present problem

Species name	Specified fixed log Activity*	ΔH of reaction
Hydroxyapatite	-44.333	0
Dolomite (disordered)	-16.54	-46.4
Dolomite (ordered)	-17.09	-39.5
Calcite	-8.48	-8
Aragonite	-8.336	-8
Vaterite	-7.913	-8
Ca ₃ (PO ₄) ₂ (beta)	-28.92	54
CaCO ₃ xH ₂ O(s)	-7.144	-8
Huntite	-29.968	-107.7798
Magnesite	-7.46	20

2. Choose “Specify possible solids phases” and input all supersaturated solids that determined in step A-3

Components in the present problem

Component name	Total concentration* Molal	Act guess?*
H+1	3.2187E-02	<input checked="" type="checkbox"/>
Ca+2	2.0967E-02	<input checked="" type="checkbox"/>
Mg+2	1.2401E-02	<input checked="" type="checkbox"/>
Na+1	2.0187E-02	<input checked="" type="checkbox"/>
PO ₄ -3	3.2284E-06	<input checked="" type="checkbox"/>
CO ₃ -2	3.2370E-02	<input checked="" type="checkbox"/>
NO ₃ -1	4.6577E-03	<input checked="" type="checkbox"/>
Cl-1	4.9700E-02	<input checked="" type="checkbox"/>

3. Input total dissolved cation and anion concentration determined in step A-3

4. Click “Run” button and start the program

Solid	Equilibrium amount (mol/l)
Calcite	6.1740E-03
Dolomite (or...)	2.0348E-03
Hydroxyapatite	2.4131E-07

5. Record theoretical solids type and amount.

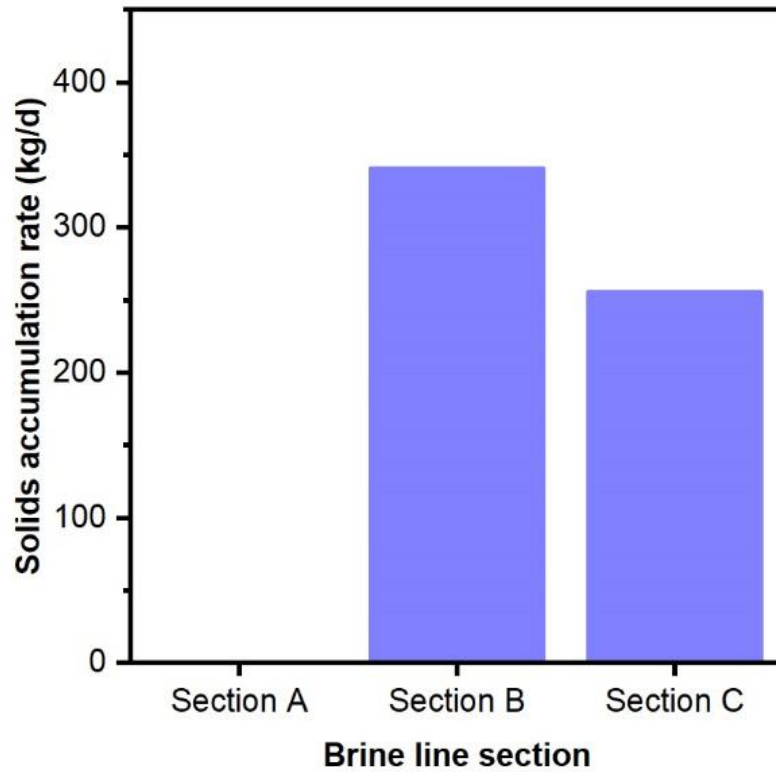


Figure S1. Solids accumulation rate in different sections of brine line. (Solids accumulation rate was calculated by multiplying flow rate with ΔFSS at each section of brine line. $\Delta FSS = FSS_{\text{Start point}} - FSS_{\text{End point}}$. Flow rate of section A, B, C is 1744, 16462, 22817 m³/day respectively)

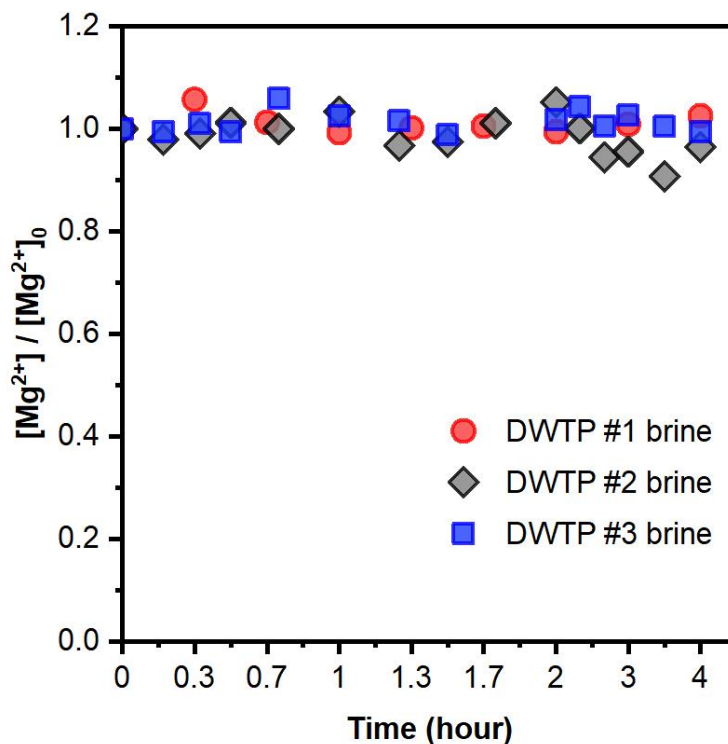


Figure S2. Dissolved magnesium concentration profile from induction time experiments with brines from three inland desalination treatment plants (DWTPs #1, #2 and #3 at Site S0, Site S6 and Site S3, respectively). Stirring rate = 700 rpm. Only residual primary antiscalants were present in these three brine samples. $[Mg^{2+}]_0$ refers to initial dissolved magnesium concentration. $[Mg^{2+}]$ refers to dissolved magnesium concentration at designated time point.

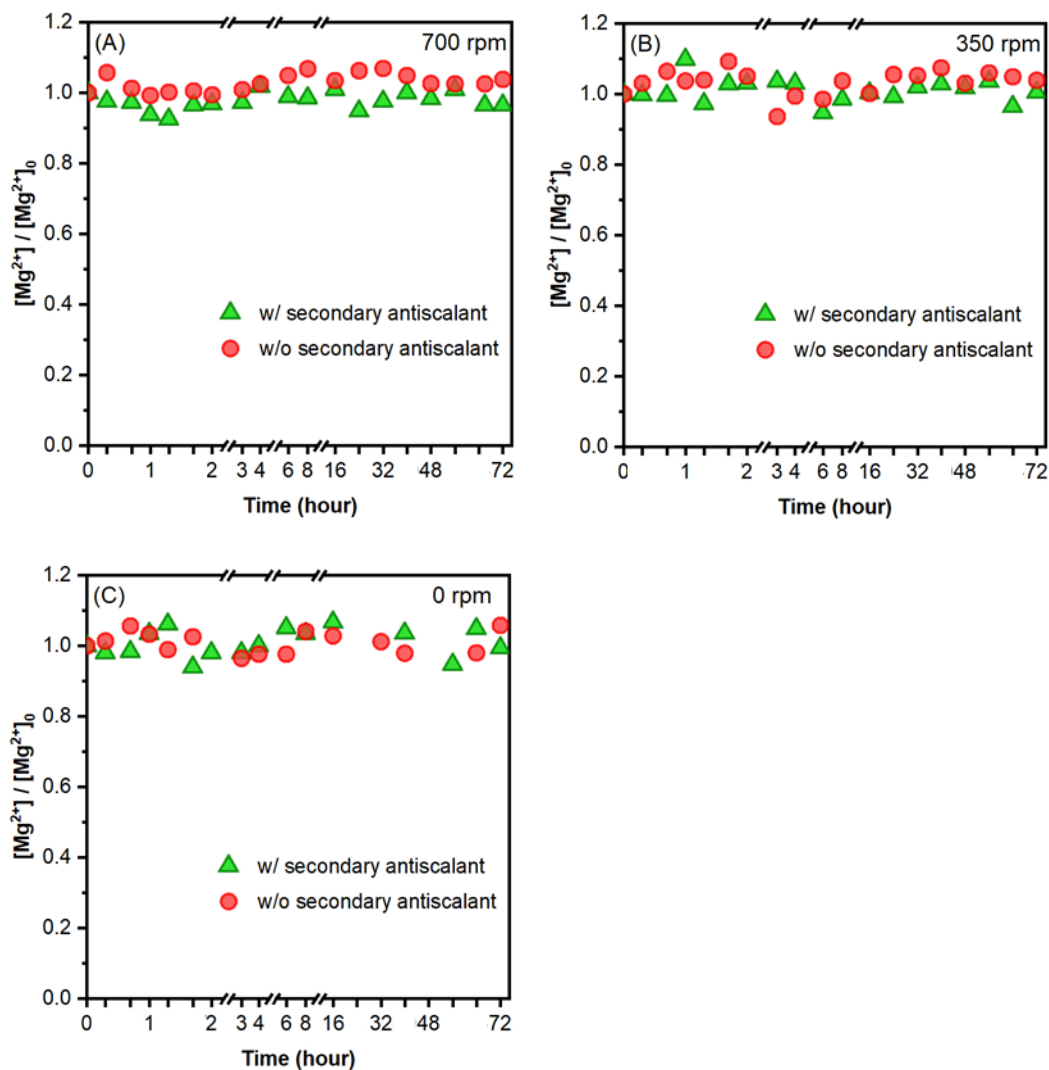


Figure S3. Effects of secondary antiscalant on magnesium precipitation in oversaturated desalination brine from desalination plant DWTP #1 under different stirring rates in lab simulation experiments. (A) stirring rate = 700 rpm; (B) stirring rate = 350 rpm; (C) stirring rate = 0 rpm. Experiments were conducted under room temperature and all brine samples were acquired at onsite sampling sites. The brine samples all contain primary antiscalant.

Appendix B

Supporting Information for chapter 3

Previously published in *Environmental Science: Water Research & Technology*

Kum, S., Tang, X., & Liu, H. (2023). Treatment of Brackish Water Inland Desalination Brine via Antiscalant Removal Using Persulfate Photolysis. *Environmental Science: Water Research & Technology*, 9(4), 1137-1146. DOI:10.1039/d2ew00924b.

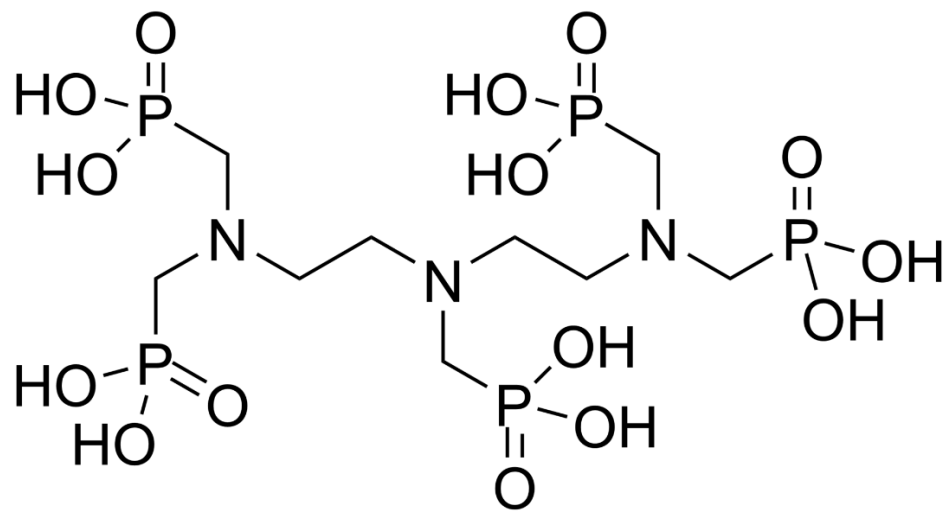
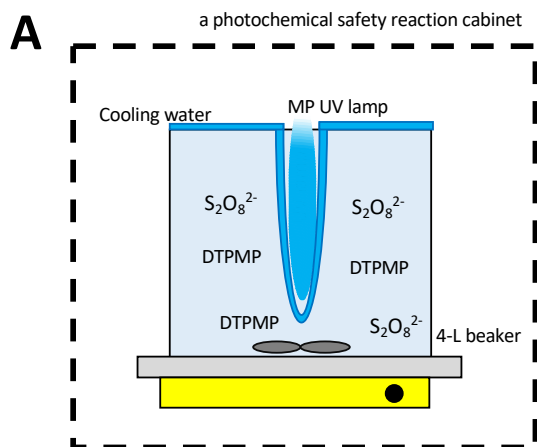
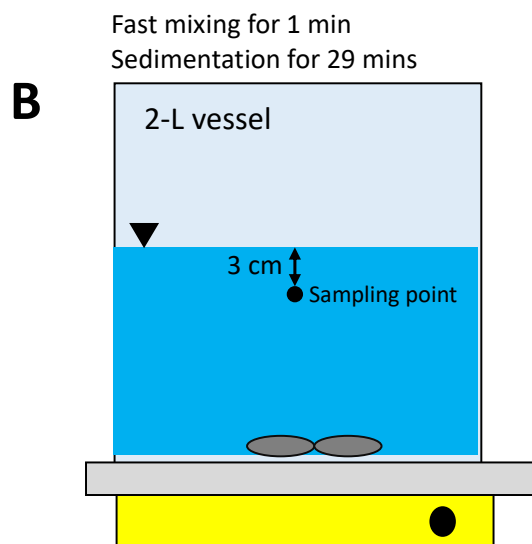


Figure S1. The molecular structure of the antiscalant diethylenetriamine pentamethylene phosphonic acid (DTPMP) investigated in this study.



A bench scale UV reactor system



A batch precipitation reactor

Figure S2. Experimental setup for (A) UV/PS and (B) CDM experiments.

Text S1. The details of UV/PS experiments

A bench-scale UV reactor consisted of a 4-L beaker, magnetic stirrer, and a 450-W medium pressure UV immersion lamp (Ace Glass, Inc.) with a water-cooling jacket to minimize temperature increase in the reactor. The UV lamp with 42 mW/cm² light intensity and spectrum of wavelengths ranging between 200 and 850 nm was placed in the centerline of the 4-L beaker and immersed into feed water to enhance penetration of UV light. Oxidation experiments were carried out in a photochemical safety reaction cabinet. The lamps were warmed up for 10 min prior to the reaction to ensure stable output, and then prepared 3.5-L feed solution was transferred to the 4-L beaker (time zero).

DTPMP degradation and ortho-phosphate kinetic experiment were conducted for 30 minutes with 3.5-L Ca²⁺ absent synthetic brine solutions containing 4 mM persulfate and 0.1 mM DTPMP. To accomplish the UV/PS operating condition investigation, 3.5-L synthetic brine solutions containing 2 -5 mM persulfate and 0.1 mM DTPMP (equivalent of 15.5 mg P/L) were prepared and experiments were conducted for 60 minutes to evaluate the impact of UV irradiation time on the DTPMP degradation. For UV/PS pre-treatment before CDM process, 3.5-L synthetic brine solutions containing 4 mM persulfate and 0.1 mM DTPMP (\cong 15.5 mg P/L) were prepared.

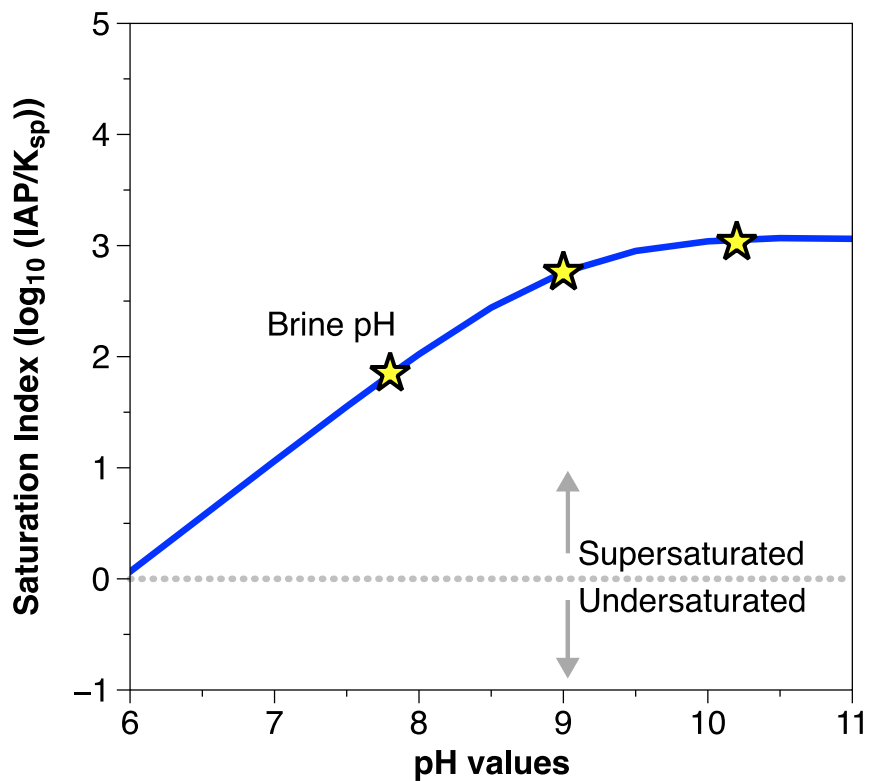


Figure S3. Calcite saturation index of the Inland Empire Brine at different pH. The saturation index of calcite is defined as: $SI_{CaCO_3} = \log\left(\frac{IAP}{K_{sp,CaCO_3(s)}}\right)$, where **IAP** is the ion activity product, while, $K_{sp,CaCO_3(s)}$ is the solubility products calcium carbonate ($K_{sp,CaCO_3} = 10^{-8.48}$).

Text S2. The details of microfiltration experiments

An Amicon stirred cell (200 mL capacity; Millipore Sigma, Burlington, MA) with 28.7 cm² of active membrane area was used for the solid/liquid separation after the UV/PS-CDM process. Flat sheet polyvinylidene fluoride (PVDF) membrane with a nominal pore size of 0.1 μm (Durapore[®], Millipore Sigma, Burlington, MA) was used in this research. Nitrogen was applied to pressurize the MF cell at 0.5 bar for the membranes.

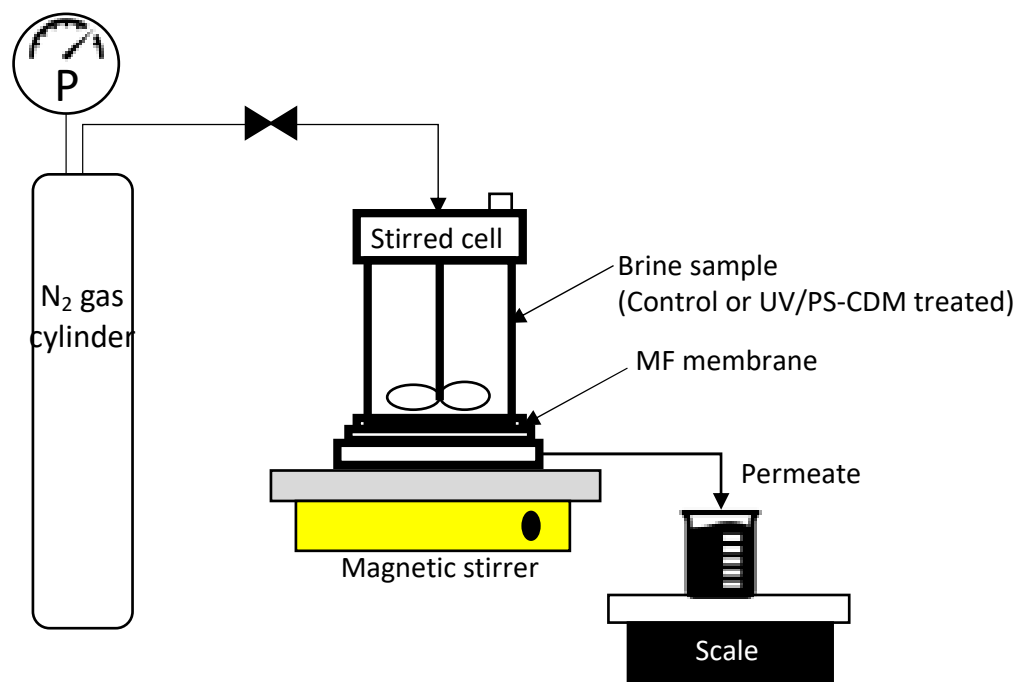


Figure S4. A schematic of dead-end microfiltration membrane setup.

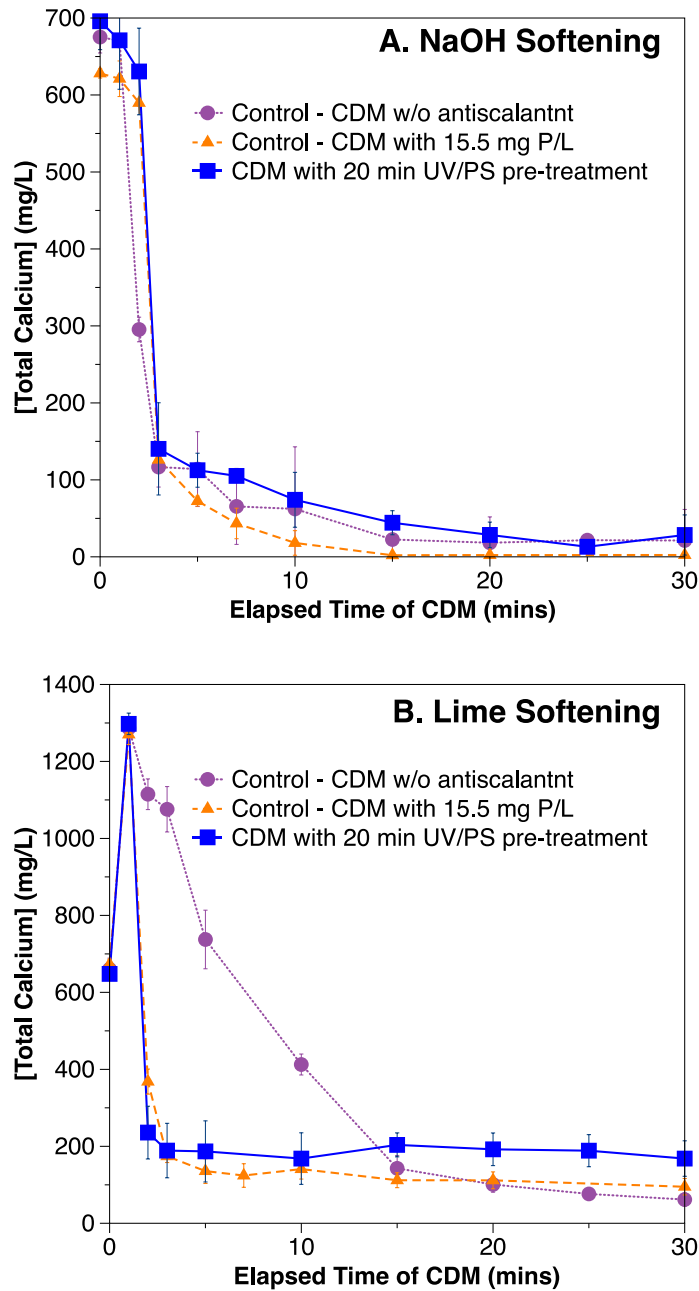


Figure S5. Impact of the addition of orthophosphate to the brine on the removal of total calcium during the CDM process. (A): NaOH softening CDM; (B): Lime softening CDM.

Text S3. Calculation on saturation index of calcite

SI as a function of the secondary RO water recovery was calculated based on the water quality after the microfiltration process (Table S1). Control stands for no UV/PS-CDM treatment (direct use of brine). Initial water quality data (0% water recovery) for calcite saturation index calculations in the secondary RO concentrate are shown in Table S1. As the secondary RO water recovery increases, the saturation index in the secondary RO concentrates increases. The concentration of the secondary RO concentrate ($C_{concentrate}$) at different water recoveries was calculated based on Equation (S1).

$$C_{concentrate} = \frac{C_{in}(1 - r(1 - R))}{1 - r} \quad (S1)$$

Where, C_{in} is the initial concentration, r is the fractional recovery, and R is the fractional removal efficiency. We assumed 100% salts rejection at the secondary RO, meaning R is 1. Saturation index calculations in Figure 7 were performed through Visual Minteq (Version 3.1) for a pH of 7.8 at different water recovery.

Table S1. Input data for saturation index calculations for calcite in the secondary RO concentrate; the input data are water quality measured after the microfiltration process (CDM with 20 minutes UV/PS pre-treatment in Fig. 6).

Chemical constituent	Untreated brine	UV/PS-CDM-MF treated brine (NaOH softening)	UV/PS-CDM-MF treated brine (Lime softening)
Calcium	16.5	0.8	3.3
Sodium	54.7	76.5	71.0
Chloride	60.9	60.9	60.9
Bicarbonate	21.3	4.0	3.3
Perchlorate	5.5	5.5	5.5
pH	7.8	7.8	7.8

Appendix C

Supporting Information for chapter 4

Previously published in *Separation and Purification Technology*

Kum, S., Tang, X., & Liu, H. (2024). Recovery of fresh water and minerals from inland brackish desalination brine via persulfate-based photochemical treatment and demineralization. *Separation and Purification Technology*, 342, 126994.
<https://doi.org/10.1016/j.seppur.2024.126994>.

Text S1. Details of Bench-scale Reverse Osmosis System

The reverse osmosis (RO) system was composed of a feed water vessel, membrane cell, bleed lines, and a permeate collection line (Fig. S1). The active membrane area of the crossflow RO apparatus (Model CF042 Membrane Cell, Sterlitech, USA) is 42 cm². The flow rate of feed was fixed at 1250 mL·min⁻¹, pumped from the feed vessel with a variable-speed diaphragm pump (Model M-03S, HydraCell, USA), and pump speed was controlled by variable frequency drive (Emerson commander SK, USA). The Filmtec BW30LE membrane was used for the experiment. BW30LE is a low-energy polyamide membrane that is commonly applied to brackish water treatment to reduce salinity and has a negatively charged surface with a molecular weight cut-off of 100 Da.¹⁻⁴ The temperature of the feed solution was maintained at 23±1°C with a chiller. The operating pressure was maintained at the target pressure using a back-pressure regulator. The pre-conditioning of the membrane is required to stabilize the permeate flux and was performed at 10.3 bar (150 psig) with MilliQ DI water for 2 h before the actual start of the experiment. The brine feed solution was introduced after the pre-conditioning step by switching the pre-conditional solution with the brine solution. When the actual feed solution was introduced to the RO system, the RO operation was paused for less than 1 min, but the pressure was not released. The RO membrane system was stabilized immediately after the feed solution was introduced, and the measurement of permeate flux was started 1 min after the system was running. 3-L of experimental solution was employed for RO experiments and the RO system was operated as partial recycling (concentrate recycled but permeate withdrawn from the system) mode for 24 h. The

permeate mass was continuously measured by an electronic balance and permeate mass data were collected by a laptop with a data acquisition equipment throughout the experiments.

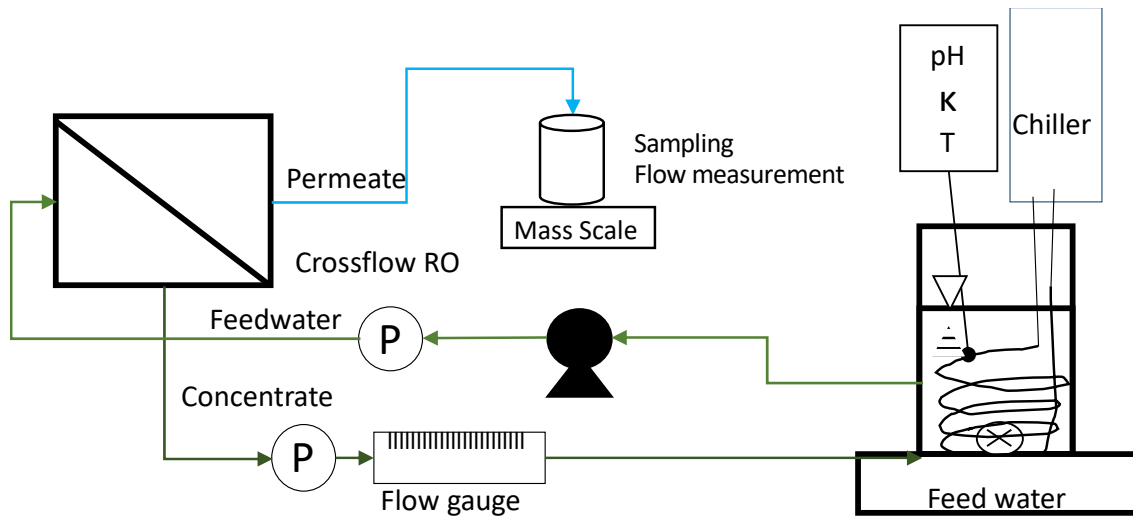


Figure S1. Schematic of the laboratory-scale RO system.

Text S2. Normalized Permeate Water Flux Calculation

The permeate water flux ($L \cdot m^{-2} \cdot h^{-1}$), J_w , can be calculated by equation S1

$$J_w = \frac{Q_p}{A_m} \quad (S1)$$

where Q_p is a measured permeate flowrate (L/h) and A is the effective area of the membrane (0.0042 m^2) The hydraulic pressure-normalized permeate flux, J ($L \cdot m^{-2} \cdot h^{-1} \cdot \text{bar}^{-1}$), is calculated by Equation S1 divided by a transmembrane pressure (TMP, $P_{\text{feed}} - P_{\text{permeate}}$, bar, eq. S2). Note that the calculated hydraulic pressure-normalized permeate flux is not a permeance because it does not consider the osmotic pressure of the feed water in the calculation of the driving force. This research applied constant pressure throughout the fouling test and assumed that P_{permeate} is negligible.

$$J = \frac{J_w}{TMP} \quad (S2)$$

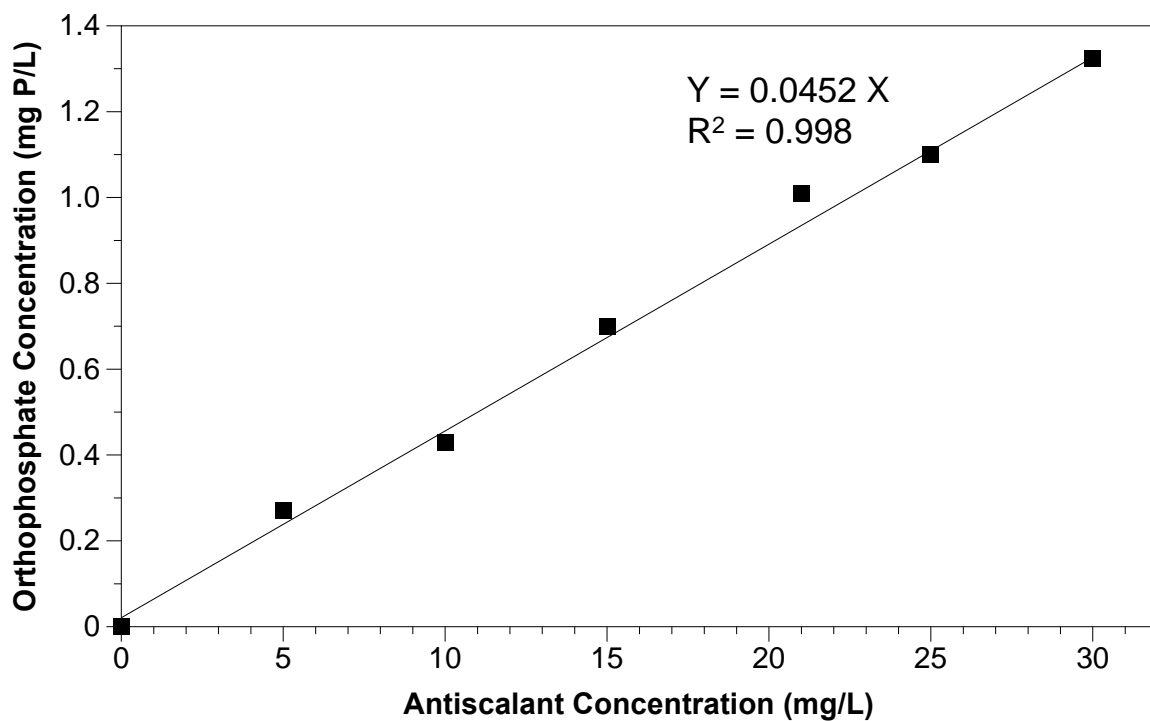


Figure S2. Orthophosphate generation by the UV/Persulfate system at various primary antiscalant concentration. Experimental condition: $[\text{Persulfate}]_0 = 4.0 \text{ mM}$; initial pH = 7.8. UV photolysis time = 30 minutes with a 450-W medium pressure UV immersion lamp (Ace Glass, Inc.). Note: orthophosphate concentration was recorded when the concentration reached plateau during photolysis experiments.

Text S3. Details of chemical analysis on the recovered minerals from the brine

XRD analyses

All XRD analyses were carried out by using a PANalytical Empyrean Series 2 instrument. All samples are in solid powder form and collected after the chemical demineralization process without UV/PS pre-treatment (CDM) and with UV/PS pre-treatment (UV/PS-CDM). 2θ range is from 10 to 90 degree.

XPS analyses

All XPS analyses were carried out by using a Kratos AXIS ULTRA DLD XPS system equipped with an Al Ka X-ray source and a 165-mm mean radius electron energy hemispherical analyzer. Mineral samples used for XPS were dried in vacuum overnight before analysis. Survey scans were collected from -5 eV to 1200 eV electron binding energy with a resolution of 1 eV and a pass energy of 80 eV. Narrow scans were performed to obtain detailed chemical bonding information of the mineral samples. These high-resolution (i.e., 0.1 eV, pass energy=20 eV) scans were performed for the elements in Table S1.

Table S1. XPS measurement parameters

Element	Start Core Level (eV)	End Core Level (eV)
Mg 1s	1310	1290
Na 1s	1280	1260
O 1s	540	520
C 1s	300	275
Ca 2p	360	340
Cl 2p	210	190
Si 2p	110	95
Mg 2p	60	40

A charge neutralizer was used to minimize sample charging during XPS analyses. XPS spectra were analyzed in CasaXPS (Casa Software Ltd., Teignmouth, UK). Baseline background subtraction was performed using a Shirley background and peak deconvolution implemented Gaussian-Lorentzian shapes. Binding energies were calibrated with respect to the C 1s peak at 284.7 eV corresponding to adventitious carbon; this approach has been considered arbitrary due to the complexity and heterogeneity of adventitious carbon.⁵

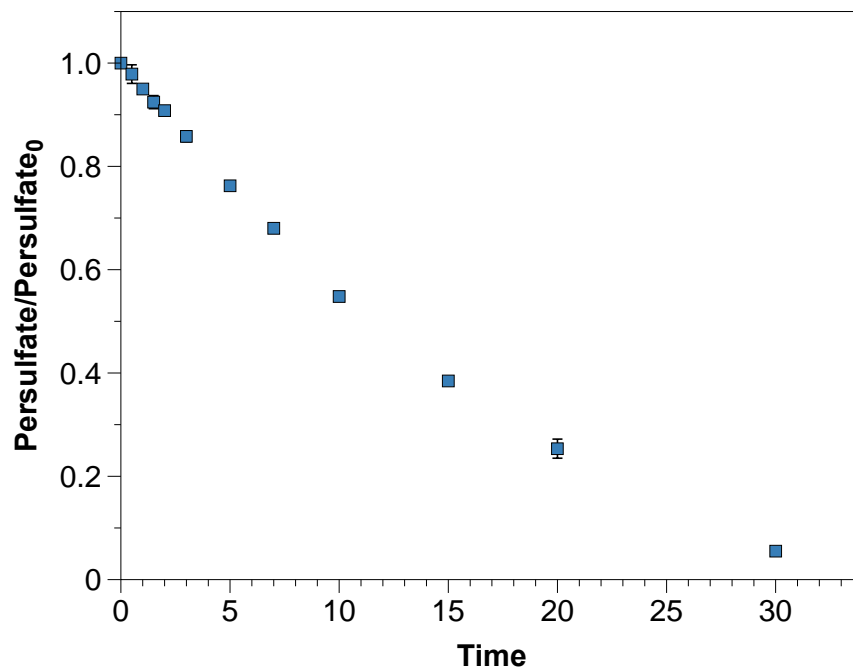


Figure S3. Persulfate degradation by the UV/Persulfate system. Experimental condition: $[\text{Persulfate}]_0 = 1 \text{ mM}$; initial pH = 7.8. Note: This persulfate degradation result is from the 1 mM persulfate experiment in Fig. 2.

Table S2. The saturation index and theoretical solid amount calculation of raw brine and brine feeded into the CDM process with pH adjustment in the absence of antiscalant.

Mineral	Raw brine (pH=7.8)			Brine feeded into the CDM process (pH=10.2)		
	Saturati on index	Theoretic al solids amount (mg· L ⁻¹)	Percenta ge* (%)	Saturati on index	Theoretic al solids amount (mg· L ⁻¹)	Percenta ge* (%)
Calcite β-CaCO _{3(s)}	2.0	416	39%	3.2	514	32%
Dolomite CaMg(CO ₃) _{2(s)}	4.0	550	51%	6.3	996	62%
Silica α-SiO _{2(s)}	1.3	103	10%	0.7	103	6%

* Percentage (%) = $\frac{\text{Specific Mineral amount}}{\text{Total solids amount}} \times 100\%$

Text S4. Detailed explanation of the recovered mineral amount calculation procedure in

Fig. 4

Recovered minerals ($2 \text{ g} \cdot \text{L}^{-1}$) from the CDM process were dissolved in nitric acid, and the concentrations of calcium, magnesium, and silicon were measured by ICP-MS. Based on the measured concentration of each cation, the chemical formula of major precipitates, and the molar mass of calcite (CaCO_3), dolomite ($\text{CaMg}(\text{CO}_3)_2$), and silica (SiO_2), the weight of recovered solids were calculated.

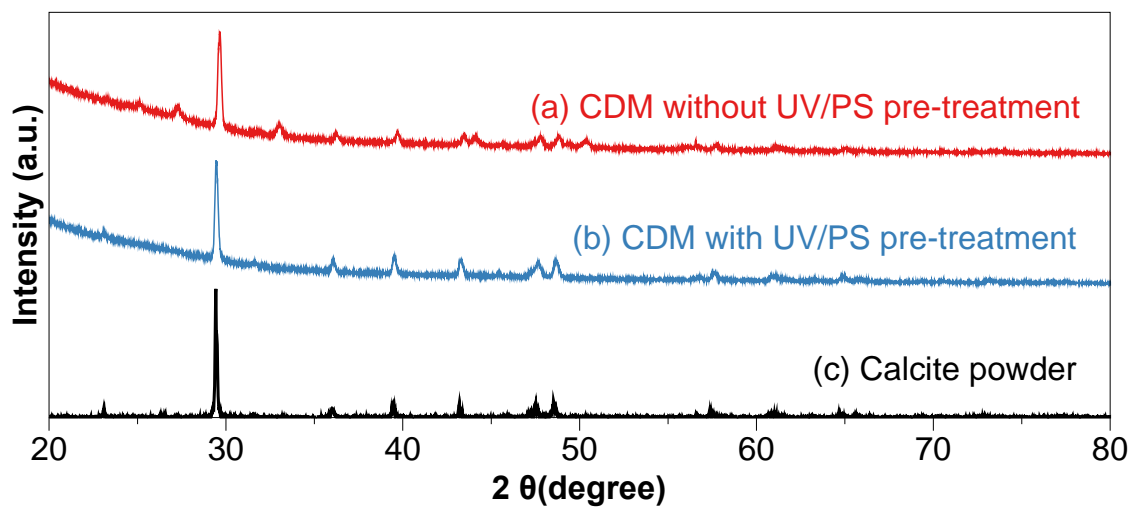


Figure S4. XRD patterns of recovered minerals from CDM without UV/PS pre-treatment (a), recovered resources from CDM with UV/PS pre-treatment (b), and calcite powder R050128 with reference pattern (c).⁶

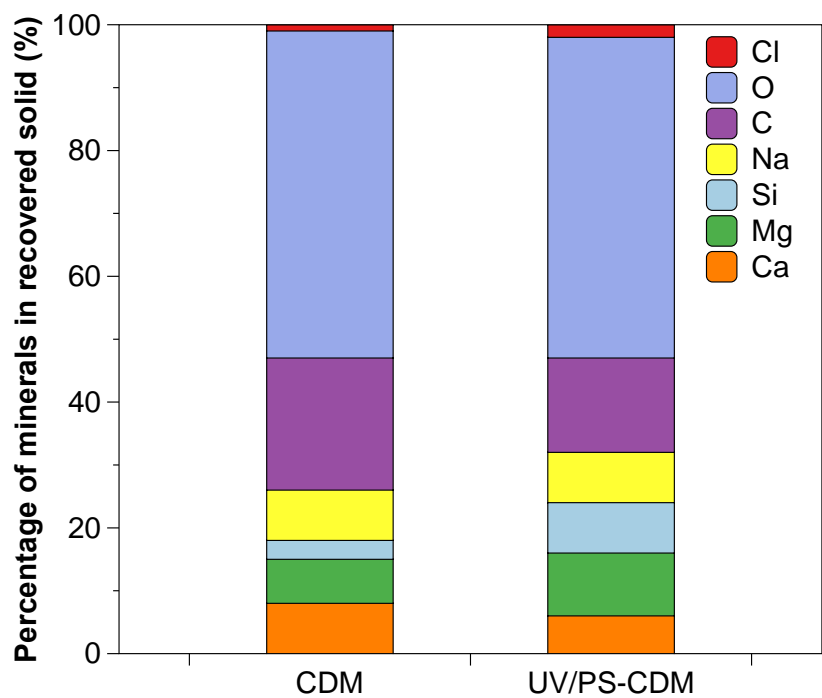


Figure S5. Surface atomic compositions XPS results of recovered minerals from the CDM process without UV/PS pre-treatment (CDM) and with UV/PS pre-treatment (UV/PS-CDM).

Table S3. The concentrations of major cations and TDS in the RO permeate without and with UV/PS pre-treatment. Note: removal efficiencies were calculated using ion concentrations in the RO permeate and the RO feedwater.

pH	Pre-treatment	Na Removal (%) [*]	Mg Removal (%) [*]	Ca Removal (%) [*]	Total Dissolved Solids (mg/L) [*]
5	UV/PS-CDM	93.5 ±0.7	98.6 ±0.9	98.6 ±1.3	382 ±10
	CDM	94.5 ±0.8	98.5 ±0.8	98.5 ±1.1	425.5 ±52
7.8	UV/PS-CDM	93.8 ±2.9	99.0 ±0.9	98.4 ±2.6	302 ±78
	CDM	94.8±1.0	99.2 ±0.3	99.4 ±1.0	280 ±36
10.2	UV/PS-CDM	96.1 ±0.8	99.6 ±0.5	99.5 ±0.6	269 ±114
	CDM	94.0±1.8	99.5 ±0.7	99.6 ±0.5	222 ±42

^{*}± indicates 95% confidence intervals.

Text S5. Energy Consumption Calculation of the UV/PS-CDM-MF-RO System

Energy consumption in this treatment train is mainly caused by UV/PS photochemical treatment, mixing during chemical demineralization, MF pump energy consumption, and secondary RO desalination process. Hence, the total energy consumption of the UV/PS-CDM-MF-RO System was calculated as a summation of each stage's energy consumption.

Electrical Energy per Order calculation of UV process:

Electrical Energy per Order (EEO) ($\text{kWh} \cdot \text{m}^{-3} \cdot \text{order}$) of UV/PS photochemical treatment was calculated by equation S3 below.⁷

$$EEO = \frac{P \cdot n \cdot f \cdot t}{V \cdot -\log(C/C_0)} \quad (\text{S3})$$

Where P is the power consumption of medium pressure UV lamp (kW), which is 0.45 kW. n is the number of lamps, which is 1. f is the fraction of the emitting portion of the lamp submerged in the solution, which is 1. t is the treatment time (h), which is 0.33h. V is the reactor volume (m^3), which is 0.0035 m^3 . C/C_0 is the degradation ratio, which is 0.001. Based on the above equation and parameters, EEO equals $14.14 \text{ kWh} \cdot \text{m}^{-3} \cdot \text{order}$.

Mixing energy consumption:

Our mixing is performed by the Fisher Scientific mixer (CAT NO: 11-100-49S, P = 0.02kW). In the demineralization process, we set 1 minute ($t = 0.017\text{h}$) 700 rpm mixing period. Treated volume V is 3.5L (0.0035m^3)

$$\text{Mixing energy consumption} = \frac{P \cdot t}{V}$$

Where P is mixing power (kW), t is the mixing period (hour), and V is the treated water volume (m^3). Based on the equation above, the estimated EE/O for the mixing process is around $0.1 \text{ kWh} \cdot \text{m}^{-3}$.

Energy Consumption of MF and RO process:

Energy consumption of the MF and RO process was determined based on the literature to estimate more realistic values. According to Tow et al., the energy consumption of an MF process is approximately $0.18 \text{ kWh} \cdot \text{m}^{-3}$.⁸ For the RO system with BW30 membrane and treating similar feed concentration, Richards et al. found that specific energy consumption was $2.3 \text{ kWh} \cdot \text{m}^{-3}$ to treat feedwater with $5.3 \text{ g} \cdot \text{L}^{-1}$ TDS.⁹ Shen et al. found that the RO process with BW30 membrane consumes 3.21 to $4.24 \text{ kWh} \cdot \text{m}^{-3}$ to treat water with $4 \text{ g} \cdot \text{L}^{-1}$ TDS.¹⁰

Reference

- (1) Hafiz, M. A.; Hawari, A. H.; Alfahel, R.; Hassan, M. K.; Altaee, A. Comparison of Nanofiltration with Reverse Osmosis in Reclaiming Tertiary Treated Municipal Wastewater for Irrigation Purposes. *Membranes (Basel)* **2021**, *11* (1), 1–13. <https://doi.org/10.3390/membranes11010032>.
- (2) Yangali-Quintanilla, V.; Maeng, S. K.; Fujioka, T.; Kennedy, M.; Amy, G. Proposing Nanofiltration as Acceptable Barrier for Organic Contaminants in Water Reuse. *J Memb Sci* **2010**, *362* (1–2), 334–345. <https://doi.org/10.1016/j.memsci.2010.06.058>.
- (3) Alsarayreh, A. A.; Al-Obaidi, M. A.; Farag, S. K.; Patel, R.; Mujtaba, I. M. Performance Evaluation of a Medium-Scale Industrial Reverse Osmosis Brackish Water Desalination Plant with Different Brands of Membranes. A Simulation Study. *Desalination* **2021**, *503* (October 2020), 114927. <https://doi.org/10.1016/j.desal.2020.114927>.
- (4) Idil Mouhoumed, E.; Szymczyk, A.; Schäfer, A.; Paugam, L.; La, Y. H. Physico-Chemical Characterization of Polyamide NF/RO Membranes: Insight from Streaming Current Measurements. *J Memb Sci* **2014**, *461*, 130–138. <https://doi.org/10.1016/j.memsci.2014.03.025>.
- (5) Greczynski, G.; Hultman, L. X-Ray Photoelectron Spectroscopy: Towards Reliable Binding Energy Referencing. *Prog Mater Sci* **2020**, *107* (April 2019), 100591. <https://doi.org/10.1016/j.pmatsci.2019.100591>.
- (6) Lafuente, B.; Downs, R. T.; Yang, H.; Stone, N. *The Power of Databases: The RRUFF Project*; 2016. <https://doi.org/10.1515/9783110417104-003>.
- (7) Qanbarzadeh, M.; DiGiacomo, L.; Bouteh, E.; Alhamdan, E. Z.; Mason, M. M.; Wang, B.; Wong, M. S.; Cates, E. L. An Ultraviolet/Boron Nitride Photocatalytic Process Efficiently Degrades Poly-/Perfluoroalkyl Substances in Complex Water Matrices. *Environ Sci Technol Lett* **2023**, *10* (8), 705–710. <https://doi.org/10.1021/acs.estlett.3c00363>.
- (8) Tow, E. W.; Hartman, A. L.; Jaworowski, A.; Zucker, I.; Kum, S.; AzadiAghdam, M.; Blatchley, E. R.; Achilli, A.; Gu, H.; Urper, G. M.; Warsinger, D. M. Modeling the Energy Consumption of Potable Water Reuse Schemes. *Water Res X* **2021**, *13*, 100126. <https://doi.org/10.1016/j.wroa.2021.100126>.
- (9) Richards, B. S.; Capao, D. P. S.; Schafer, A. I. The Effect of Energy Fluctuations on Performance of a Photovoltaic Hybrid Membrane System. *Environ Sci Technol* **2008**, *42* (12), 4563–4569.

- (10) Shen, J.; Jeyhanipour, A.; Richards, B. S.; Schäfer, A. I. Renewable Energy Powered Membrane Technology: Experimental Investigation of System Performance with Variable Module Size and Fluctuating Energy. *Sep Purif Technol* **2019**, *221* (March), 64–73. <https://doi.org/10.1016/j.seppur.2019.03.004>.

Appendix D

Supporting Information for chapter 5

Previously published in *ACS ES&T Water*

Tang, X., & Liu, H. (2024). Mechanisms of Alleviating Gypsum Scaling by Antiscalants during Membrane Desalination: Implications on Agricultural Drainage Water Reuse. *ACS ES&T Water*, 4(8), 3486-3494. <https://doi.org/10.1021/acsestwater.4c00298>

Text S1: Lab-scale RO desalination setup description and preparation

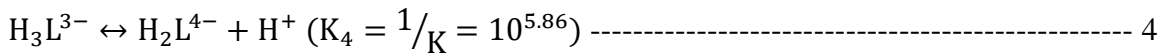
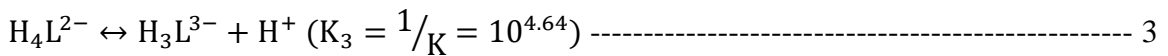
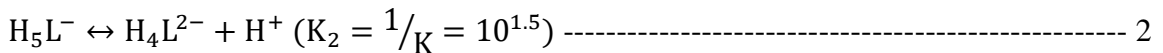
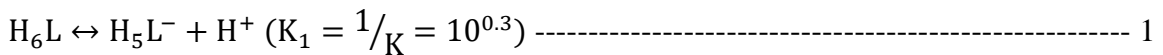
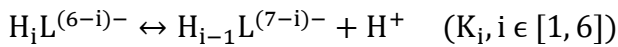
Our lab-scale membrane desalination unit comprises several components, including a cross-flow membrane module (CF042 cell assembly, Sterlitech), a mass scale, a chiller (NSC0250-FROST, North Slope), inlet and outlet pressure gauges, a pump and a 10-L feedwater reservoir (Figure S1). To prepare the new RO membrane for use, it was cut to fit the membrane module and soaked into 25% isopropanol for 30 min before being rinsed with DI water. The RO membrane was then placed in the membrane module, and the chiller was turned on to maintain the temperature at 25°C. Feedwater was pumped from the feedwater reservoir into the membrane module at a flow rate of 1.2 L/min (Flow rate suggested by manufacturer is 0.6 – 2.7 L/min). The system's operating pressure was maintained at 150 psi, following the recirculation mode, and thus permeate was generated vertically from the membrane module. The permeate was collected on the mass scale, and the weight was automatically recorded on a laptop, while the concentrate flowed back into the feedwater reservoir. The recirculation mode is feasible for lab-scale desalination experiments because it can provide flux curve analysis with a compact setup. Before the start of each RO experiment, DI water was used as the feedwater for 30 min to optimize the RO membrane performance before switching to the target feedwater.

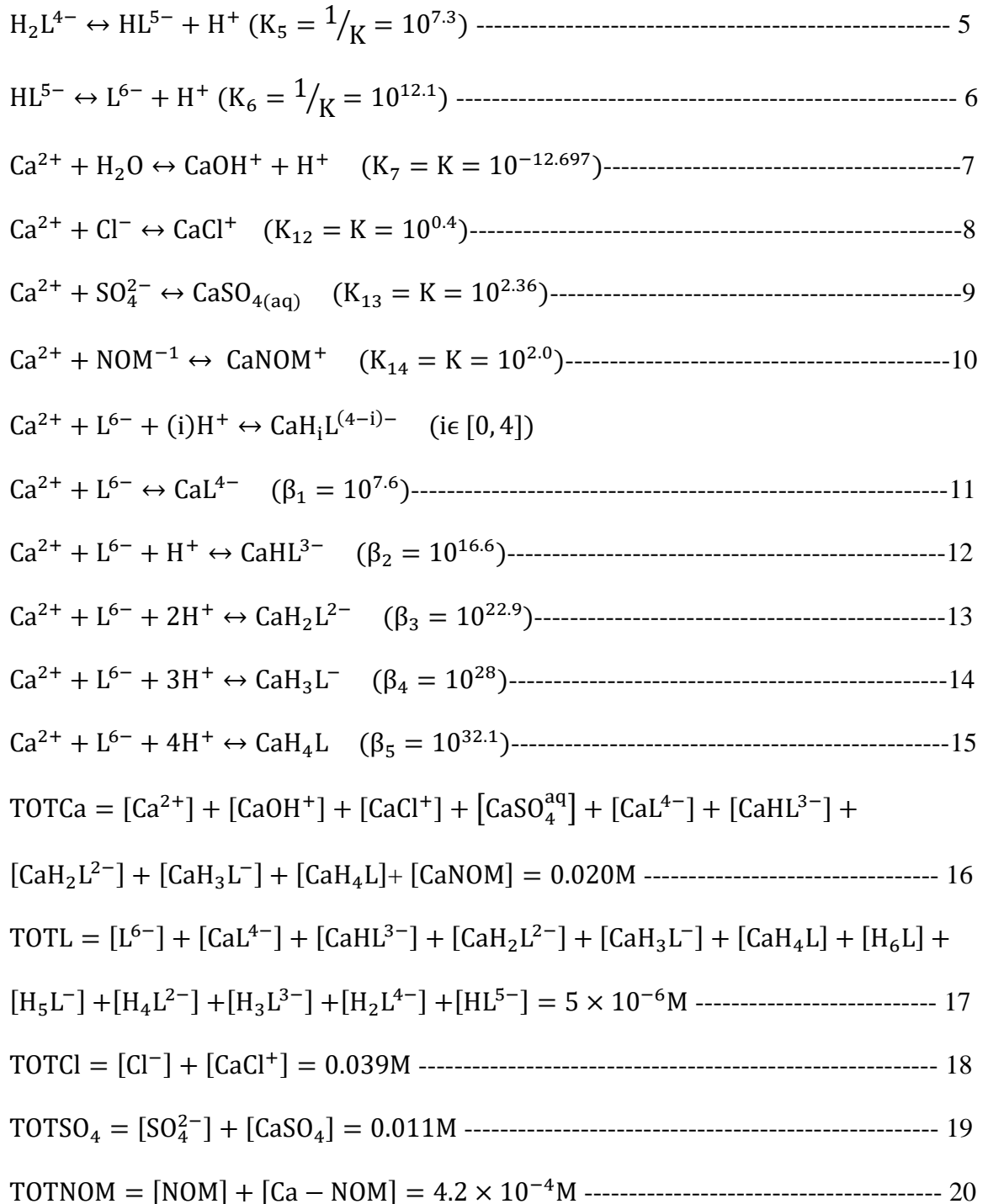
Text S2: theoretical calculations of total charge of antiscalants aqueous species in the drainage water.

In this study, complexations between one mole of calcium and one mole of antiscalant or inorganic anions were considered only. The available equilibrium constants sourced from the current literature only include complexation between one mole of calcium and one mole of antiscalant. Therefore, we did not consider other forms of complexation in our theoretical calculations. As for inorganic anions, such as chloride and sulfate, they are monodentate when complex with calcium.¹ We believe that the currently available data is sufficient to support conclusions drawn in this study.

In addition, this theoretical calculation assumed that NOM 100% exist as negatively charged base molecule NOM^{-1} that can form aqueous complex with calcium with molar ratio 1:1. The equilibrium constant value of this complexation is determined through equations developed by KIRISHIMA, et al., 2010.² In this study, K of complexation between different humic acids and fulvic acids and calcium was developed and listed in table 2 of KIRISHIMA, et al., 2010.

NTMP calculation:





By combining 20 equations above, an equation that only contains $[\text{Ca}^{2+}]$ unknown can be got:

$$a[\text{Ca}^{2+}]^5 + b[\text{Ca}^{2+}]^4 + c[\text{Ca}^{2+}]^3 + d[\text{Ca}^{2+}]^2 + e[\text{Ca}^{2+}] + f = 0$$

Define:

$$A = \beta_1 + \beta_2[\text{H}^+] + \beta_3[\text{H}^+]^2 + \beta_4[\text{H}^+]^3 + \beta_5[\text{H}^+]^4$$

$$B = 1 + K_1K_2 \dots K_6[\text{H}^+]^6 + K_2K_3 \dots K_6[\text{H}^+]^5 + K_3K_4 \dots K_6[\text{H}^+]^4 + K_4K_5K_6[\text{H}^+]^3 + K_5K_6[\text{H}^+]^2 + K_6[\text{H}^+]$$

Then

$$a = A\left(1 + \frac{K_7}{[\text{H}^+]}\right)K_8K_9K_{10}$$

$$b = \left(1 + \frac{K_7}{[\text{H}^+]}\right) \left(AK_{10}(K_8 + K_9) + K_8K_9(A + BK_{10}) \right) + A \cdot \text{TOTCl} \cdot K_8K_9K_{10} + A \cdot \text{TOTSO}_4 \cdot K_8K_9K_{10} + A \cdot \text{TOTL} \cdot K_8K_9K_{10} + A \cdot \text{TOTNOM} \cdot K_8K_9K_{10} - A \cdot \text{TOTCa} \cdot K_8K_9K_{10}$$

$$c = \left(1 + \frac{K_7}{[\text{H}^+]}\right) \left(A(K_8 + K_9 + K_{10}) + B(K_8K_9 + K_8K_{10} + K_9K_{10}) \right) + \text{TOTCl} \cdot (A \cdot K_8K_9 + A \cdot K_8K_{10} + B \cdot K_8K_9K_{10}) + \text{TOTSO}_4 \cdot (A \cdot K_8K_9 + A \cdot K_9K_{10} + B \cdot K_8K_9K_{10}) + \text{TOTL} \cdot A \cdot (K_8K_9 + K_8K_{10} + K_9K_{10}) + \text{TOTNOM} \cdot (A \cdot K_8K_{10} + A \cdot K_9K_{10} + B \cdot K_8K_9K_{10}) - \text{TOTCa} \cdot (A(K_8K_9 + K_8K_{10} + K_9K_{10}) + B(K_8K_9K_{10}))$$

$$d = \left(1 + \frac{K_7}{[\text{H}^+]}\right) \left(B(K_8 + K_9 + K_{10}) + A \right) + \text{TOTCl} \cdot (A \cdot K_8 + B \cdot K_8K_9 + B \cdot K_8K_{10}) + \text{TOTSO}_4 \cdot (A \cdot K_9 + B \cdot K_8K_9 + B \cdot K_9K_{10}) + \text{TOTL} \cdot A \cdot (K_8 + K_9 + K_{10}) + \text{TOTNOM} \cdot (A \cdot K_{10} + B \cdot K_9K_{10} + B \cdot K_8K_{10}) - \text{TOTCa} \cdot (A(K_8 + K_9 + K_{10}) + B(K_8K_9 + K_8K_{10} + K_9K_{10}))$$

$$e = \left(1 + \frac{K_7}{[H^+]}\right) \cdot B + \text{TOTCl} \cdot B \cdot K_8 + \text{TOTSO}_4 \cdot B \cdot K_9 + \text{TOTL} \cdot A + \text{TOTNOM} \cdot B \cdot$$

$$K_{10} - \text{TOTCa} \cdot (A + B(K_8 + K_9 + K_{10}))$$

$$f = -\text{TOTCa} \cdot B$$

Then 20 unknowns can be solved: Ca^{2+} , CaL^{4-} , CaHL^{3-} , $\text{CaH}_2\text{L}^{2-}$, CaH_3L^- , CaH_4L , CaOH^+ , CaCl^+ , CaSO_4 , SO_4^{2-} , Cl^- , H_6L , H_5L^- , H_4L^{2-} , H_3L^{3-} , H_2L^{4-} , HL^{5-} , L^{6-} , Ca-NOM , NOM .

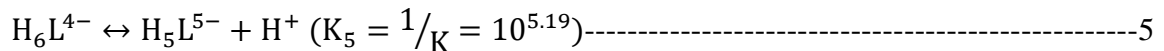
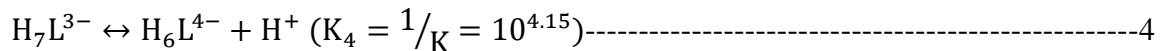
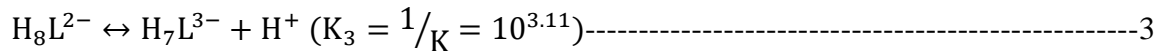
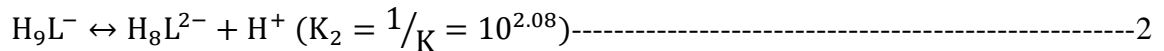
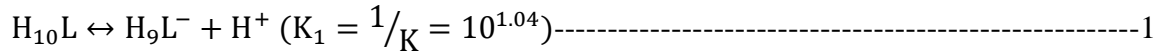
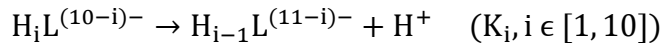
If NOM is not considered, then remove equation 10, 20 and $[\text{CaNOM}]$ in equation 16.

Then problem becomes 18 equations solve 18 unknowns. And final equation in the form of $[\text{Ca}^{2+}]$ becomes:

$$a[\text{Ca}^{2+}]^4 + b[\text{Ca}^{2+}]^3 + c[\text{Ca}^{2+}]^2 + d[\text{Ca}^{2+}] + e = 0$$

By using equation above, $[\text{Ca}^{2+}]$ and other species concentration can be solved at different pH. Then total charge of antiscalant species Φ is calculated by equation 3 in the main text.

DTPMP calculation:



$H_5L^{5-} \leftrightarrow H_4L^{6-} + H^+ (K_6 = 1/K = 10^{6.23})$	-----6
$H_4L^{6-} \leftrightarrow H_3L^{7-} + H^+ (K_7 = 1/K = 10^{7.23})$	-----7
$H_3L^{7-} \leftrightarrow H_2L^{8-} + H^+ (K_8 = 1/K = 10^{8.3})$	-----8
$H_2L^{8-} \leftrightarrow HL^{9-} + H^+ (K_9 = 1/K = 10^{11.18})$	-----9
$HL^{9-} \leftrightarrow L^{10-} + H^+ (K_{10} = 1/K = 10^{12.58})$	-----10
$Ca^{2+} + H_2O \leftrightarrow CaOH^+ + H^+ (K_{11} = K = 10^{-12.697})$	-----11
$Ca^{2+} + Cl^- \leftrightarrow CaCl^+ (K_{12} = K = 10^{0.4})$	-----12
$Ca^{2+} + SO_4^{2-} \leftrightarrow CaSO_{4(aq)} (K_{13} = K = 10^{2.36})$	-----13
$Ca^{2+} + NOM^{-1} \leftrightarrow CaNOM^+ (K_{14} = K = 10^{2.0})$	-----14
$Ca^{2+} + H_iL^{(10-i)-} \leftrightarrow CaH_iL^{(8-i)-} (\beta_i, i \in [2, 9])$	
$Ca^{2+} + H_2L^{8-} \leftrightarrow CaH_2L^{6-} (\beta_1 = 10^{5.04})$	-----15
$Ca^{2+} + H_3L^{7-} \leftrightarrow CaH_3L^{5-} (\beta_2 = 10^{4.41})$	-----16
$Ca^{2+} + H_4L^{6-} \leftrightarrow CaH_4L^{4-} (\beta_3 = 10^{3.78})$	-----17
$Ca^{2+} + H_5L^{5-} \leftrightarrow CaH_5L^{3-} (\beta_4 = 10^{3.5})$	-----18
$Ca^{2+} + H_6L^{4-} \leftrightarrow CaH_6L^{2-} (\beta_5 = 10^{2.52})$	-----19
$Ca^{2+} + H_7L^{3-} \leftrightarrow CaH_7L^- (\beta_6 = 10^{1.89})$	-----20
$Ca^{2+} + H_8L^{2-} \leftrightarrow CaH_8L (\beta_7 = 10^{1.26})$	-----21
$Ca^{2+} + H_9L^- \leftrightarrow CaH_9L^+ (\beta_8 = 10^{0.63})$	-----22
TOTCa = $[Ca^{2+}] + [CaOH^+] + [CaCl^+] + [CaSO_4^{aq}] + [CaH_2L^{6-}] + [CaH_3L^{5-}] +$ $[CaH_4L^{4-}] + [CaH_5L^{3-}] + [CaH_6L^{2-}] + [CaH_7L^-] + [CaH_8L] + [CaH_9L^+] + [CaNOM]$	
----- 23	

$$\begin{aligned} \text{TOTL} = & [\text{L}^{10-}] + [\text{CaH}_2\text{L}^{6-}] + [\text{CaH}_3\text{L}^{5-}] + [\text{CaH}_4\text{L}^{4-}] + [\text{CaH}_5\text{L}^{3-}] + [\text{CaH}_6\text{L}^{2-}] + \\ & [\text{CaH}_7\text{L}^-] + [\text{CaH}_8\text{L}] + [\text{CaH}_9\text{L}^+] + [\text{H}_{10}\text{L}] + [\text{H}_9\text{L}^-] + [\text{H}_8\text{L}^{2-}] + [\text{H}_7\text{L}^{3-}] + [\text{H}_6\text{L}^{4-}] \\ & + [\text{H}_5\text{L}^{5-}] + [\text{H}_4\text{L}^{6-}] + [\text{H}_3\text{L}^{7-}] + [\text{H}_2\text{L}^{8-}] + [\text{HL}^{9-}] \text{-----} 24 \end{aligned}$$

$$\text{TOTCl} = [\text{Cl}^-] + [\text{CaCl}^+] \text{-----} 25$$

$$\text{TOTSO}_4 = [\text{SO}_4^{2-}] + [\text{CaSO}_4] \text{-----} 26$$

$$\text{TOTNOM} = [\text{NOM}] + [\text{Ca} - \text{NOM}] \text{-----} 27$$

By combining 27 equations above, an equation that only contains $[\text{Ca}^{2+}]$ unknown can be got:

$$a[\text{Ca}^{2+}]^5 + b[\text{Ca}^{2+}]^4 + c[\text{Ca}^{2+}]^3 + d[\text{Ca}^{2+}]^2 + e[\text{Ca}^{2+}] + f = 0$$

Define:

$$\begin{aligned} A = & 1 + K_{10}[\text{H}^+] + K_{10}K_9[\text{H}^+]^2 + K_{10}K_9K_8[\text{H}^+]^3 + K_{10}K_9 \dots K_7[\text{H}^+]^4 \\ & + K_{10}K_9 \dots K_6[\text{H}^+]^5 + K_{10}K_9 \dots K_5[\text{H}^+]^6 + K_{10}K_9 \dots K_4[\text{H}^+]^7 \\ & + K_{10}K_9 \dots K_3[\text{H}^+]^8 + K_{10}K_9 \dots K_2[\text{H}^+]^9 + K_{10}K_9 \dots K_1[\text{H}^+]^{10} \end{aligned}$$

$$\begin{aligned} B = & K_{10}K_9\beta_1[\text{H}^+]^2 + K_{10}K_9K_8\beta_2[\text{H}^+]^3 + K_{10}K_9 \dots K_7\beta_3[\text{H}^+]^4 + K_{10}K_9 \dots K_6\beta_4[\text{H}^+]^5 \\ & + K_{10}K_9 \dots K_5\beta_5[\text{H}^+]^6 + K_{10}K_9 \dots K_4\beta_6[\text{H}^+]^7 + K_{10}K_9 \dots K_3\beta_7[\text{H}^+]^8 \\ & + K_{10}K_9 \dots K_2\beta_8[\text{H}^+]^9 \end{aligned}$$

$$C = 1 + \frac{K_{11}}{[\text{H}^+]}$$

Then

$$a = \text{BCK}_{12}K_{13}K_{14}$$

$$b = C(BK_{14}(K_{12} + K_{13}) + K_{12}K_{13}(B + AK_{14})) + B \cdot \text{TOTCl} \cdot K_{12}K_{13}K_{14} + B \cdot \text{TOTSO}_4 \cdot K_{12}K_{13}K_{14} + B \cdot \text{TOTL} \cdot K_{12}K_{13}K_{14} + B \cdot \text{TOTNOM} \cdot K_{12}K_{13}K_{14} - B \cdot \text{TOTCa} \cdot K_{12}K_{13}K_{14}$$

$$c = C(B(K_{12} + K_{13} + K_{14}) + A(K_{12}K_{13} + K_{12}K_{14} + K_{13}K_{14})) + \text{TOTCl} \cdot (B \cdot K_{12}K_{13} + B \cdot K_{12}K_{14} + A \cdot K_{12}K_{13}K_{14}) + \text{TOTSO}_4 \cdot (B \cdot K_{12}K_{13} + B \cdot K_{13}K_{14} + A \cdot K_{12}K_{13}K_{14}) + \text{TOTL} \cdot B \cdot (K_{12}K_{13} + K_{12}K_{14} + K_{13}K_{14}) + \text{TOTNOM} \cdot (B \cdot K_{12}K_{14} + B \cdot K_{13}K_{14} + A \cdot K_{12}K_{13}K_{14}) - \text{TOTCa} \cdot (B(K_{12}K_{13} + K_{13}K_{14} + K_{12}K_{14}) + A(K_{12}K_{13}K_{14}))$$

$$d = C(A(K_{12} + K_{13} + K_{14}) + B) + \text{TOTCl} \cdot (B \cdot K_{12} + A \cdot K_{12}K_{13} + A \cdot K_{12}K_{14}) + \text{TOTSO}_4 \cdot (B \cdot K_{13} + A \cdot K_{12}K_{13} + A \cdot K_{13}K_{14}) + \text{TOTL} \cdot B \cdot (K_{12} + K_{13} + K_{14}) + \text{TOTNOM} \cdot (B \cdot K_{14} + A \cdot K_{13}K_{14} + A \cdot K_{12}K_{14}) - \text{TOTCa} \cdot (B(K_{12} + K_{13} + K_{14}) + A(K_{12}K_{13} + K_{12}K_{14} + K_{13}K_{14}))$$

$$e = C \cdot A + \text{TOTCl} \cdot A \cdot K_{12} + \text{TOTSO}_4 \cdot A \cdot K_{13} + \text{TOTL} \cdot B + \text{TOTNOM} \cdot A \cdot K_{14} - \text{TOTCa} \cdot (B + A(K_{12} + K_{13} + K_{14}))$$

$$f = -\text{TOTCa} \cdot A$$

Then 27 unknowns can be solved: Ca^{2+} , CaOH^+ , CaCl^+ , CaSO_4 , SO_4^{2-} , Cl^- , L^{10-} , $\text{CaH}_2\text{L}^{6-}$, $\text{CaH}_3\text{L}^{5-}$, $\text{CaH}_4\text{L}^{4-}$, $\text{CaH}_5\text{L}^{3-}$, $\text{CaH}_6\text{L}^{2-}$, CaH_7L^- , CaH_8L , CaH_9L^+ , H_{10}L , H_9L^- , H_8L^{2-} , H_7L^{3-} , H_6L^{4-} , H_5L^{5-} , H_4L^{6-} , H_3L^{7-} , H_2L^{8-} , HL^{9-} , Ca-NOM, NOM

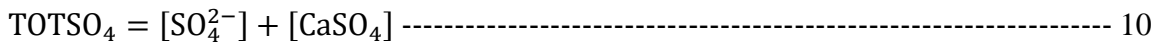
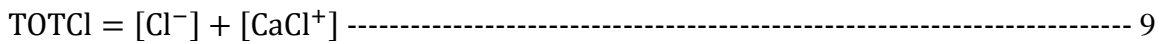
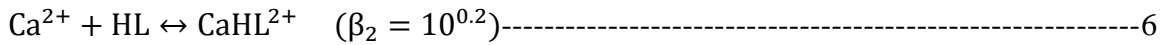
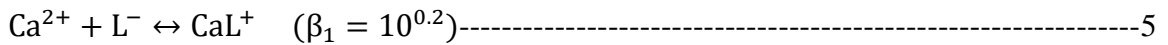
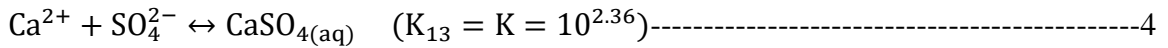
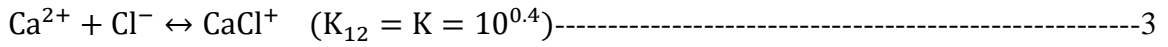
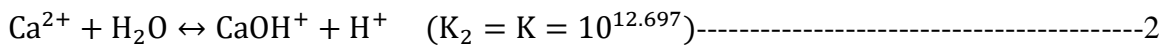
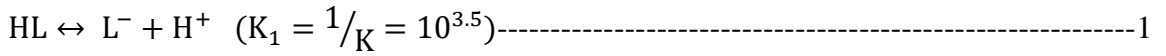
If NOM is not considered, then remove equation 14, 27 and [CaNOM] in equation 23.

Then the problem becomes 25 equations solving 25 unknowns. And the final equation in the form of $[\text{Ca}^{2+}]$ becomes:

$$a[\text{Ca}^{2+}]^4 + b[\text{Ca}^{2+}]^3 + c[\text{Ca}^{2+}]^2 + d[\text{Ca}^{2+}] + e = 0$$

By using equation above, $[Ca^{2+}]$ and other species concentration can be solved at different pH. Then total charge of antiscalant species Φ is calculated by equation 3 in the main text.

PAA calculation:



Total charge of antiscalant species calculation follows same procedure as DTPMP and NTMP calculation.

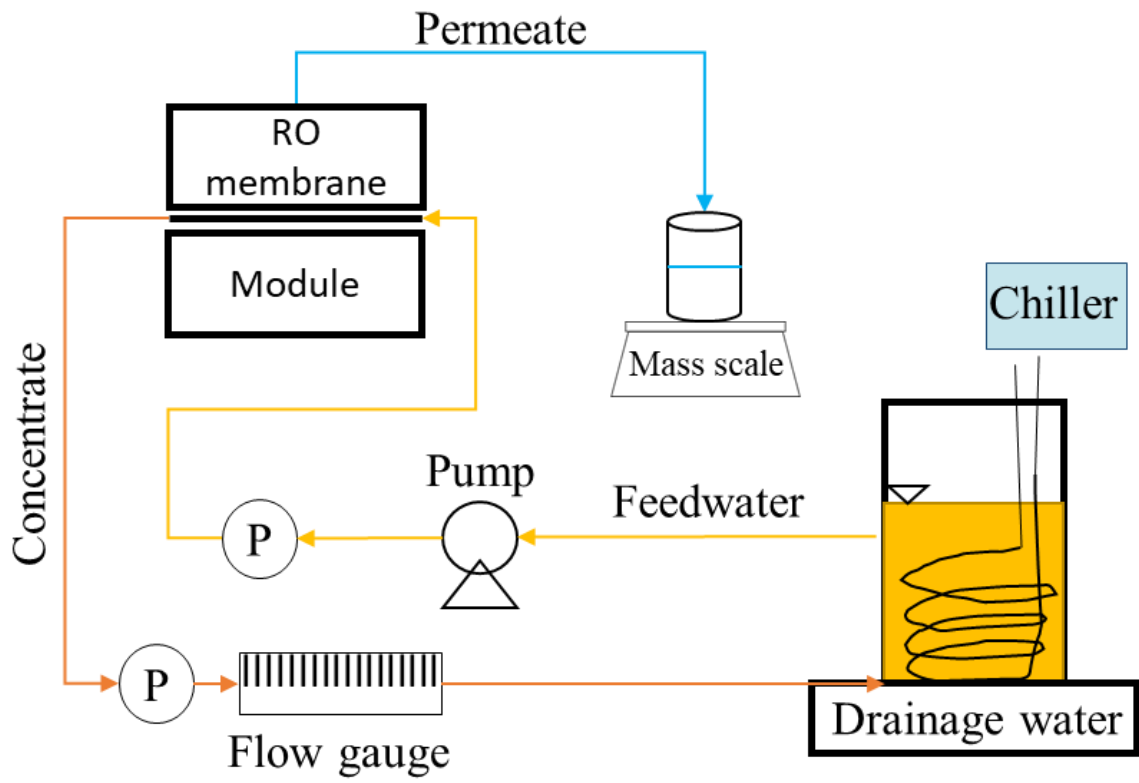


Figure S1. Schematic diagram of lab-scale RO desalination setup.

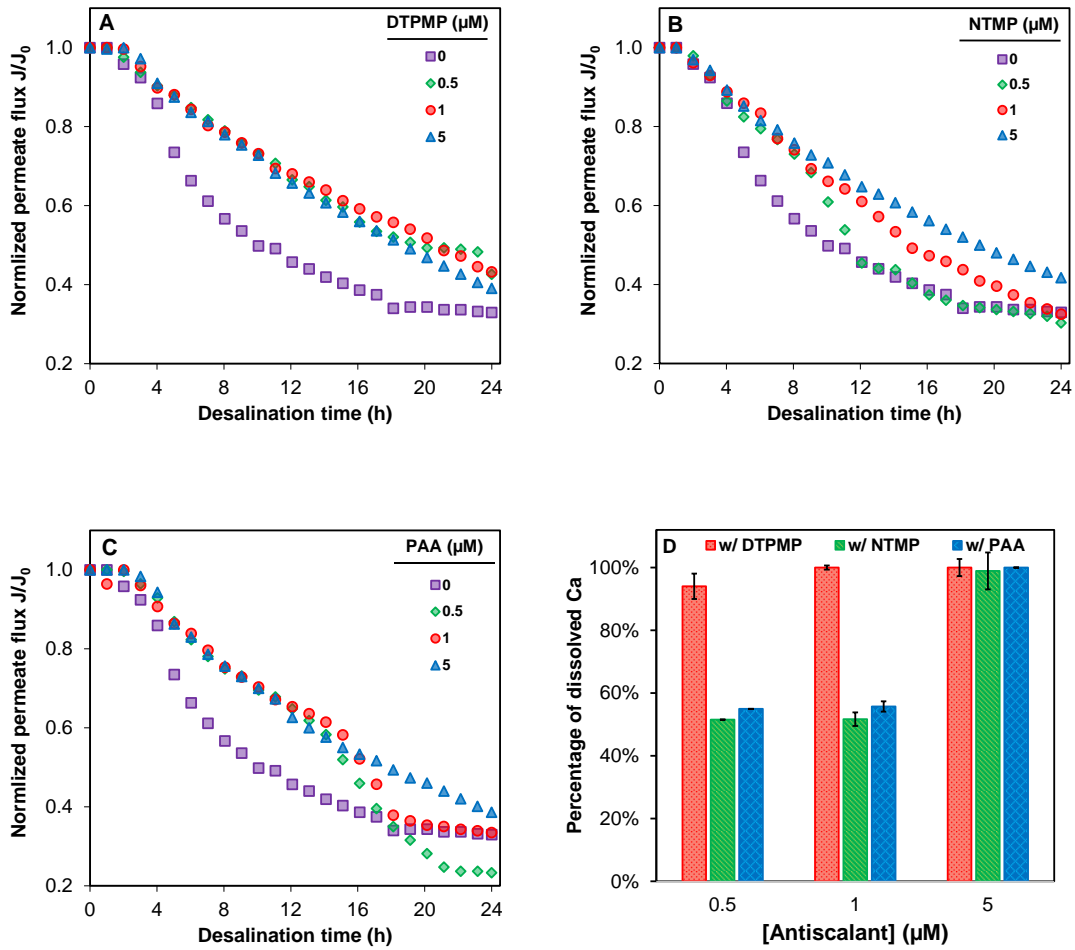


Figure S2. Effect of antiscalant type and concentration on 24 hours RO permeate flux. A) DTPMP = [0.5, 5] μM, B) NTMP = [0.5, 5] μM, C) PAA = [0.5, 5] μM. D) Effect of antiscalant type and concentration on percentage of dissolved Ca at 24 hours of desalination. Feedwater using synthetic drainage water I.

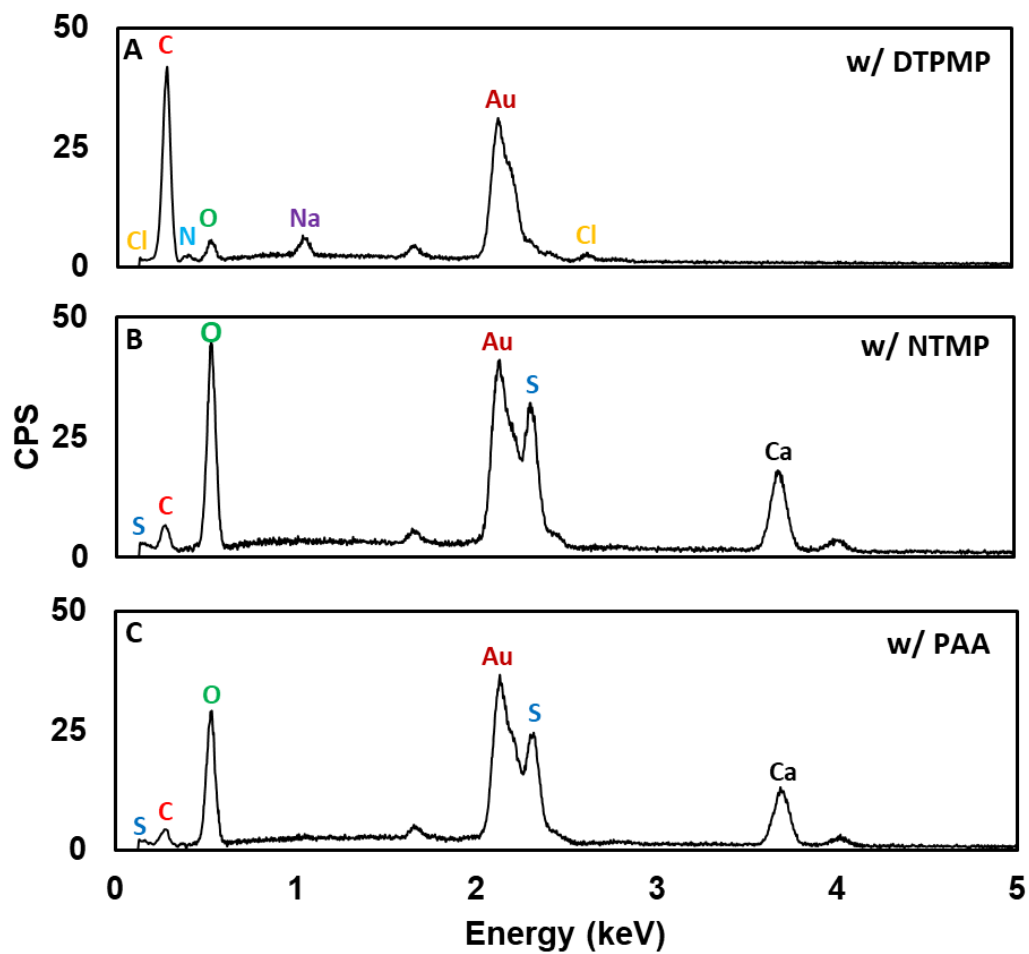


Figure S3. EDS spectra of membrane surface after 24 hours RO desalination with A) 1 μ M DTPMP, B) 1 μ M NTMP, C) 1 μ M PAA. Feedwater using synthetic drainage water I. Peaks not identified are Au, which is used to coat the sample before SEM analysis.

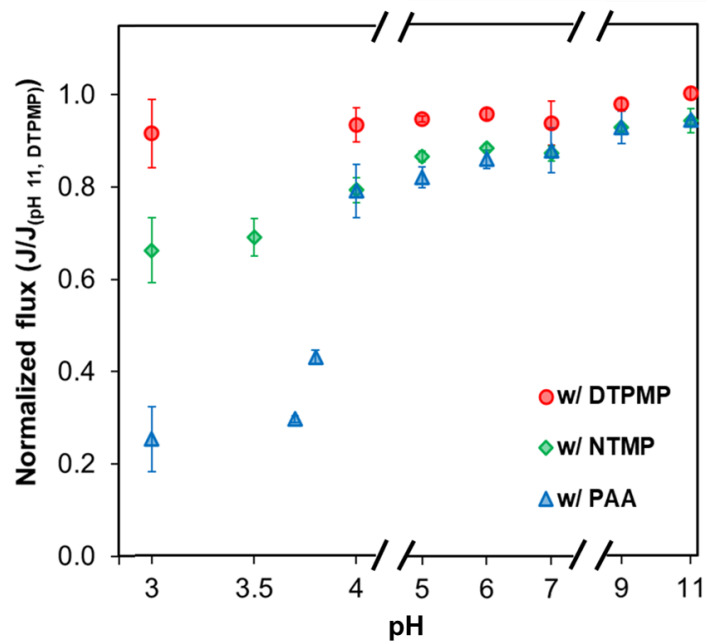


Figure S4. Effect of pH on normalized flux (flux / flux (pH 11, 5 μ M DTPMP)) at 24 hours with different antiscalants. Feedwater using synthetic drainage water I with 5 μ M NTMP or DTPMP or PAA under various pH.

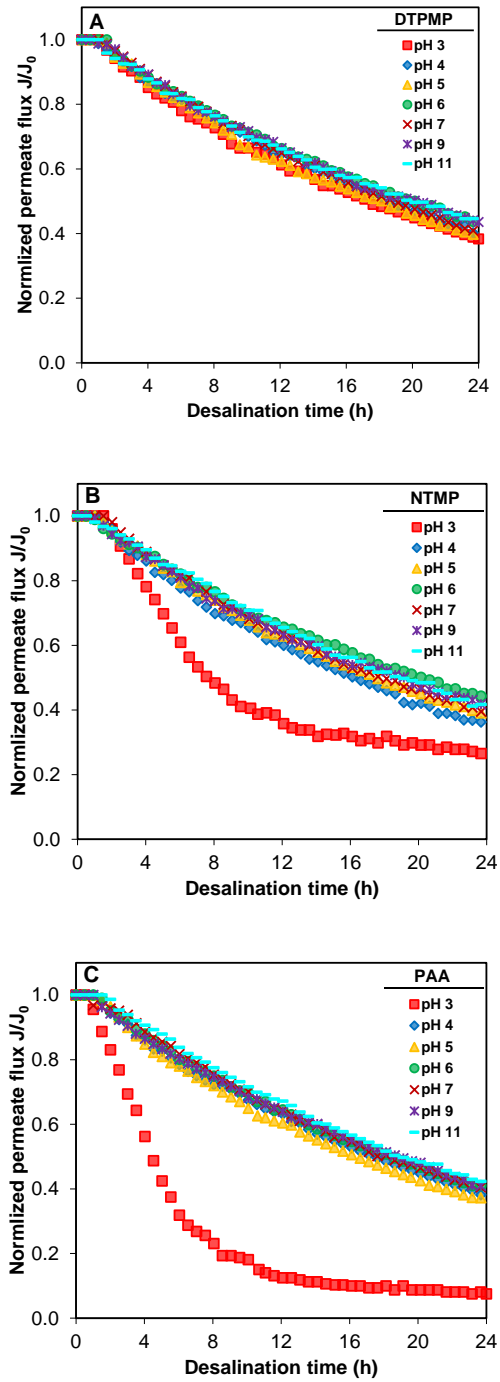


Figure S5. Effect of pH on 24 hours RO permeate flux with addition of 5 μ M A) DTPMP, B) NTMP, C) PAA. Feedwater using synthetic drainage water I.

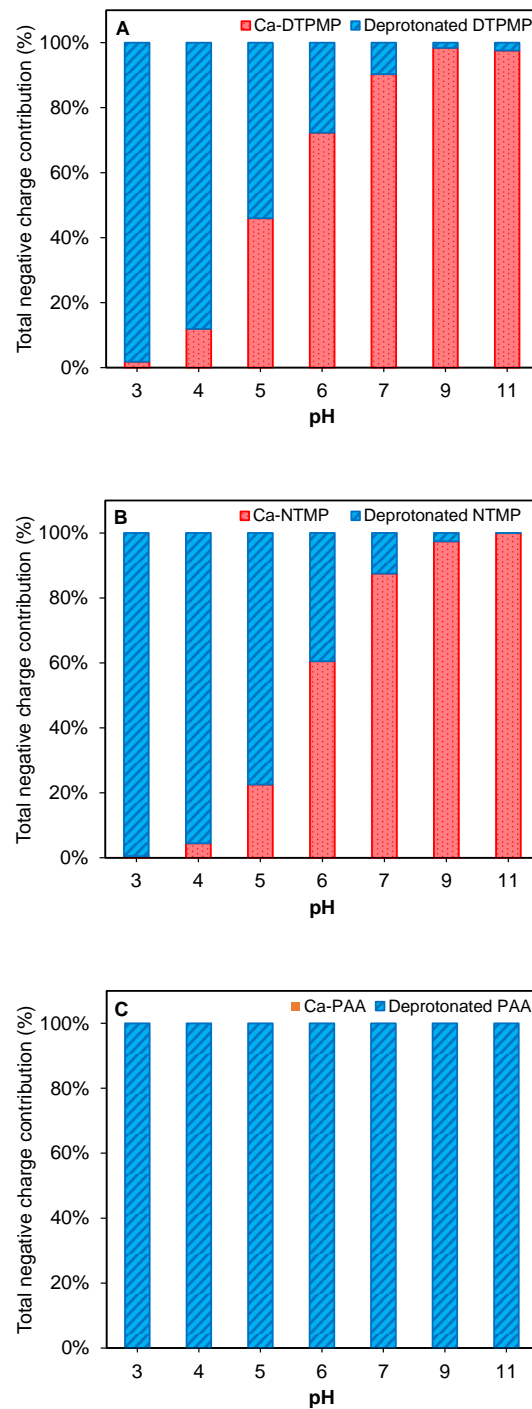


Figure S6. Effect of pH on contributions of total negative charge of different antiscalant species. A) DTPMP, B) NTMP, C) PAA.

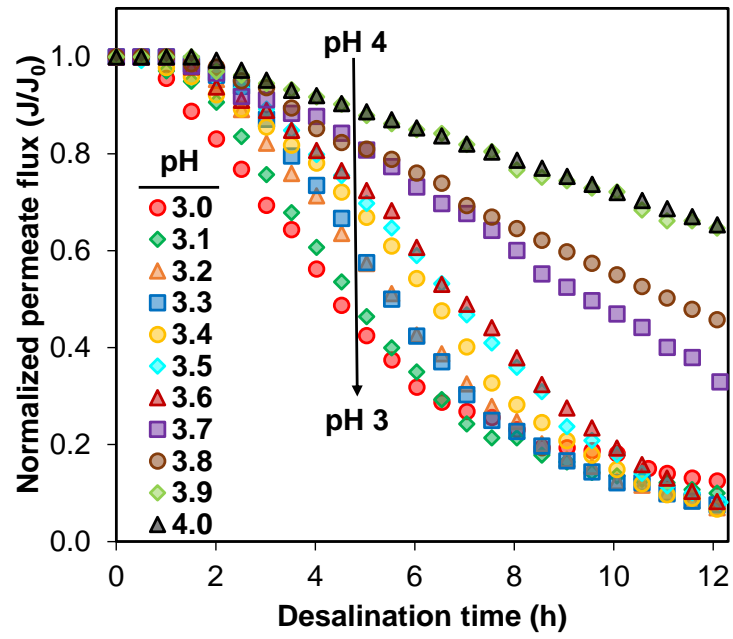


Figure S7. Effect of acidic pH on 24 hours RO permeate flux. Feedwater using synthetic drainage water I with 5 μ M PAA.

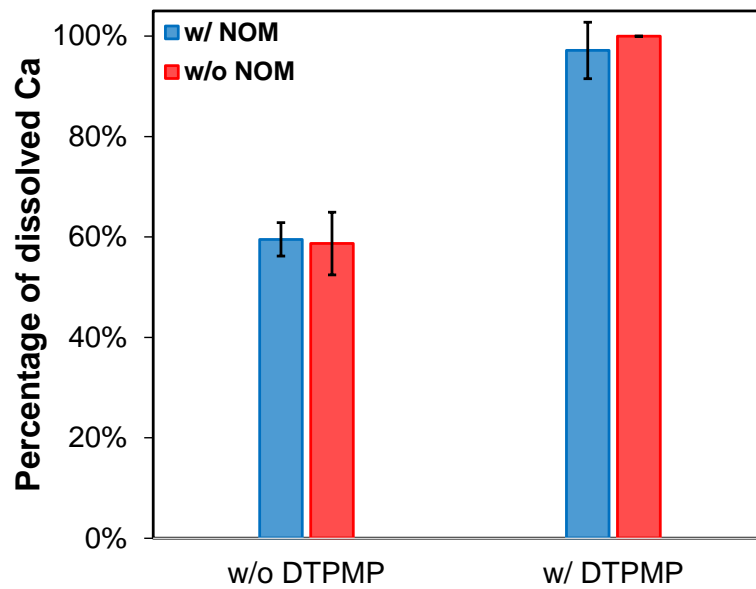


Figure S8. Effect of 1 μM DTPMP on dissolved calcium percentage at 24 hours RO desalination with or without 5 mg C/L NOM. Feedwater using synthetic drainage water I.

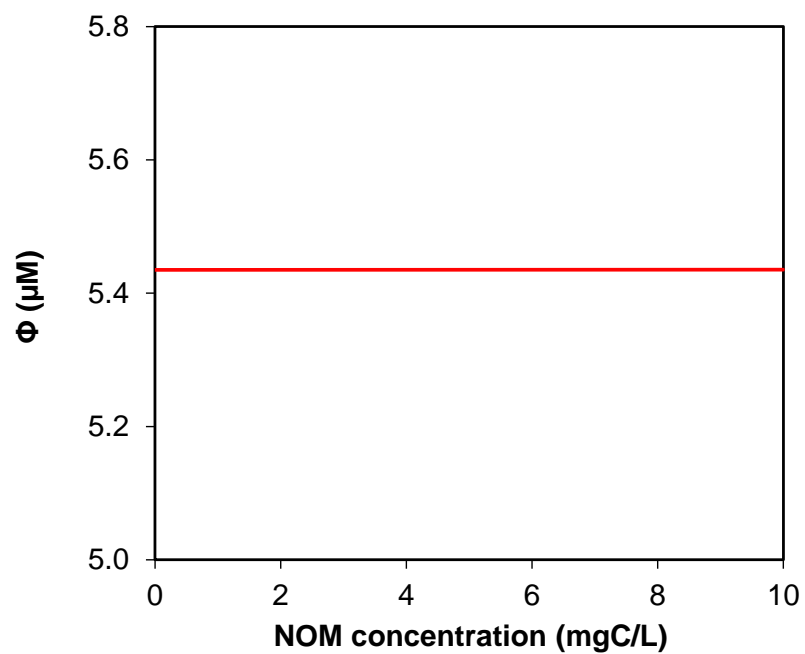


Figure S9. Effect of NOM on concentration of total charge of DTPMP species.

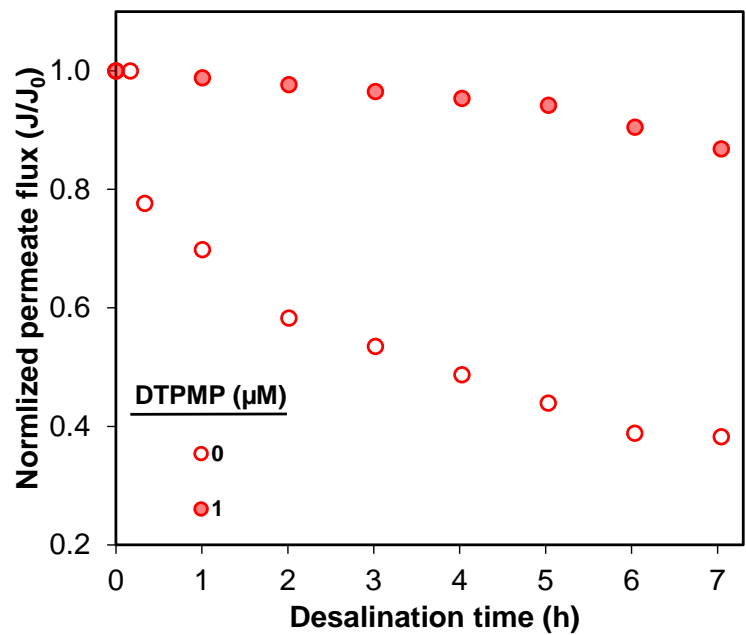


Figure S10. Effect of optimized antiscalant condition on RO permeate flux. Feedwater using synthetic drainage water II.

Table S1. Molecular structure of selected antiscalants

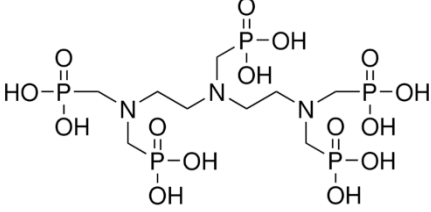
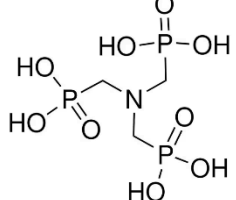
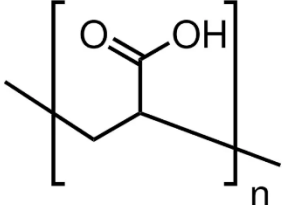
Antiscalant name	CAS#	Molecular structure
DTPMP	15827-60-8	 <p>The structure shows a central diethylenetriamine (DET) molecule with three nitrogen atoms. Each nitrogen atom is bonded to two methylene groups. Each of these six methylene groups is further bonded to a phosphonic acid group (-CH₂-P(=O)(OH)₂), resulting in a total of six phosphonic acid groups per molecule.</p>
NTMP	6419-19-8	 <p>The structure shows a central nitrilotriamine (NTA) molecule with three nitrogen atoms. Each nitrogen atom is bonded to one methylene group. Each of these three methylene groups is further bonded to a phosphonic acid group (-CH₂-P(=O)(OH)₂), resulting in a total of three phosphonic acid groups per molecule.</p>
PAA	9003-01-4	 <p>The structure shows the repeating unit of polyacrylic acid (PAA) enclosed in square brackets with a subscript 'n'. The repeating unit consists of a carbon atom bonded to a methyl group, a hydrogen atom, and a carboxylic acid group (-COOH).</p>

Table S2. Normalized average molar concentration (%) fraction of different elements on membrane surface after 24 hours RO desalination with different antiscalants. Feedwater using synthetic drainage water I.

Element Antiscalant	C	N	Ca	S	O	Scaling mineral
1 μM DTPMP	75.04	8.74			13.11	
1 μM NTMP	13.16		14.33	14.84	57.67	CaSO _{4(S)}
1 μM PAA	12.20		14.94	15.36	57.50	CaSO _{4(S)}

Reference:

- (1) Mark M. Benjamin. *Water Chemistry*; 2015.
- (2) KIRISHIMA, A.; OHNISHI, T.; SATO, N.; TOCHIYAMA, O. Simplified Modelling of the Complexation of Humic Substance for Equilibrium Calculations. *J Nucl Sci Technol* **2010**, 47 (11), 1044–1054.
<https://doi.org/10.1080/18811248.2010.9711669>.